POLITECNICO DI MILANO
Facoltà di Ingegneria Industriale e dell'Informazione

Corso di laurea magistrale in
Materials Engineering and Nanotechnology

QUASI-1D HIERARCHICAL TITANIUM OXYNITRIDE NANOSTRUCTURES FOR METHANOL OXIDATION

Relatore: Prof. Andrea Casalegno
Correlatori: Fabio di Fonzo
Andrea Perego

Tesi di laurea di:
Antonio Bellizzi
Matricola 837556

Anno accademico 2015/2016

Ringraziamenti

Grazie alla mia famiglia che mi ha sempre supportato
ai miei amici del gruppo di via Grossich, compagni di studio e di vita

Grazie al professor Casalegno e all'Istituto Italiano di Tecnologia per avermi dato l'occasione
di seguire questo progetto.
Grazie agli amici dell'IIT con i quali ho trascorso quest'ultimo anno
Un ringraziamento particolare va a Fabio, Andrea e Giorgio per l'incredibile aiuto datomi
nella realizzazione di questa tesi.

Abstract

One of the main efficiency losses in Direct Methanol Fuel Cell is the high anodic overpotential caused by the sluggish methanol oxidation reaction (MOR). In order to overcome this problem, the role of the catalyst is fundamental and for this reason, up to now, bimetallic Pt – Ru supported over carbon is the state of the art catalyst causing a net increase of the costs of the device. Research is moving toward cheaper and more stable materials and titanium oxynitride (TiON) can play both the role of a stable catalyst support replacing carbon and that of co-catalyst toward the MOR with a consequent reduction of the catalytic loading and the costs of the device. Furthermore, to enhance the methanol oxidation reaction, TiON, being a semiconductor, can exploit a photocatalytic effect after a correct engineering of the band gap.

In this thesis work, we fabricate quasi 1D-hierarchical TiN nanostructures by Pulsed Laser Deposition (PLD) to produce a high surface area scaffold. TiN thin films are then oxidized to TiON passing from a metal-like material to a semiconductor with tunable band gap and consequently, Pt nanoparticles are deposited over the surface by pulsed electrodeposition. The final TiON/Pt catalyst is characterized by performing different electrochemical measurements to show the activity of the fabricated active layer toward MOR both in dark and under illumination condition to verify the benefit of the photocatalysis toward the elimination of the poisoning intermediates during the reaction.

Keywords: Pulsed Laser Deposition, Methanol oxidation reaction, Titanium oxynitride, photocatalysis

Sommario

Una delle principali perdite di efficienza nelle celle a combustibile a metanolo (DMFCs) risiede nell'elevato sovrapotenziale anodico causato dalla lenta reazione di ossidazione del metanolo (MOR). Al fine di risolvere questo problema, il ruolo del catalizzatore è fondamentale e al giorno d'oggi, lo stato dell'arte è il catalizzatore bimetallico Pt-Ru supportato su nanoparticelle di carbonio con conseguente aumento del costo del dispositivo. La ricerca è indirizzata verso nuovi materiali più economici e al tempo stesso più stabili e, l'ossinitruro di titanio (TiON) risponde sia al ruolo di supporto stabile rimpiazzando il carbonio che quello di co-catalizzatore verso l'ossidazione del metanolo con conseguente riduzione del carico catalitico e del costo del dispositivo. Inoltre, essendo il TiON un semiconduttore, questo può favorire la reazione di ossidazione sfruttando un effetto fotocatalitico a seguito di una corretta ingegnerizzazione del band gap.

In questa tesi, vengono fabbricate nanostrutture gerarchiche di TiN attraverso Pulsed Laser Deposition (PLD) al fine di produrre un supporto con un'elevata area superficiale. I film sottili di TiN sono in seguito ossidati a ossinitruro di titanio passando da un materiale semimetallico ad un semiconduttore con un band gap variabile e, successivamente, le nanoparticelle di platino vi sono depositate tramite elettrodeposizione pulsata. Il catalizzatore completo TiON/Pt è caratterizzato attraverso diverse misure elettrochimiche al fine di mostrare l'attività del materiale verso la MOR sia in buio che simulando condizioni di illuminazione per verificare il beneficio della fotocatalisi verso l'eliminazione degli intermedi avvelenanti prodotti durante le reazioni.

Parole chiave: Pulsed Laser Deposition, ossidazione del metanolo, ossinitruro di titanio, fotocatalisi

List of contents

Introduction

Energy systems will evolve in a more environmental friendly way to reduce the CO_2 emission as a result of a progressive abandon of fossil fuels along with the use of renewable energy carriers. Among these, hydrogen is extremely interesting since it can be produced in a clean way by gasification of biomasses or by electrolytic processes like water-splitting exploiting solar power.

Hydrogen can be transformed into heat and mechanical energy by combustion or directly converted in electrical energy using fuel cells, for example in Polymer Electrolyte Fuel Cells (PEMFCs) technology. In this type of devices, the electrical energy is produced by an electrolytic process involving the oxidation on hydrogen (fuel) to produce current and water (product) with no generation of CO_2. In this way, PEMFCs can be optimized for energy production, in particular for automotive applications. Nevertheless hydrogen has different drawbacks: it has a low volumetric energy density (one-third that of methane) and it's gaseous in normal operation conditions so dangerous and difficult to handle. Even when the fuel is stored as liquid in a cryogenic tank or in a compressed hydrogen storage tank, the volumetric energy density [mJ/l] is small relative to that of gasoline and, especially for automotive application, highly pressurized gas tanks are difficult to stock and relatively dangerous. Finally, fuel infrastructures are not compatible for hydrogen since they operate with liquid fuels.

To overcome these issues, a promising way seems to employ methanol as a fuel since its liquid and with a higher volumetric energy density. Direct Methanol Fuel Cells (DMFCs) can operate with a direct feed of methanol

and water simplifying hardware since no pressurized gas are present leading so to promising characteristic for portable applications.

DMFC produce CO_2 as byproduct so the choose of methanol as an environmental friendly fuel seems misleading but considering that it can be produced from biomasses, it won't alter the total CO_2 balance differently from fossil fuels. Methanol has the simplest structure of all the possible organic fuels nevertheless it doesn't have a straightforward reaction mechanisms but a complicated pathway difficult to analyze. The full oxidation to CO_2 is accompanied by different reaction steps that finally influence the yield of the process. Studying the reaction process is a fundamental step to ideate an efficient device.

Chapter I

Fuel Cells Technology, Electrode Materials and Methanol Oxidation

1.1 Fuel cells

A fuel cell is an electrochemical device that exploits redox reactions to convert the chemical energy from a fuel into electrical energy. Differently from batteries, they can generate electricity as long as they are fed with fuel. There are different types of fuel cells according to the operating temperature and choice of the electrolyte but they are all characterized by the presence of an anode, of a cathode and of an electrolyte membrane that allow the protons to move from one to the other electrode. Fuels reach the anode where with the aid of a thin catalyst layer it undergoes oxidation with generation of protons (hydrogen ions) and electrons. The hydrogen ions permeate through the electrolyte while electrons move to the cathode through an external circuit generating a current. At the cathode side a reduction reaction involve hydrogen ions, electrons and oxygen to form water.

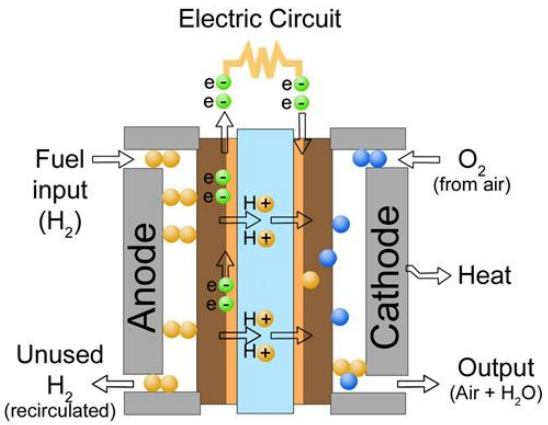

Figure 1: Schematics of a PEMFC

The generation of current is due to a direct conversion from chemical energy into electrical energy through redox reactions and the product generated in the process are mainly water and heat but, depending on the type of fuel cell also amounts of CO_2 can be produced.
Since the generation of energy is different from a combustion process, fuel cells can obtain higher efficiencies reaching values of 40 – 60 %.

The main classification of fuel cell is done by the type of electrolyte and the operating temperature range that will also define the application area: portable, stationary and transport.

Polymer Electrolyte Membrane Fuel Cells (PEMFCs) are the most diffused low temperature fuel cells. They are characterized by the use of a proton conductive polymeric membrane as electrolyte (Nafion®) and they are fed with Hydrogen (H_2) that is oxidized to water with generation of current.
Nafion® is a modified PTFE containing a fraction of pendant sulfonic acid groups.
To conduct H^+, the membrane must be hydrated so proton conductivity is strongly dependent on the water content of the membrane. The water in the membrane is localized to the hydrophilic groups where the hydrated protons are transported by diffusion and via proton transfer between hydrated clusters [1].

A PEMFC can be described as a series of different layers characterized by a specific function:

- **Bipolar plates**: Made of different materials (metals, graphite based, carbon-polymer composites) they are essential for a multicell configurations connecting the anode of one cell to the cathode of the adjacent cell (series connection)
- **Gas Diffusion Layer** (GDL): A layer between the catalyst and bipolar plates, it provides a pathway for the reactant gas and for water to reach and abandon the active area but also it provides mechanical support to the Membrane Electrode Assembly
- **Electrodes**: In a PEMFC it's a thin catalyst layer placed between the membrane and the GDL, supported by a porous and conductive material. Electrochemical reactions take place on the catalyst surface. The most common catalyst in PEM fuel cells for both oxygen reduction and hydrogen oxidation reactions is platinum in the form of nanoparticles (5 nm) finely dispersed on the conductive support material that is typically carbon powders (40 nm).

1.2 Direct Methanol Fuel Cell

As aforementioned, the main limitation of the use of hydrogen as a fuel for a PEMFC is linked to its low volumetric energy density and to the fact that is a gas in normal operative conditions with consequent limitations in application due to safety issues of the compressed gas tanks.
The main solution to this problem is to choose a different type of polymer electrolyte fuel cell and in particular, the Direct Methanol Fuel Cell (DMFC) is able to operate with a fed of liquid fuel i.e. methanol in a range of temperature around 100°C eliminating the problem linked to the use of a gaseous fuel and being so an interesting device for portable applications. [2]
In a DMFC, the methanol/water mixture is injected at the anode site where is oxidized following the reaction:

$$CH_3OH + H_2O \rightarrow CO_2 + 6H^+ + 6e^- \qquad E_0 = 0.046V \qquad (1.2.1)$$

While at the cathode site, oxygen reduction takes place (ORR):

$$6H^+ + 6e^- + 3/2O_2 \rightarrow 3H_2O \qquad E0 = 1.23V \qquad (1.2.2)$$

With an overall reaction:

$$CH_3OH + 3/2O_2 \rightarrow CO_2 + 3H_2O \qquad E_0 = 1.18V \qquad (1.2.3)$$

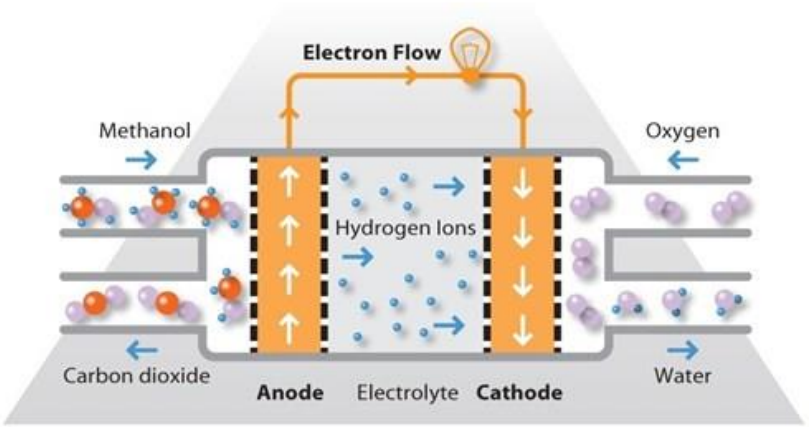

Figure 2: Schematics of a DMFC

Even if the standard thermodynamic cell potential is similar to the H_2-PEMFC, the operating voltage is much lower due to high polarization losses on the anode site. The main reason for this high overpotential can be attributed to the sluggish oxidation reaction. In addition, methanol shows a high diffusion rate through the membrane reaching the cathode site where it reacts with air without generation of useful current. This phenomena is called methanol crossover and is due to the fact that methanol has a high affinity with water and so is dragged with it through the polymer membrane by diffusion. Once methanol has reached the cathode compartment, it reacts with oxygen causing a fuel waste and a mixed potential at the electrode. In particular, mixed potential is expressed as the potential of an electrode against a suitable reference electrode when appreciable fraction to the anodic or cathodic current arises from species of two or more different redox couples according to IUPAC definition [3].
Crossover and mixed potential will decrease the cell potential under operation that will always be lower than the standard potential. The measured voltage will also decrease during the current flow due to polarization losses. This kind of losses can be represented through a voltage/current density curve called polarization curve.

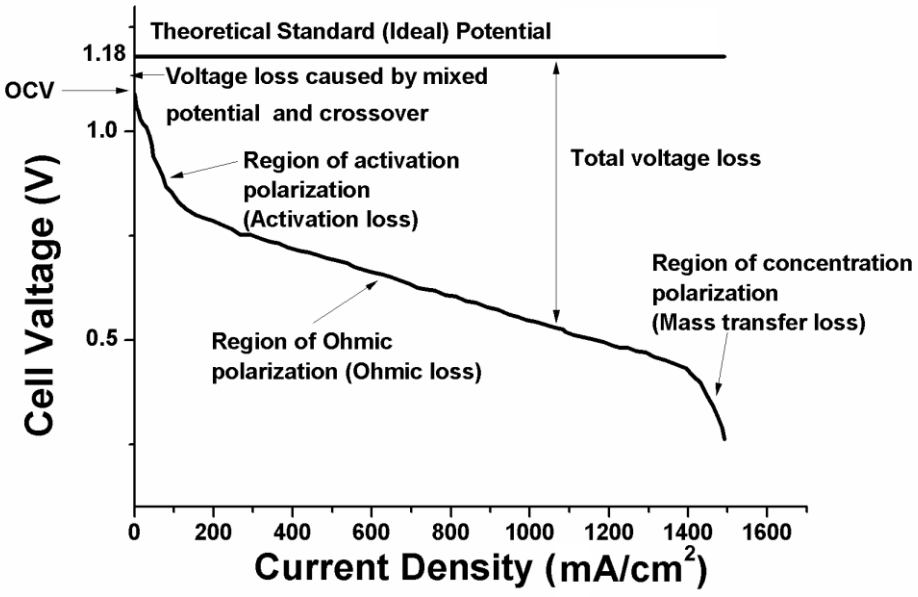

Figure 3: Polarization curve of a DMFC

Three main polarization losses can be identified in the graph:

- At low current density, the voltage drop is caused by activation losses: the process is limited by the reaction kinetic so, in order to overcome the activation energy, a portion of voltage is needed
- The linear region is the region of Ohmic polarization where resistive ohmic losses (membrane and contact resistances) affect the characteristic influencing the slope of the curve
- At high current density, mass transfer losses occur: in this situation, the reaction is sufficiently rapid to lower the concentration of the reactants below that of bulk solution so the rate of the reaction is limited by the ability of these to reach the electrode

Since activation losses are extremely severe in a DMFC and since they are mainly related to methanol oxidation reaction, particular attention to this topic will be given in this thesis work with the aim of understanding its mechanics and consequently try to overcome these issues.

1.3 Methanol oxidation

1.3.1 Introduction

Severe losses in DMFC efficiency are attributed to high anodic overpotential caused by the slow kinetic of methanol oxidation. [4]
In the oxidation of a single methanol molecule to CO_2, six electrons are involved and the complex mechanism has several intermediate steps.
A simplified reaction scheme is shown:

$CH_3OH \rightarrow (CH_3OH)_{ads}$ *Methanol adsorption* (1.3.1)
$(CH_3OH)_{ads} \rightarrow (CO)_{ads} + 4H^+ + 4e^-$ *C-H bond dissociation* (1.3.2)
$(CO)_{ads} + H_2O \rightarrow CO_2 + 2H^+ + 2e^-$ *CO oxidation* (1.3.3)

There are two different pathways:

- **Indirect pathway**: characterized by the presence of a strongly adsorbed intermediate that is carbon monoxide (CO). The bottleneck of this reaction path is the difficulty to remove the strongly adsorbed CO that work as a catalyst poison and so inhibit catalyst sites for further oxidation.
- **Direct pathway**: involving formaldehyde and formic acid as weakly bonded and partially dissolved intermediates. [4]

$$(CH_3OH)_{ads} \rightarrow \text{adsorbed intermediates} \begin{cases} \nearrow (CO)_{ads} \rightarrow CO_2 \\ \searrow HCHO, HCOOH \rightarrow CO_2 \end{cases} \quad (1.3.4)$$

Both of these pathways require a catalyst able to dissociate the C-H bond and facilitate the reaction of the resulting residue with O-containing species to form CO_2 (or HCOOH) [5].
Platinum is known to be the most efficient material since it favors the C-H bond dissociation but the support material and the presence of a co-catalyst are extremely important.

1.3.2 Methanol adsorption

Methanol adsorption takes place in several steps, forming different species due to cleavage of the C-H bonds each one on a different and adjacent Pt site. Since Pt is initially covered by adsorbed H and since methanol alone cannot displace it, the adsorption can start at 0,2 V vs RHE. [4][6]
The dehydrogenation reactions lead to formation of adsorbed hydrogen atoms and successively an electron transfer reaction occurs to form a proton and an electron. [7]
For an indirect pathway this process will occur different times until the methanol molecule will be completely deprotonated to adsorbed CO. The formation of CO intermediate is a critical step in the methanol electro oxidation mechanism since it acts as a catalyst poisoner toward Pt sites.
Depoisoning of CO and consequent oxidation to CO_2 is extremely important and will be discussed in the next chapter.

1.3.3 CO depoisoning

Poisoning of platinum by CO is one of the most severe problems in fuel cell anode catalysis. CO is a strongly bonded intermediate in methanol oxidation and its depoisoning can start only with the presence of a water molecule following the Langmuir–Hinshelwood (LH) mechanism suggested by Gilman [8].
Water needs to be splitted on a free site on the surface, leading to a surface OH that will be the oxygen donor for the final oxidation of CO to CO_2. [4]
On pure Pt electrode, a strong interaction of water with the catalyst surface is only possible at high potentials. This difficulty can be overcome by adding a co-catalyst able to dissociate water more easily. One of the best co-catalyst is Ruthenium (Ru) and for this reason, Pt-Ru is the most efficient couple since now.
Pt is efficient in the adsorption and dissociation of methanol while Ru is able to oxidize the CO due to the easier dissociation of water on its surface. The cooperative effect of these two catalysts is usually called *bifunctional mechanism* and is a fundamental process in methanol oxidation. [5]
A necessary condition for the LH mechanism are both an high CO diffusion on the surface in order to reach OH adsorbed on the partner co-

catalyst and at the same time an efficient distribution of the two precious metals. Schematically, the LH mechanism can be described in *Equation 1.3.5*:

$$Pt(CO)_{ads} + Ru(OH)_{ads} \rightarrow CO_2 + Pt + Ru + H^+ + e^- \quad (1.3.5)$$

With this mechanism, CO coverage is reduced and the number of active sites for methanol oxidation is recovered.

Beside the bifunctional mechanism, another important effect is attributed to ruthenium and it's usually called *intrinsic mechanism* or *electronic effect*. Different authors [9] [10] have investigate the effect of alloying Pt with Ru and discovered that the second metal in the catalyst modifies the electronic properties of the pure noble metal. As a consequence, the chemisorption properties of CO are also modified.
Before investigating this effect we must first describe briefly a transition metal-CO bond and the orbitals involved.

1.3.4 Pt-CO bonding

Carbon monoxide bonds to transition metals with a synergic process in which three main components constitute the bond. A sigma bond between the nonbonding sp-hybridized electron pair on carbon with empty d orbitals on the metal while a pair of π bonds is caused by the overlap of filled d-orbitals on the metal with a pair of π-antibonding orbitals of CO. [11]

According to [9], the adsorption of CO on platinum is stabilized by two effects:

- electronic transfer from the filled 5σ-orbital of CO to the empty d-band of platinum
- back donation of electrons from metal dπ to the empty 2π* antibonding orbital of CO

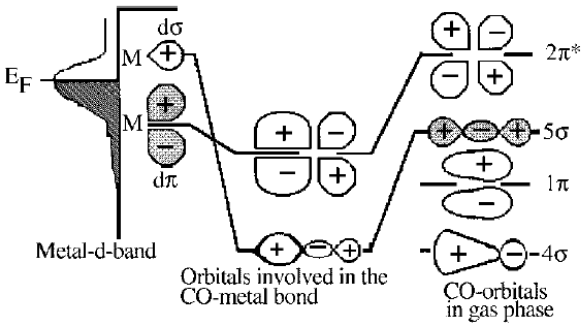

Figure 4: Orbitals involved in Pt-CO bond

When electrons from the metal fill the π-antibonding orbital of CO, the carbon-oxygen bond result to be weakened while the metal-carbon bond is strengthened. [12]
An effective way to reduce Pt poisoning so will consist in modifying the electronic structure of Pt in order to reduce the Pt back donation creating so a destabilizing effect.

1.3.5 Electronic effect

In order to achieve a modification of the electronic structure of a metal, the study of Rodriguez and Goodman [10] is focused on understanding the physical and chemical properties of solids that have heteronuclear metal-metal bonds.
As suggested, the properties of a metal center depend on: the metal itself, the species bonded to the metal and the geometrical structure of the system.
The formation of a heteronuclear metal-metal bond can induce large changes in the electron density and so affecting the cohesive energy and chemical properties of the metal.
In particular, the chemical properties of the bimetallic system are investigated studying the chemisorption of CO on different metals. Referring to the surface system palladium (Pd) – ruthenium respect to pure Pd, the authors explain the weakening of the Pd – CO bond by considering a charge transfer between the two metal: they are able to demonstrate that a net charge transfer occur from Pd to underneath metal leaving a positive charge on Pd.
This positive charge is consistent with a reduction in the Pd – CO bond strength mainly because it hinders the backdonation to the 2π orbitals of

the CO. X ray photoelectron spectroscopy (XPS) is a useful tool to look at the amount of backdonation by measuring the shift in the core level peak position of Pd indicating a reduced backdonation for the bimetal system. [10] [13]
Giorgi et al. [9] investigated the role of Ru as an alloying metal with Pt and found the same results: looking at the 4f core level of Pt they attributed a positive shift of the level toward higher binding energy due to a charge transfer from the Pt to Ru leaving vacancies in the Pt d-band and consequently reducing the stabilizing backdonation from Pt to CO finally lowering the Pt – CO bond strength.

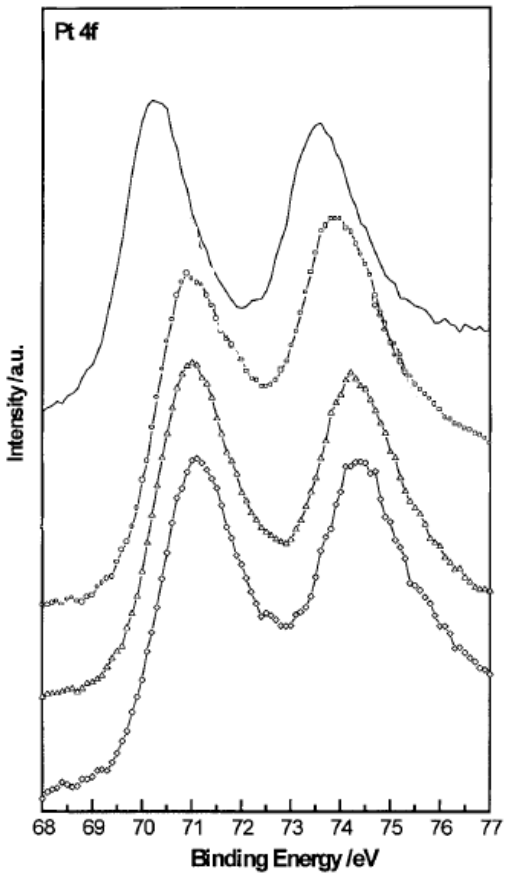

Figure 5: XPS of Pt 4f spectra of Pt bulk (solid line) and Pt-Ru/C catalysts with different compositions (3:1 circle, 1:1 triangle, 1:3 diamond symbol)

Accordingly, also Buatier et al. found the same results with a study on CO adsorption and oxidation on bimetallic Pt/Ru. [14]

1.3.6 Structure effect

Methanol and CO oxidation are complex processes and the reactions have a strong sensitivity to the surface structure. [6][15]
In particular, CO oxidation is promoted on defect sites like steps and kinks respect to highly coordinated sites like terraces. It has been reported by [7] that CO initially adsorbed at or near steps diffuse toward this sites where they react with OH to finally obtain CO_2.
Considering Pt surfaces, Pt(110) seems the most promising surface due to its low coordinated sites (steps) respect to Pt(111) terraces.

As already described, bifunctional mechanism, electronic effect and structure effect are fundamental mechanism for enhancing the methanol oxidation reaction on the anode side of a DMFC so, this thesis work will focus on the choose of a material able to exploit this phenomena in order to increase the efficiency of the whole process.
Ruthenium is considered up to now the state of the art cocatalyst for the MOR because is able to exploit both the bifunctional mechanism and the electronic effect playing so a synergic role in the oxidation process helping the platinum catalyst to be depoisoned from CO intermediate. At the same time, the role of the catalyst support is fundamental since it allows a good dispersion of the catalyst even if it isn't usually active in the oxidation process.
The best performance so will be obtained with a meticulous choice of the catalyst and catalyst support able to cooperate on the MOR in a synergic way with an active material able to both provide its support ability to the catalyst and at the same time promote the reaction.
Before describe the innovative support materials, a brief description of classical supports will be done in order to show their limitations.

1.4 Support materials for DMFC anode catalyst

1.4.1 Carbon-based supports

The thin anode catalyst layer, usually Pt-Ru for methanol oxidation must be supported and contacted both with the GDL and with the polymeric membrane. In order to efficiently transfer protons to Nafion® and at the same time be fed by the methanol solution, the catalyst layer require a three-phase contact with adjacent layers.
It's clear that to have a high active surface area, a fundamental parameter is the dispersion of the catalyst.
Consequently, the electrode is composed of the active phase i.e. the catalyst (nanoparticles in the order of 4nm) finely dispersed on a catalyst support that will require also to be porous and conductive to extract the charge carriers.
The most common support for DMFC catalyst is carbon since it can be easily disperse as nanoparticles with high surface are and has a good conductivity.
Liu et al. [16] classified Carbon-based supports in three main categories:

- **Carbon Black**: Different types of Carbon black like Acetylene Black, Vulcan XC-72, Ketjen Black are the most common supports and are mainly produced by pyrolyzing hydrocarbons. Specific surface area is an important parameter and can reach high value with Ketjen Black even if this type of carbon black shows bad performance due to high ohmic losses during operation.
  Pore size and distribution also affect the performance of carbon black supported catalysts since catalyst nanoparticles can sunk into the micropores giving no electrochemical activity. [16]

- **Nanostructured carbon**: Nanostructured carbon materials are very interesting supports for DMFC due to peculiar structural properties. Carbon nanotubes (CNTs) belong to this group and show increased performances compared to carbon black. As shown by [16], a CNTs supported Pt can achieve higher fuel cell voltage and power density respect to carbon black supported Pt. Furthermore, a higher catalytic activity was observed due to larger surface area of carbon nanotube architecture. CNT synthesis, metal loading and electrode preparation based on CNT supports still face some challenges,

especially when applied to fuel cells. CNTs are usually synthesized by carbon-arc discharge, laser ablation of carbon, or chemical vapor deposition (CVD) suffering in terms of largescale production and costs.

- **Mesoporous carbon**: To achieve high performance at DMFC anode, the three-phase reaction zone at nanoscale must be large. It also important to have an efficient transport passage for liquid-phase reactants and products so too small support nanoparticles (2nm) decrease catalyst utilization due to mass transport problems while too large particles (50nm) reduce the surface area. Mesoporous carbon has tunable pore size and highly integrated interconnected pore systems with periodic order being able to solve both problems and so can be implemented as an efficient carbon based catalyst support. [16]

1.4.2 Limitations of carbon-based supports

Despite Carbon has very good property as catalyst support (high conductivity, low cost material, high surface area) it suffers from Carbon Corrosion when subject to acidic environment during fuel cell work operation and the presence of Pt catalyze the process creating a synergic effect.
The amount of oxygen in the anode is negligible so the overall reaction is

$$C + H_2O \rightarrow CO_2 + 4H^+ + 4e^- \quad (1.4.1)$$

Carbon corrosion leads to a low durability of the catalyst finally leading to a loss or agglomeration of platinum and consequently a reduction of the electrochemical surface area (ECSA). [15][17]

1.4.3 Non carbon based supports for DMFCs

In order to overcome problems of corrosion and consequent catalyst loss with a reduction of performances, research is moving toward non-carbon based supports. A key role choosing the material is its stability in harsh environment to avoid degradation. At the same time, it's interesting to

find materials able to have an active role during fuel cell operation promoting reactions and helping the catalyst in methanol oxidation.
The catalyst is expensive due to the high cost of the precious metals Pt and Ru so, a great way to reduce DMFCs costs would be the reduction of the catalyst amount or even the replacement with cheaper materials. Furthermore, ruthenium, despise its extremely useful properties for methanol oxidation suffer from stability problems due to dissolution ad migration from anode to cathode compartment following this reaction path [18]:

1.Anode:	$Ru + 3H_2O \rightarrow Ru(OH)_3 + 3H^+ + 3e^-$	(1.4.2)
2.	Ru^{3+} *migration through membrane*	(1.4.3)
3.Cathode:	$2Ru(OH)_3 + 1/2O_2 \rightarrow 2RuO_2 + 3H_2O$	(1.4.4)

An extremely interesting class of material for catalyst support is represented by metal oxides, already implemented in various fields with a wide range of applications. In general, metal oxides are cheap, abundant and chemically stable materials and in particular, for fuel cells applications they can be useful due to the high corrosion resistance.

Tungsten oxide (WO_3) ad example has been used as a support for Pt catalyst with positive effect toward methanol oxidation due to its ability to enhance the Pt dehydrogenation and depoisoning from strongly bounded intermediates. [19]
Furthermore, tungsten oxide forms hydrogen tungsten bronze and the subsequent oxidation of hydrogen at anodic potentials called spillover effect, ensures a better efficiency of Pt active sites on the dehydrogenation step. Finally, also the formation of adsorbed water or OH_{ads} on WO_3 has been studied resulting in an enhanced methanol oxidation reaction thanks to the bifunctional mechanism. [20]
Also Cerium oxide (CeO_2) has been studied as an active support for Pt in methanol oxidation reaction and the result was an enhanced activity of the catalyst due to a synergic effect between the two materials. In particular the better catalysis could be ascribed to the ability of CeO_2 to adsorb OH groups on its surface i.e. the bifunctional mechanism. [21]

In this thesis work, particular interest is given to Titanium oxide (TiO_2) and its sub-stoichiometric phase known as Magnéli Phase (Ti_nO_{2n-1}).
Since we are dealing with semiconductors, it's important to recall some fundamentals of semiconductor electrochemistry, in particular the

difference between a semiconductor-electrolyte interface and a metal-electrolyte interface.

1.4.4 Electrode – electrolyte interface

Metal - electrolyte

Normally in electrochemistry the electrodes are made of metals and once they are in contact with a liquid electrolyte the situation is shown in the following scheme:

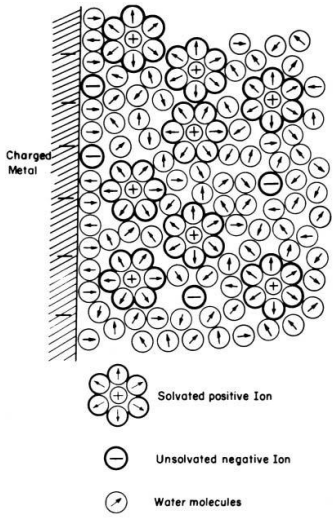

Figure 6: Metal electrolyte interface

A metal can be described as a lattice of positive ions and a cloud of free electrons. When it's charged with an excess charge density, the surface will accommodate this either positive or negative excess of free electrons. Consequently, the solutions will be perturbed by this surface charge and will respond rearranging its molecules. Adjacent to the metal surface a first row of water molecules will be oriented according to the charge on the metal. This thin layer of water molecules is called hydration sheath. Going deeper in the solution, solvated ions will form the so called outer Helmholtz plane (OHP). [22]
The simplest model of the electrified interface was done by Helmholtz and Perrin and considers that the charge on the metal would rearrange the randomly dispersed ions in solution in a counter-layer of a charge of an opposite sign. The electrified interface will consist of two sheets of charge with the name "double layer". This model simply describes the

process as a capacitor with a linear drop in potential between the two plates.

Simply the potential difference V will be expressed as:

$$V = \frac{d}{\varepsilon\varepsilon_0} q_M \tag{1.4.5}$$

And the capacity of the interface as:

$$V = \frac{dq}{dV} = \frac{\varepsilon\varepsilon_0}{d} \tag{1.4.6}$$

Being d the distance between the plates, ε is the dielectric constant of the material between the plates, and ε_0 is the permittivity of free space ($\varepsilon_0 = 8.854\times10^{-12}$ F/m).

However, the description made by Helmholtz and Perrin appears to be too much simple to describe the real behavior of the interface especially because there is no freedom of the charges in the solution restricted only to a sheet.

Gouy and Chapman realized a different model in which the ions are not constrained by a sheet parallel to the electrode. In particular, they considered that the excess-charge density on the OHP is not equivalent to that on the metal, but diffuse further in the solution decreasing with the distance until, sufficiently far into the solution, the net charge density is zero because positive and negative ions are equal. [22]

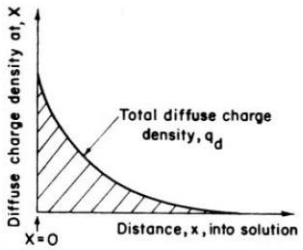

Figure 7: Gouy–Chapman model

The corresponding gradient of potential at a distance x from the electrode is given by the expression:

$$\frac{d\Psi}{dx} = \sqrt{\frac{8kTc_0}{\varepsilon\varepsilon_0}} sinh \frac{ze_0\Psi_x}{2kT} \tag{1.4.7}$$

Where c_0 is the concentration of the different species in the solution and ψ_x is the potential difference between a point x from the electrode and the bulk of the solution.

This model still has some errors ad example it neglects ion–ion interactions important at high concentrations, it assume point charge ions and not modify the dielectric constant between the electrode and the bulk solution. [22]
A more complete model for the description of an electrified interface is given by the Stern model and it is the union of the Helmholtz-Perrin model and the Gouy–Chapman diffuse model.
First it eliminates the point-charge approximation of the diffuse-layer theory placing the ion centers at a distance a far away from the electrode then it divide the solution charge in two contributions given by both the Helmholtz (q_H) and the Gouy (q_G) model.

$$q_s = q_H + q_G \tag{1.4.8}$$

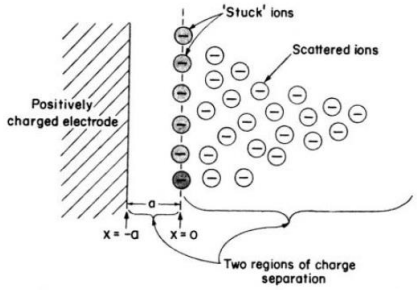

Figure 8: Stern model

Consequently there is a linear variation in the first region according to the Helmholtz–Perrin model and an exponential potential drop in second region according to the Gouy–Chapman model [22]. So finally, the whole system can be described as a series of two capacitor named C_H and C_G and so the total capacity C is calculated by:

$$\frac{1}{C} = \frac{1}{C_H} + \frac{1}{C_G} \tag{1.4.9}$$

Semiconductor - electrolyte

The potential – distance relation for a semiconductor in a solution is different from that of a metal and is show below.
It can be clearly seen that nearly all the potential drop at the interface is in the semiconductor while a minimum drop is in the solution. This can

be explained by the fact that the electronic conduction of a semiconductor is many order of magnitude less than that of a metal and electrons at the interface are not concentrated on the surface (as for a metal) but are more distributed inside and consequently the counter ions in the solution spread out. [23]

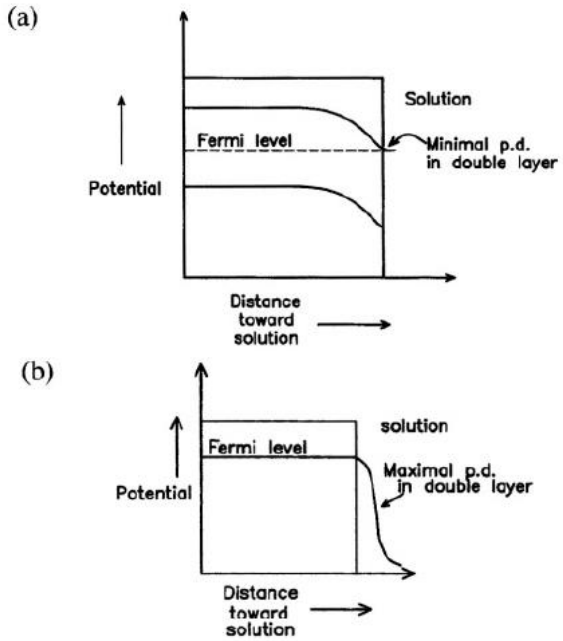

Figure 9: (a) semiconductor/solution interface, (b) metal/solution interface

Nerst equation gives the electrochemical potential of electrons in a redox electrolyte:

$$E_{\text{redox}} = E^{\circ}{}_{\text{redox}} + \frac{RT}{nF} \ln\left[\frac{c_{\text{ox}}}{c_{\text{red}}}\right] \tag{1.4.10}$$

Where C_{ox} and C_{red} are the concentrations of the oxidized and reduced species respectively. The redox potential E_{redox} can be linked to the fermi level in the electrolyte $E_{f\text{-}redox}$ by:

$$E_{\text{F,redox}} = -4.5\ \text{eV} - e_o E_{\text{redox}} \tag{1.4.11}$$

Considering the electron energy in vacuum as reference instead of the SHE.

When a semiconductor is immersed in an electrolyte, an equilibration process occurs between the two phases with a consequent flow of charge and the band bending finally leading to the equilibration of the fermi levels ($E_f = E_{f\text{-}redox}$) and the rise of a built in voltage V_{SC}. [24]

The characteristic region in which the charge has been removed by the equilibration process is called space charge region or depletion region and the voltage dependence on the distance from interface can be described in a simple way as:

$$V_{SC} = -\left(\frac{e_o N_D}{2\varepsilon_s}\right) W^2 \tag{1.4.12}$$

Where W is the depletion layer width, e_o is the electronic charge, ε_s is the dielectric constant of the semiconductor and N_D is the donor density for an n-type semiconductor (or N_A for a p-type semiconductor). [24]

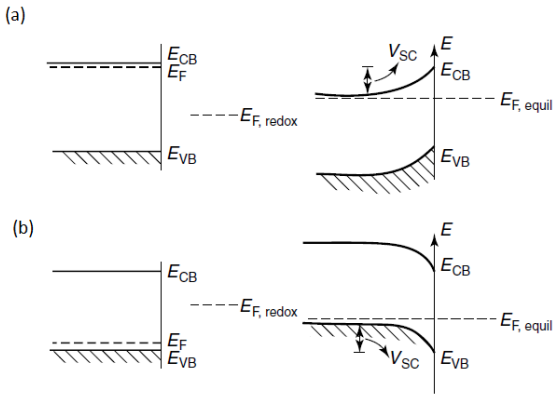

Figure 10: semiconductor-electrolyte interface before (left) and after (right) equilibration. (a) n-type semiconductor, (b) p-type semiconductor

1.4.5 Titanium oxide

Titanium dioxide (TiO_2) is an indirect semiconductor metal oxide with a band-gap of 3.2 eV. It presents different polymorphic forms: Rutile, Anatase and Brookite.

Anatase is a well-known photo catalyst under UV light and its photocatalytic properties were discovered for the first time by Fujishima in 1967 for the photocatalytic water splitting. [25]

TiO_2 is also a cheap, non-toxic and high corrosion resistant material and therefore it's studied as PEMFCs and DMFCs material especially in its nanostructured forms to exploit a large surface area.

Furthermore it's also chosen for its ability to dissociate water and form OH groups on its surface. In particular, TiO_2 surface is characterized by the presence of terminal Ti atoms 5-fold coordinated (Ti_t) and bridging oxygen atoms 2-fold coordinated($>O_{2br}$) so, when in contact with water,

OH^- will interact with Ti_t behaving like Lewis acid site while H^+ will interact with O_{2br} (Lewis base site).
As consequence TiO_2 surface will covered by two different hydroxyl species named terminal OH^-_t and bridging OH^-_{br}. [26]

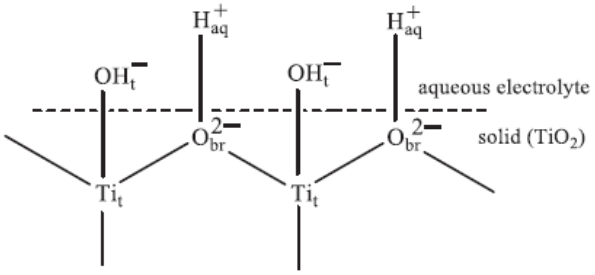

Figure 11: Surface hydroxyl groups resulting from the dissociative adsorption of water

1.4.6 Light absorption and carrier generation

Titanium oxide is an indirect semiconductor with a wide band gap of 3.2 eV. In order to effectively produce an electron-hole pair it must be illuminated with UV light. Optical excitation result in a delocalized electron in the conduction band (CB) and a delocalized hole in the valence band (VB). Considering the semiconductor-electrolyte interface, the electron-hole pairs can be generated both in the field free and in the depletion region where an electric field is present. The direction of the electric field will affect the holes (minority carriers for an n-type semiconductor) moving them toward the surface while the electrons will move in the opposite direction toward the ohmic contact.
Considering that the diffusion length for holes can be described as $L_p = (kT\mu_p\tau_p)^{1/2}$ where μ_p is the hole mobility and τ_p is the hole lifetime, the region in which carriers can effectively be separated is $L_D = Lp + W$ and is called Debye length being W the space charge length. [24]

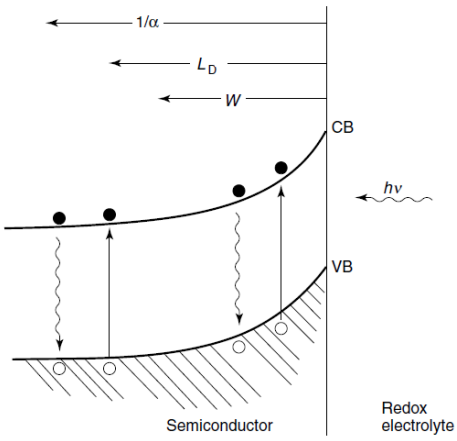

Figure 12: Photogeneration of electron-hole pairs in the field free region and in the space charge region of an n-type semiconductor/electrolite interface

The photogenerated holes generated in the valance band of the semiconductor (h^{+}_{VB}) are trapped by $>OH^{-}_{br}$ and finally form OH radicals ($OH^{\bullet}$) extremely active toward methanol oxidation. [26]
The fact that TiO_2 is covered by OH species on its surface makes this material extremely interesting for application in DMFCs as a support material and co-catalyst with Pt due to an optimization of the bifunctional mechanism.
Different studies have demonstrated that TiO_2 can effectively increase efficiency in methanol oxidation for DMFCs applications as an active support in the catalyst layer.

- Su et al. [27] synthetized Pt nanoparticles by plasma-induced method supporting them over TiO_2 nanotubes prepared by anodization. Through electrochemical measurements the research group demonstrated that TiO_2 was a suitable material for Pt nanoparticle support and exhibit higher performances respect to Pt/C catalyst layer toward methanol oxidation. Firstly ECSA value obtained by Pt/TiO_2 catalyst resulted higher than Pt/C indicating a larger area for Pt anchoring over the substrate. Secondly the ratio between forward and backward scan peak during cyclic voltammetry that has a direct correlation with Pt tolerance to CO poisoning was higher for Pt/TiO_2 catalyst suggesting that the addition of TiO_2 nanotubes cause the easy adsorption of OH species on the catalyst surface and further promote the removal of CO_{ads} intermediate species. Finally an electronic effect between TiO_2 nanotubes and Pt was shown by XPS

measurements: a positive shift of the binding energy of Pt 4f peak is obtained for Pt/TiO_2 catalyst respect to Pt/C suggesting an increase of the Pt d-vacancy in the valence band and consequent weaker adsorption strength of poisoning adsorbate.

- Qin et al. [28] further investigated the electronic effect of TiO_2 on Pt with XPS analysis of Pt core levels. In particular the Pt 4f signal was deconvoluted into two pair of doublets attributed to Pt(0) (metallic platinum) and Pt(II) (PtO or $Pt(OH)_2$). Pt(0) shifted from 71,2 eV for Pt/C catalyst to 71,8 eV for Pt/TiO_2-C suggesting an electron transfer from Pt to TiO_2.

  In order to increase the conductivity of the active substrate, the group used TiO_2 doped with carbon prepared by a sol gel process.
- Polo et al. [29] studied $Pt/Ru/TiO_2$ as photoelectrocatalyst for methanol oxidation. The catalyst was prepared by polymeric precursor method by mixing metallic salts H_2PtCl_6, $RuCl_3*3H_20$ with TiO_2 nanoparticles, ethylene glycol and citric acid finally mixing to carbon black (Vulcan XC-72R). The suspension was thermally treated at 400 ◦C for 2 h under N_2 atmosphere. Chronoamperometric experiments carried out at 0.5V under UV light showed an improved performance of the anodic current of up to 18% in comparison to the performance in the dark.
- Drew et al. [30] created an hybrid electrode made of TiO_2 nanoparticles as photocatalyst and Pt-Ru electrocatalyst. The group tested the photoelectrochemical behavior of the TiO_2 photocatalyst by irradiating the electrode with UV light and recorded the photocurrent at different applied potentials and with different concentration of TiO_2. They were able to harvest more UV photons with higher TiO_2 concentrations and they observed an increased photocurrent generation. However, at higher loadings, the coverage of TiO_2 was too high with a resulting lower efficiency of electron extraction. The photoresponse was analyzed using a monochromatic light and with cyclic voltammetry TiO_2/Pt-Ru electrode showed an increased anodic current when accompanied by UV irradiation. Higher anodic current were recorded even in the dark for the TiO_2/Pt-Ru catalyst respect to the one without TiO_2 confirming the fact that TiO_2 coupled with Pt- causes the overall performance to improve.

1.4.7 Problems associated to Titanium oxide

Even if titanium oxide shows interesting properties for methanol oxidation, its application in a working device is still problematic since TiO_2 presents critical drawbacks that limit its use.
First of all TiO_2 alone cannot fulfill one of the most important requirement for a catalyst support in fuel cells i.e. the electrical conductivity since it is many order of magnitude less than carbon.
Secondly, TiO_2 is a semiconductor with a wide band gap (3.2eV for Anatase) and it absorbs only UV radiation making it a non-ideal material for solar radiation absorption since the solar spectrum has only a limited portion (less than 10%) in the UV region. As consequence, band gap engineering is required to increase TiO_2 absorption in the visible range and is obtained through doping and in particular, nitrogen is one of the most used elements.
Yoshida et al. [31] performed a nitrogen doping of TiO_2 thin films prepared by Pulsed Laser Deposition technique (PLD). The doping was achieved through N^+ ion implantation and as consequence the absorbance in the visible light region from 420 to 540 nm increased.
Asahi et al. [32] studied visible light photocatalysis in doped TiO_2. In particular, the team describes three main requirements that a doping element must fulfill to effectively achieve visible light activity in doped TiO_2 and are:

- Introduction of states inside band gap that absorb visible light
- No variation of conduction band minimum (CBM) respect to TiO_2 (for photoreduction activity)
- The states in the gap must overlap with the TiO_2 states to transfer photoexcited carriers

The last two conditions were fulfilled by choosing anionic species instead of cationic ones since they were able to effectively narrow the band gap of TiO_2 instead of introducing mid gap states that act as recombination centers. [32]
Among different doping elements for substitutional doping as C,N,S,F and P, nitrogen was chosen as the most effective because its p states contribute to the band gap narrowing of TiO_2 by mixing with O 2p states.
The team calculated density of states (DOSs) by full-potential linearized augmented plane wave (FLAPW) formalism in the framework of the local density approximation (LDA) showing the effective reduction of TiO_2 band gap with N doping [32].

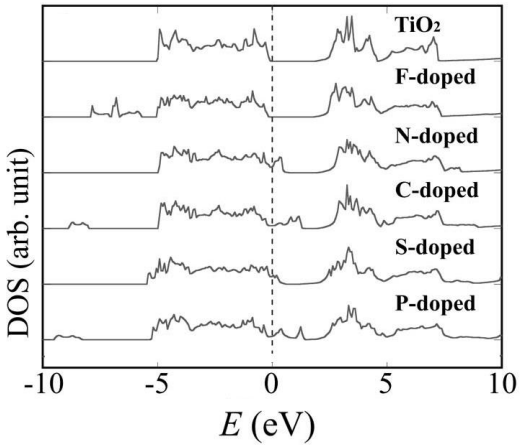

Figure 13: Total DOSs of doped TiO_2. The energy is measured from the top of the valence bands of TiO_2

They prepared $TiO_{2-x}N_x$ films by sputtering a TiO_2 target in a N_2/Ar gas and successively annealing it at 550°C in nitrogen atmosphere for 4 hours.
To confirm the band gap thinning of the material they recorded a shift of the absorption edge to a lower energy with an active wavelength below 500 nm. Finally, the $TiO_{2-x}N_x$ showed a good stability in acid and alkaline environments and a photocatalytic performance for more than 3 months.
Cui et al. [33] obtained $TiO_{2-x}N_x$ thin films starting by titanium nitride (TiN). The group performed an oxidation of the TiN film by annealing it in air at 350°C for 1h. The photoelectrochemical properties of the annealed film versus a TiO_2 film were carried out with photopotential and photocurrent measurements under white light and visible light illumination. Results showed that $TiO_{2-x}N_x$ was active under visible light respect to TiO_2 making it a suitable material for visible light photocatalysis.

1.4.8 Titanium nitride

Titanium nitride (TiN) is a transition metal nitride characterized by a good acid corrosion resistance and a relatively high electrical conductivity. It is extremely hard and therefore is often used as a coating. Some of the TiN properties are reported in the table below.

Titanium Nitride properties [34][35][36]	
Chemical formula	TiN
Molar mass	61.874 g/mol
Density	5.22 g/cm^3
Melting point	2930°C
Vickers hardness	2490HV
Modulus of elasticity	251 GPa
Thermal expansion coefficient	9.35×10^{-6} K^{-1}
Crystal structure	Cubic cF8
Coordination geometry	Octahedral
Electrical resistivity	30–70 μΩ·cm

Table 1: TiN properties

Titanium nitride has a rock salt structure where Ti and N atoms are placed in interpenetrating f.c.c lattice. In this way, each Ti atoms has six N neighbors organized in an octahedral geometry. [34]

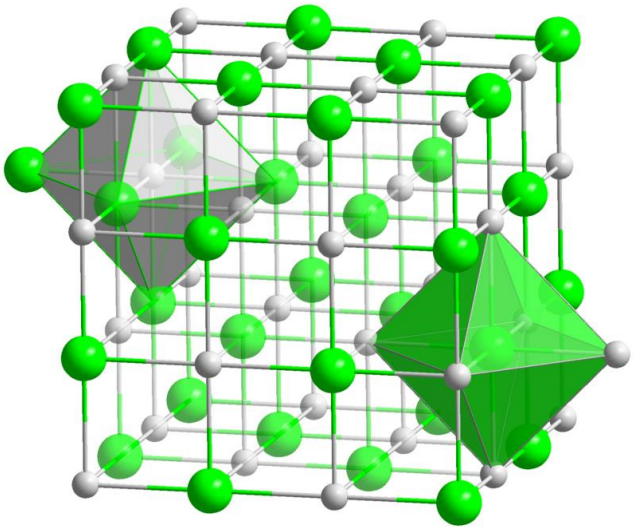

Figure 14: TiN crystal structure

TiN has a peculiar electronic structure that will grant interesting properties. In particular, there is a transfer of part of s and d electrons of the Ti atoms to the 2p-states of the N atoms. The depletion of the electron population of the d-band near the Fermi level makes TiN a good electron acceptor and consequently its able to make covalent bonds with foreign atoms [37]. The metal like behavior of this material arise from the fact that the bonding states in the TiN electronic structure are filled by eight electrons and since TiN molecules has nine electrons, one of these occupies an anti-bonding states with consequent non zero electron density at Fermi level. [34]
TiN is well known for its oxidation resistance property due to the presence on its surface of a native oxynitride layer formed by atmospheric oxidation that prevents further oxidation. [37]
The high electrical conductivity coupled with a good corrosion resistance makes TiN a good candidate as support material in the catalyst layer for DMFCs.
Additionally, TiN is studied also as a co-catalyst being able to assist Pt during methanol oxidation reaction due to strong synergic effect with Pt:

- Bifunctional mechanism
- Electronic effect caused by a strong metal support interaction (SMSI).
- Structure effect induced by TiN to Pt sites

Musthafa et al. [38] reported high performance of platinized titanium nitride catalyst toward methanol oxidation prepared by electrodeposition of Pt over a TiN substrate. TiN alone resulted to be inactive toward methanol oxidation while Pt/TiN showed better properties than Pt-C due to the enhanced stability of the support material combined with the formation of Ti-OH species on TiN surface responsible for the bifunctional mechanism.
Roca et al. [15] investigated the role of Titanium based carbides and nitrides as support materials and co-catalyst for CO and methanol oxidation. In particular, to evaluate the better catalytic activity of Ti based supports, CO stripping experiments were performed. Considering that CO oxidation reaction is easier at low coordinated sites i.e. steps and kinks respect to highly coordinated terraces, cyclic voltammetry shown different anodic peaks at different potential linked to CO oxidation on catalytic sites of different nature. Pt/TiN presented a CO oxidation peak at lower overpotential respect to Pt-C catalyst demonstrating the higher activity of Pt/TiN toward this reaction consequence of the high density of

low-coordinated sites and the presence of smaller amount of (111) terraces respect to Pt-C.
Thotiyl et al. [39] realized an efficient electrode for the oxidation of methanol by electrodepositing Pt nanoparticles on titanium nitride thin film. With XPS measurements the team was able to demonstrate that the Pt/TiN catalyst was stable after a prolonged potential cycling measuring the relative intensities of the peaks corresponding to Pt(0) (metallic Pt) and Pt(II) (PtO, $Pt(OH)_2$). Considering that only Pt(0) is active toward methanol oxidation, an high area ratio between Pt(0) and Pt(II) before and after cyclic voltammetry measurements confirms the good stability of the Pt-TiN catalyst. Furthermore the presence of an oxynitride layer on TiN was recorded with positive consequence on methanol oxidation.
Pt/TiN and Pt-Ru/TiN catalyst activity toward methanol oxidation were measured with a direct comparison between cyclic voltammetry peak currents in function of cycles for the two materials. Pt/TiN showed higher currents respect to Pt-Ru/TiN and the two materials were further compared by polarization measurements showing that while Pt-Ru/TiN feels an increase in the Tafel slope with cycling, Pt/TiN shows the opposite trend.
The good performance of Pt/TiN were ascribed to the propensity of TiN to form OH adsorbed species on its surface as well as the ability of Pt/TiN to easily get depoisoned from CO due to the interfacial behavior of Pt–TiN which weaken the Pt–CO bonding: the equilibration of Fermi levels leads to electron flow from Pt to TiN creating d-orbital vacancies which will result in a decreased back donation to the CO bonding orbital.
An in situ FTIR study at different potentials was carried out showing that TiN can effectively promote methanol oxidation by adsorbing on its surface OH groups even at low potentials. Furthermore, intensity of the band associated to linearly bonded CO shows the ability of the material to remove the poisonous adsorbate with increasing potential.[39]

1.4.9 Stability of Ti-based support

Verify the effective stability of titanium nitride – titanium oxynitride support during DMFC operative condition is a crucial step to determine if the proposed material is better than carbon nanoparticles as catalyst support for DMFC anodes. As already expressed, carbon NP undergo corrosion in a fuel cell environment with consequent loss of performance

due to a reduction of electrochemical surface are. Corrosion of carbon is caused by the harsh environment in which fuel cell anodes must work and occurs with generation of gaseous products (CO_2) and as consequence, a loss of anode material and platinum catalyst is observed. The behavior of a material in a corrosive environment can be different and some of them can react with a creation of a surface passive layer able to avoid further corrosion.
Titanium nitride is an extremely interesting material because its oxidation is hindered by the creation on the surface of a native titanium oxynitride layer able to stop the diffusion of oxygen and preventing so further oxidation [37]. A thermodynamic favorable oxidation reaction occurs when TiN is exposed to air:

$$2TiN + 2O_2 \rightarrow 2TiO_2 + N_2 \quad \Delta G = -611.8\ kJ/mol\ (298\ K) \qquad (4.1.1)$$

And the reaction consists of 3 main stages:

- Diffusion of oxygen inside the lattice and replacement of N atoms
- Formation of sub stoichiometric titanium oxide (Ti_nO_{2n-1})
- Further slow oxidation of the remaining non oxidized TiN

The replaced nitrogen is first released in the interstitial position of the lattice and finally expelled from the surface with the ongoing oxidation.[37]
The titanium - oxygen - nitrogen system is well known and the native layer is made by a non-uniformly distributed mixture of oxynitride and oxide. The formation of this thin layer on TiN is due to atmospheric oxidation but the oxynitride components are also formed during electrochemical potential scanning conditions. [37]
Knowledge on the electrochemical behavior of titanium nitride and oxynitride is fundamental and will be discussed in the next chapter.

1.4.10 Electrochemical behavior of TiN

In order to study the electrochemical behavior of titanium nitride at different values of pH, Pourbaix diagram of TiN is shown

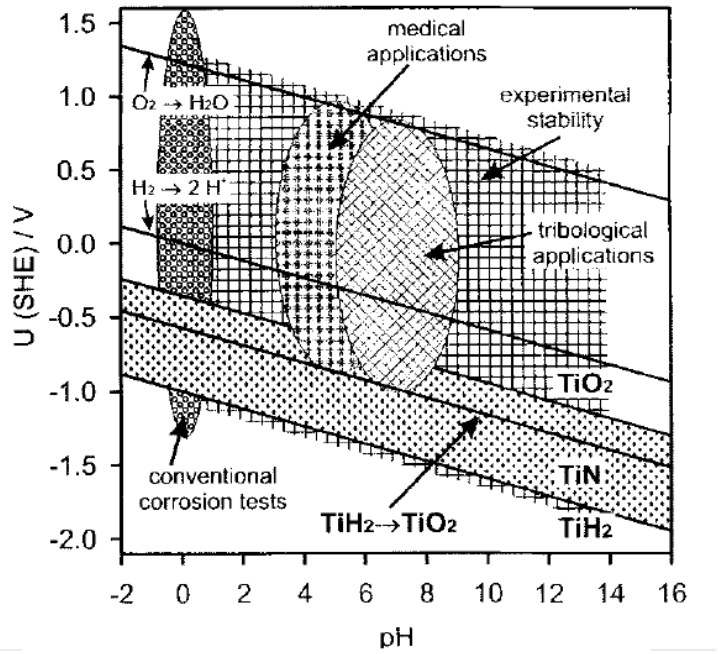

Figure 15: Pourbaix diagram of TiN

The Pourbaix diagram shows the equilibrium phases of the material in different potential and pH regions [58]. As can be seen, at pH = 0, TiN undergoes the reaction to TiO_2 for values of potential higher of -0.36 V vs SHE. In particular, the reaction is:

$$TiN + H_2O \rightarrow TiO_2 + 1/2N_2 + 4H^+ + 4e^- \qquad (4.1.2)$$

As described by [37], the formation of oxide/oxynitride on the surface in the rage of potential 0.5 – 0.9 V vs SHE leads to the retardation of a further oxidation while at higher potentials between 1.0 – 1.5 V another kind of reaction occurs:

$$TiN + 3H_2O \rightarrow Ti(OH)_3 + N_2 + 3H^+ + 3e^- \qquad (4.1.3)$$
$$TiN + 3H_2O \rightarrow TiO_2 \cdot H_2O + 1/2N_2 + 4H^+ + 4e^- \qquad (4.1.4)$$

That is the formation of hydroxides more soluble and less protective than the oxides.

As already described, the formation of the oxynitride component on the surface of TiN (TiO_xN_y) act as a barrier reducing the further oxidation of TiN in the acidic media. The stable behavior of TiN vs. carbon NP when cycled in acidic media is shown by [37] and confirms the fact that TiN is a promising for catalyst support for fuel cells.

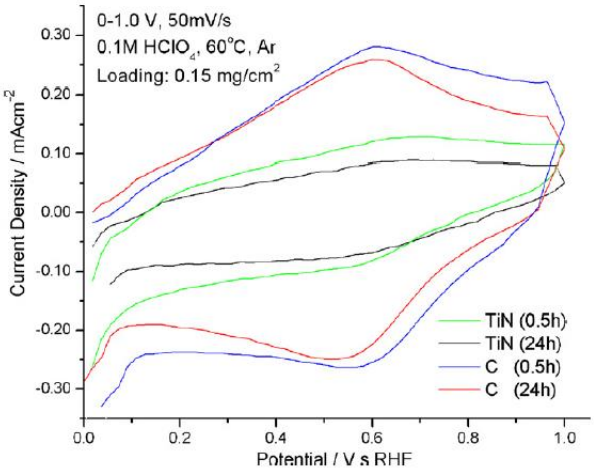

Figure 16: Cyclic voltammetry (CV) of TiN and carbon black after potential cycling between 0 - 1V vs RHE in an inert-gas saturated 0.1M $HClO_4$ at 60 ◦C

In the graph is shown the cyclic voltammetry in acidic media (0.1M $HClO_4$) of both TiN and carbon and the lower current densities of TiN witness the inert nature of this material compared to carbon that instead undergoes corrosion as shown by the peak at ~0.55V corresponding to the hydroquinone/quinone peak [37]. Furthermore, the oxidation of TiN is reduced after 24h (lower current densities) respect to carbon because of the creation of the oxynitride layer on top. The behavior of the different oxides present on the surface of TiN is different and in particular the oxynitride TiO_xN_y has a stronger acid resistance due to its lower oxygen content respect to the sub stoichiometric titanium oxides and hydroxides that instead undergo dissolution.
An important characteristic of TiO_xN_y is the fact that it has good electrical conductivity consequence of its NaCl crystal structure similar to TiN and so it is an ideal material for a catalyst support.

Aim of the work

This thesis work will be focused to the fabrication and characterization of a Titanium oxynitride support as anode for DMFCs. As described by the literature, this material should provide excellent stability and good conductivity as support material for Pt nanoparticles as well as being an active co-catalyst toward methanol oxidation. Furthermore, the material will be tuned in order to achieve an enhanced efficiency toward MOR thanks to a photocatalytic effect when irradiated by visible light.

The fabrication process will consist in different steps:

- Deposition through Pulsed Laser Deposition(PLD) of nanostructured TiN thin films in order to achieve a material with an high surface area
- Annealing of the as deposited thin films in vacuum in order to provide a good crystallinity of the material
- Annealing in air at different temperatures in order to partially oxidize the titanium nitride to titanium oxynitride (TiON)
- Deposition of the Pt catalyst over the active substrate via pulsed electrodeposition technique

The catalyst layer will be physically characterized by SEM, UV-vis and XRD measurements and successively electrochemically characterized by cyclic voltammetry (CV) and chronoamperometric measurements both in the presence and in absence of visible light to study the photocatalytic effect.

Chapter II

Fabrication and characterization methods

2.1 Pulsed Laser Deposition

Introduction

In this chapter, the main fabrication and characterization methods used in this thesis work will be briefly described in their theoretical aspects following all the steps needed to create the final catalyst starting from the deposition method via PLD of the titanium nitride thin films and analyzing also the subsequent annealing and electrodeposition.
Physical characterizations made by SEM, XRD and UV-vis spectroscopy cover a key role in the understanding of the structural and chemical properties of the bare TiN film and their variation during the fabrication steps to TiON/Pt.

Pulsed Laser Deposition

Pulsed Laser Deposition (PLD) belongs to the physical vapor deposition processes (PVD) and is characterized by high energetic laser pulses that strike on a target of known material inside an ultra-high vacuum chamber. The induced ablation that is an evaporation and ionization of the material results in the creation of a plasma plume that expands from the surface. The different constituents of the plasma plume condense on a substrate and a thin film grows. This process can occur in ultra-high vacuum or in the presence of a background gas to tune the properties of the deposited film [40].

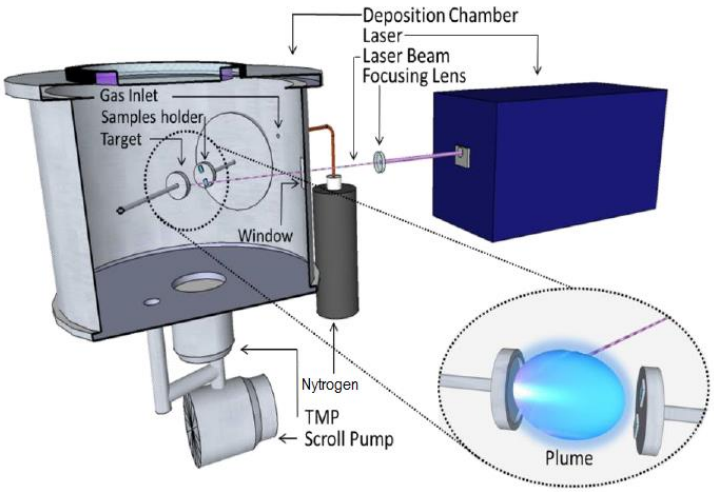

Figure 17: Illustration of a PLD vacuum chamber

According to Schou [41], the pulsed laser deposition process can be described by a sequence of five events and will be briefly described below:

- **Light absorption**: the laser energy is absorbed by the solid target and in few picoseconds is converted into heat. The fast heating rate is followed by an equilibration at high temperature of the species and this allows all target components, even if with different binding energies, to evaporate at the same time
- **Initial plume expansion***:* the local heating lead to the explosive evaporation of the different species which form a high-temperature plasma plume that further get ionized by the absorbed laser radiation
- **Free plume expansion**: the plasma plume expands adiabatically and strongly directed in the forward direction. In vacuum, the species move with a constant velocity away from the target due to the high pressure of the plume.
- **Slowing down of the plume**: the presence of a background gas slows down the plume and the atoms that diffuse away from it reach the substrate. Characteristic is the presence of a shock-wave in the region of contact between the plume and the gas and the shape of the plume is influenced by the pressure and molecular weight of the background gas.
- **Collection of the atoms on the substrate**: the atoms finally reach the substrate with enough kinetic energy to diffuse on the surface until they deposit with the creation of the film.

During PLD, the growing film properties can be tuned by properly modifying the kinetic energy of the ablated particles. To do so, different parameters can be adjusted:

Background gas pressure: the background pressure influences the kinetic energy of the ablated particles and in particular, a high background gas pressure leads to a strong slowdown of the plasma particles after the shock between the plume and the gas. A reactive background gas such as oxygen, can induce modification in the composition of the deposited film creating oxides. [41]

Substrate/target distance: the higher the distance travelled by the particles, the lower will be their kinetic energy so this parameter

influences the porosity of the film in the same way as the background pressure. [53]

Laser fluence: one of the most important parameters that affect the film morphology and the rate of deposition is the laser fluence expressed in J/cm^2 and correspond to the energy delivered per unit area. The variation of this parameter will be directly correlated to the quantity of ablated material with each pulse affecting the deposition rate and the stoichiometry.
As already stated, the variation of the film morphology and of its porosity is mainly related to the kinetic energy of the deposited particles so, high kinetic energy of the striking particles will produce a compact film, while lower energies will lead to the formation of a more porous structure.[41]

2.1.1 PLD advantages and drawbacks

PLD has some interesting advantages respect to other PVD methods:

- **Versatility of the process**: As already stated, the properties of the deposited film, both structural and compositional, can be easily tuned modifying different parameters during the deposition.
- **Stoichiometric transfer**: In many cases, during PLD the stoichiometry of the deposited film is very close to that of the used target and, therefore, it is possible to prepare stoichiometric thin films from a single alloy bulk target. Complex system can be prepared like perovskite structures. Stoichiometry is difficult to obtain from evaporation or sputtering due to the different vapor pressure and sputtering yield of the different components. During the PLD process instead, the strong heating of the laser up to 5000K in few ns will make all components evaporate at the same time. [42]
- **Deposition rate**: deposition rate can reach up to 0.1 nm per pulse [42]
- **Laser–target interaction**: this interaction at the beginning of the process is completely decoupled from other process parameters such as the type and pressure of background gas or the nature of the substrate. [41] [36]
- **Highly controlled process**: during PLD, the number of particles arriving at the substrate can be controlled precisely with the number

of pulses and the fluence. Consequently a single monolayer growth can be achieved by adjusting the number of arriving atoms so perfect surfaces and interfaces in sandwich-systems can be produced. [41]

Nevertheless PLD process has some drawbacks:

- **Sputtering of the film**: Sputtering of a growing film by the ablated particles has been recognized as an issue, for PLD at fluences exceeding 4 J/cm^2. Different authors [41] have discovered ad example a sputtering rate of 0.55 for silver at 4.5 J/cm^2 so only about one-half of the arriving Ag atoms remain on the silver film. The reason is that the kinetic energy of the ablated atoms in vacuum increases with fluence so a substantial fraction of the particles have an high kinetic energy and the sputtering yield increases proportionally
- **Hydrodynamic sputtering**: during the ablation process, undesired droplets of target material are also expelled and deposited. The ablation of these droplets originates from the fast heating and cooling processes of the target and cannot be avoided unless using off-axis geometry. [42]
- **Thickness uniformity:** since the distribution of ablated material is higher in the forward direction, the uniformity of the thickness is granted only for small angles. The practical solution to this problem is to keep the substrate under rotation. [43]

2.1.2 Substrates for PLD

The choose of Pulsed Laser Deposition in order to fabricate the TiN supports was made due to the ability of PLD to control the morphology and the composition of the fabricated up to the molecular and atomic scale. A fundamental requirement for low temperature fuel cell catalytic support is a high surface area to maximize the Pt catalyst dispersion and utilization. Therefore, the fabrication process was focused on obtaining a nanostructured film that could present both porosity (high surface area) and mechanical resistance. This was achieved thanks to a carefully choose of the background gas pressure and consequently an adequate kinetic energy of the striking particles on the substrate.

The films were deposited on different substrates each one chosen to study different properties of the film:

- GC (glassy carbon): glassy carbon has been chosen as substrate for the depositions because of its widespread use as electrode material in electrochemistry due to its extremely high electrical conductivity. GC are accurately polished before PLD to achieve a smooth flat surface

- FTO (fluorine-doped tin oxide): FTO is a type of *transparent conductive films* (TCOs), which is, an electrically conductive film deposited on glass. FTO was early chosen as transparent substrate to test oxygen-doped TiN films under illumination.

- Silicon: silicon samples obtained by cutting silicon wafer are used mainly to perform SEM measurements due to the possibility to cut the PLD deposited substrate to perform cross-section measurements.

- Glass: glass was used to perform all the physical characterization experiments of the TiN based support especially for UV-vis measurement due to its ability to transmit light up to UV.

Pulsed Laser Deposition process of a TiN thin film is reported in *Figure 18*:

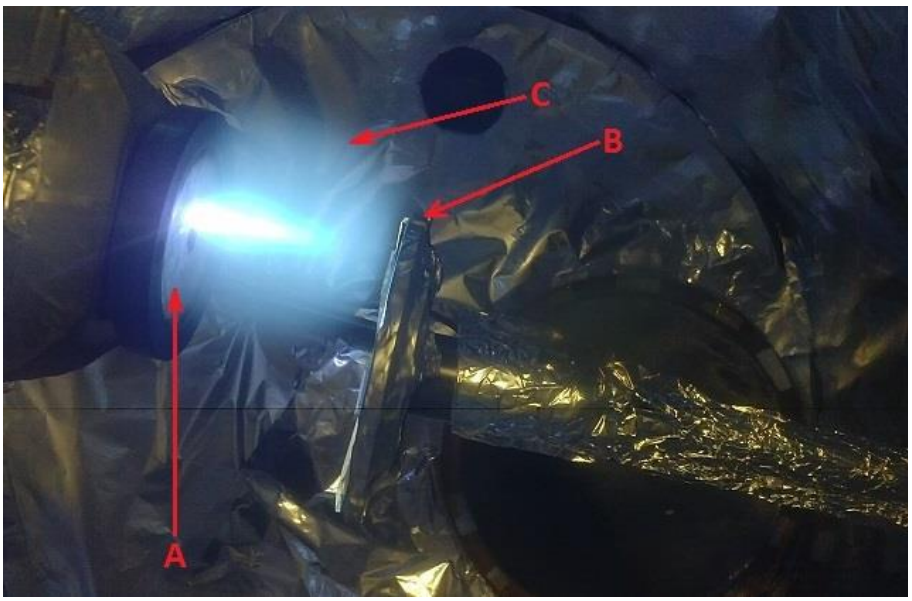

Figure 18: Pulsed laser deposition of TiN from [53]

- (A) Represents the TiN target placed in its holder and ablated by the laser pulses. The TiN is kept in continuous roto-translation in order to ablate the material in a uniform way
- (B) Is the sample holder, where the substrates are allocated. Also the sample holder is under rotation during the deposition so the particles can cover the substrate in a uniform way.
- (C) Is the plasma plume during its expansion: the spherical shape of the plume is a direct consequence of the chamber pressure.

As described by [44], as deposited PLD thin films are amorphous so, to obtain a crystalline film annealing at high temperature is required.

2.2 Annealing and oxidation

Annealing plays a fundamental role in the preparation of the material since accurately changing the annealing parameters, the TiN based supports will be optimized toward methanol oxidation.
Two different types of annealing have been performed in this thesis work:

- **Vacuum annealing**: since as deposited TiN films from PLD process result to be amorphous, a vacuum annealing is required in order to favor the crystallinity of the thin film
- **Air annealing (oxidation):** in order to obtain a partially oxidized substrate (TiON) air annealing must be performed. At high temperatures and in an oxidizing atmosphere the TiN will be partially oxidized on its surface creating a titanium oxynitride layer.

Different parameters must be considered to tune properly the annealing process and are:

- **Dwelling temperature:** is the set temperature for the annealing process both for the vacuum annealing and for the air annealing. For the air annealing treatment, dwelling temperature is a fundamental parameter since it will directly influence the oxidation state of the TiN substrate.
- **Dwelling time:** is the set time for the annealing process
- **Ramping velocity:** setting the ramping time will influence the heating and cooling rate up to reaching the dwelling temperature. Both up and down ramping velocity must be carefully chosen to avoid thermal shocking. Ramping from the dwelling temperature down to room temperature is a key parameter in order to control the crystallinity of the film. A slow cooling rate is always chosen
- **Vacuum:** for the vacuum annealing step, it is important to reach a high level of vacuum inside the tubular furnace to avoid any kind of contamination during the process and at the same time avoiding unwanted oxidations.

2.3 Electrodeposition

Electrodeposition is the technique used for depositing the catalyst precious metal on the surface of the TiON thin film. The substrate upon which the electrodeposition must be carried out is immersed along with the counter electrode in an electrolyte containing the Pt precursor.
Applying a cathodic current to the working electrode, a reduction reaction happens on the TiON substrate and so the metal ions that approached the surface, after a charge transfer reaction, deposit as metal nanoparticles on the electrode.
Electrodeposition is a tunable and versatile technique for the deposition of the Pt catalyst and the loading and the morphology of the deposited nanoparticles depends on different parameters.
Furthermore, since it is an electrochemical process, the total deposited mass can be linked to the quantity of electrical charge, using the Faraday's law. [45]

$$m_{deposited} = \frac{Q_{deposited}}{F \cdot EPI} \cdot MM_{metal} \cdot \eta_{faradaic} \tag{2.3.1}$$

The equation is used to calculate the total deposited mass and:

- $Q_{deposited}$, in [C], is the total charge transferred in the process
- F is the Faraday constant: 96485.33 sA/mol
- EPI is the *electron-per-ion* ratio corresponding to the number of electron that the metal ion must gain to be reduced in the process
- MM_{metal}, in [g/mol] is the molecular mass of the metal
- $\eta_{faradaic}$ is the faradaic efficiency that is the portion of the total charge effectively used to deposit the material while part of the current is wasted in parasitic reactions like hydrogen evolution. This parameter is always less than 100% however, it's difficult to calculate so only a rough estimation can be performed.

Electrodeposition can be performed both in potentiostatic mode in which the deposition is performed by choosing appropriate values of potential or in galvanostatic mode where differently from potentiostatic deposition, in this case the controlled parameter is the current of the pulse [49]. This typology of deposition has been chosen for the current work.

Typical in fuel cell catalyst fabrication pulsed electrodeposition is preferred. [46]
The difference from a normal electrodeposition experiment is that in pulsed methods the signal is not continuous but made by a series of pulses of equal amplitude and duration, separated by zero signal. A typical waveform is shown in *Figure 19*.

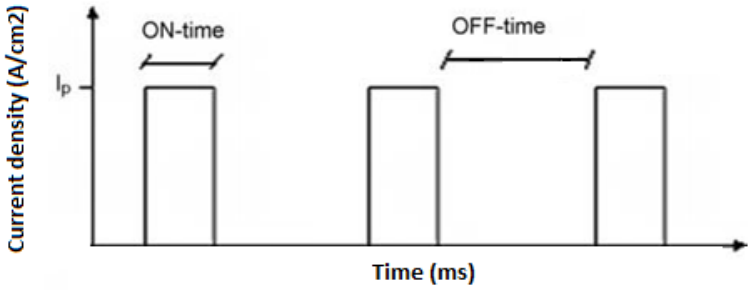

Figure 19: Waveform of a pulsed electrodeposition experiment

Different parameters can be tuned in order to variate the catalyst deposition:

- The duration of the pulse (ON-time) will influence the dimension of the catalyst nanoparticles and clusters: at higher on-time will correspond a bigger deposited particle diameter
- The OFF-time allows the discharge of the negatively charged layer formed around the cathode during the deposition process and a replenish of the solution due to diffusion of new reagents making the process more uniform [46]

2.4 Electrochemical measurements

Electrochemical measurements are a key step in the characterization of the catalysts. Thanks to these measurements we can investigate the mechanism of electrochemical reactions happening on Pt-TiON as well as the stability of the catalyst.
Electrochemical measurements were carried out in a three-electrode configuration cell. This configuration is characterized by the presence of:

- **Working electrode (WE)**: The working electrode is the electrode in an electrochemical system on which the reaction of interest is occurring and in this specific case will be the system GC-TiON/Pt. It's called either cathodic or anodic depending on whether the reaction on the electrode is a reduction ad example during the electrodeposition of Pt nanoparticles or an oxidation ad example during the MOR.
- **Reference electrode (RE)**: the reference electrode is an electrode which has a known electrode potential. The high stability of the electrode potential is reached by using a redox system with saturated concentrations of each participants of the redox reaction. In the specific case, the reference electrode used during the electrochemical experiment is an Ag/AgCl electrode with a saturated KCl solution. Since $E^{o}_{Ag/AgCl}$ is +0.197 V vs RHE at room temperature the equation for the conversion from Ag/AgCl to reference hydrogen electrode is:

  $$\boldsymbol{E}_{(RHE)} = E_{Ag/AgCl} + 0.059 \cdot pH + E^{o}_{Ag/AgCl} \qquad (2.4.1)$$

  Where the pH dependent term is also present.
- **Counter electrode (CE)**: it's also called auxiliary electrode and is used in a three-electrode electrochemical. The counter electrode functions as a cathode whenever the working electrode is operating as an anode and vice versa. It often has a surface area much larger than that of the working electrode (usually a mesh) to ensure that the half-reaction occurring on its surface is fast to not hamper the process at the working electrode. Counter electrodes are usually made of electrochemically inert material such as platinum or gold. [47]

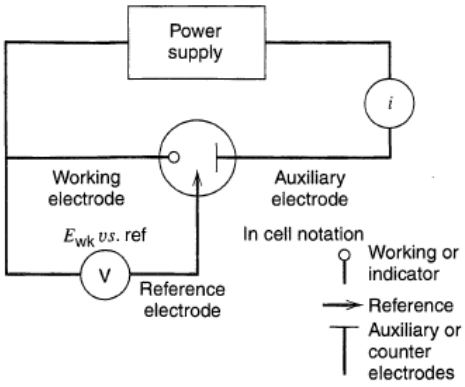

Figure 20: Three electrode cell configuration

Using a potentiostat to control voltage and current variation on the working electrode as output respect to an input during time it's possible to perform different kind of measurement obtaining information about the reaction happening on the surface of the sample.

2.4.1 Cyclic voltammetry

Cyclic voltammetry (CV) is a standard electrochemical technique able to provide information about the activity and reaction a given material has during a potential scan when immersed in an electrolyte.
In cyclic voltammetry, the potential is varied linearly versus time between an upper and a lower value. The variation of potential in time during forward and backward scan is called scan rate and is measured in V/s.

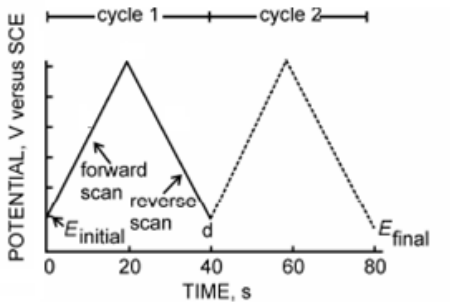

Figure 21: Cyclic voltammetry potential waveform

The current is measured between the WE and the CE and the data are plot in a current density (J) vs. potential (E) plot.

During the initial forward scan a sweep in potential between the two extreme values is applied and, if in the solution are present analytes that can be oxidized, the current will increase over this period. When the oxidation potential of the analyte is reached, the current will start to decrease as the concentration of the species is depleted. If the redox couple is reversible then during the reverse scan the oxidized analyte will start to be reduced, giving rise to a current of reverse polarity (cathodic current).
The reversibility of the redox couple is connected to the shape of the forward and backward peaks and the peak ration i_{fwd}/i_{bwd} is a direct estimation. For reversible couple infact the ratio is equal to 1 while for non-reversible ones it's different from 1. [48]

CV is a useful analysis method to test the electrochemical activity of the catalyst in different electrolyte solutions. Mainly two types of CV were performed:

- **CV in acid solution**: this type of CV is performed in a solution of sulphuric acid (H_2SO_4) with the aim of testing the stability of the materials in this harsh environment and at the same time calculate the electrochemical surface area ECSA of the electrodeposited substrates by integrating the current in the hydrogen desorption region
- **CV in Methanol solution:** this CV was performed in a known Methanol (MeOH) and H_2SO_4 solution to test the activity of the catalyst toward MOR.

2.4.2 Electrochemical surface area

The electrochemical surface area (ECSA) is the total area of a catalyst able to promote the reaction. In the specific case it is the total exposed surface of Pt nanoparticles in contact with the electrolyte and able to perform methanol oxidation.
In this thesis work, ECSA for the Pt catalyst is determined using hydrogen stripping during cyclic voltammetry. The evaluation is made using the formula (2.4.2). [53]

$$ECSA = \frac{Q_H}{q_h \cdot m_{Pt}} \quad (2.4.2)$$

- Q_H is the total charge density corresponding to the hydrogen desorption and its calculated by integrating the current density/potential curve in the hydrogen desorption region (0 - 0.4V vs. RHE) excluding the double layer current that is a non-faradaic current since it's associated to the charging of the double layer.
- q_h is the charge density needed to desorb a monolayer of hydrogen over a Pt surface and is $2{,}10 \times 10^{-4}$ C/cm².
- m_{Pt} is the catalyst loading and the most difficult parameter to determine. Its correlated to the faradaic efficiency of Pt electrodeposition and as described by literature it can have values up to 50% depending on the chosen parameters and precursors [49][50]. A preliminary method to measure the Pt loading was the use of a microbalance measuring the weight difference between the sample before and after the electrodeposition. Since the measurement was too much influenced by many external factors like water infiltration beneath the masking tape with consequent wrong estimation of the final mass, this method was discarded.

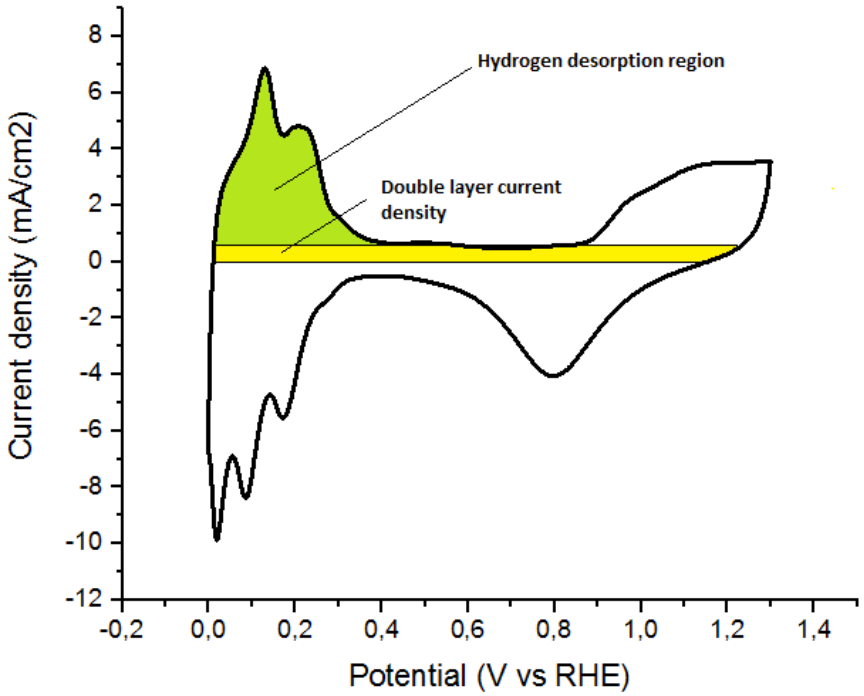

Figure 22: Cyclic voltammetry of Pt in acidic media. Hydrogen desorption area is highlighted

2.4.3 Chronoamperometry

In a chronoamperometry experiment a constant potential is imposed to an electrode over time while recording the current. The result in a fast-redox system is that the interfacial concentration of the consumed species is fixed. In such a case, the slope of the concentration profile at the interface and so the current changes over time. The faradaic current decays as described in the Cottrell equation [51].

$$i = \frac{nFAc_j^0\sqrt{D_j}}{\sqrt{\pi t}} \qquad (2.4.3)$$

Where F is the Faraday's constant, c_j^0 is the initial concentration of the analyte [mol/cm^3] and D_j is the diffusion coefficient [cm^2/s].
The capacitive current instead follow an exponential decay vs. time as $I_{cap} = e^{-kt}$ and since it decrease more rapidly respect to the faradaic current, at longer times I_{far}/I_{cap} is higher.

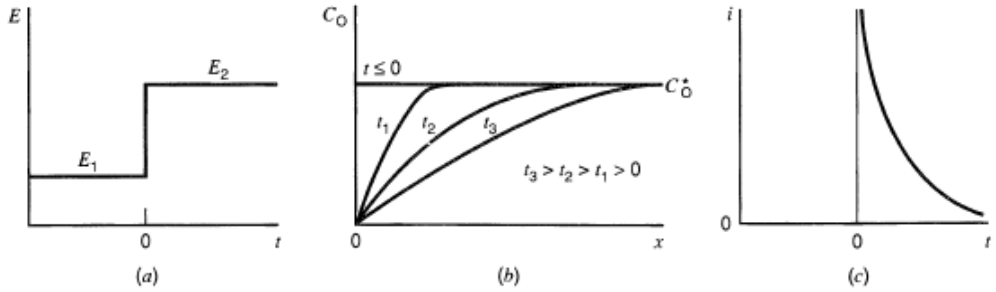

Figure 23: (a) Waveform for a potential step experiment, (b) Concentration profile vs time, (c) current flow vs time

If the chronoamperometry is performed while illuminating the device with a solar simulator (AM 1.5 1000W/m^2) chopped chronoamperometry can be performed in order to recognize the photoactivity of the catalyst. Chopping the light with a shutter will expose the catalyst to a periodic alternation of light and dark at given times named ton and t_{off}. As consequence, during light period, the measured current (I_{on}) will be higher for a photocatalytic device since the incoming radiation will promote the reaction. The percentage of photocurrent can be measured by using the formula:

$$Photocurrent_{\%} = \frac{(I_{on}-I_{off})}{I_{off}} \qquad (2.4.4)$$

2.5 Phisical analysis

2.5.1 X-ray diffraction

X-Ray Diffraction (XRD) is a characterization method used for identifying the crystalline structure of a sample exploiting the ability of a crystal to diffract x-rays. XRD is based on Bragg's Law

$$n\lambda=2d\sin\theta \qquad (2.5.1)$$

Where n is a positive integer, d is the separation among planes, λ is the wavelength of the incident x-ray and θ is the scattering angle.
A schematic representation of XRD setup experiment is reported in *Figure 24*. It consists of an x-ray source, a detector and a sample holder. X-ray striking the sample with an angle progressively increased over time is diffracted by the sample and a detector reads the intensity of the radiation received. The diffraction peaks at different 2θ values are recorded.

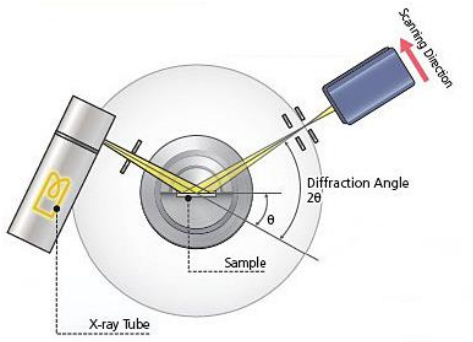

Figure 24: Schematics of an XRD setup

In the analysis of a XRD spectrum different parameters can give information on the crystal. The peak position at a given 2θ angle is used to identify the analyzed material since for each crystal, Bragg condition is verified at given angles. The peak width (FWHM) is used to measure the degree of crystallinity and the crystalline grain size by using the Scherrer equation.

XRD has been performed in order to identify the crystalline structure of the deposited thin films of TiN and to study the transformation of the material after annealing in vacuum and subsequent thermal oxidation.
XRD has been used to:

- Determine the structure and the nature of the TiN thin film after the deposition
- Study the variation during the oxidation at different temperatures

2.5.2 UV-vis spectroscopy

To study the optical properties of the deposited films, UV-Vis spectroscopy has been performed using a Perkin Elmer Lambda 1050 UV-Vis-NIR system. Using a 150mm integrating sphere, transmittance and reflectance measurement has been carried out on the as deposited TiN films, vacuum annealed TiN films and TiON films oxidized at different temperatures.
Integrating sphere is made by a fluoropolymer (Spectralon®) with high diffuse reflectance over the ultraviolet and visible regions of spectrum [51]. In this way, it is possible to have a complete light collection to the detector in total and diffuse transmittance/reflectance, also for high scattering materials.
A schematic representation of the optic pathway is shown below:

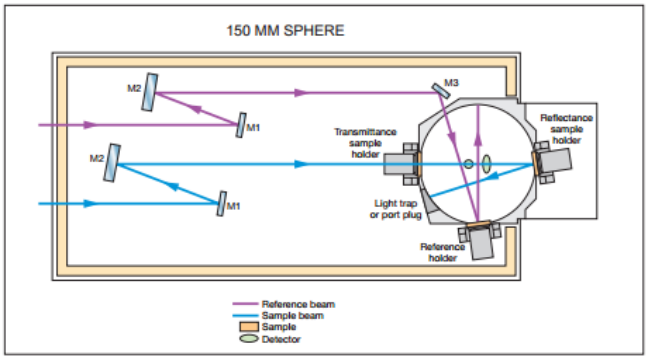

Figure 25: Optical path for an integrating sphere

The basic components of a spectrophotometer are a light source, a holder for the sample, monochromator to select the different wavelengths of light, and a detector. The radiation sources are often different types of lamp emitting in different interval of the spectrum.

Transmittance measurement is done by measuring the intensity of the light passing through the sample (I) and dividing it by the intensity of the light measured without the sample (I_0).
$T = I/I_0$
In a single beam instrument, all the light passes through the sample cell so in order to measure I_0, the sample must be removed.
In a double-beam instrument instead, the light is split into two beams named reference beam and sample beam. The reference beam intensity is taken as I_0 so the transmittance can be measured immediately.[51]
Using an integrating sphere, it's possible to perform both transmittance and reflectance measurements and the sample position is crucial for the kind of analysis:

- **Transmittance**: the sample is placed at the entrance of the integrating sphere so the beam passing through it is attenuated and then collected at the detector to measure I
- **Reflectance**: the sample is placed at the back of the sphere so the beam enters it without attenuation.

After the measurement of transmittance and reflectance, it's possible to calculate the absorptance using the formula:

$$A(\%) = 100 - T(\%) - R(\%) \quad (2.5.2)$$

Knowing the absorbance and the optical path of the material, it's possible to estimate the band gap using Tauc plots.

Tauc plot shows the quantity hν (the energy of the light) on the x-axis and the quantity $(\alpha h\nu)^{1/r}$ on the y-axis where α is the absorption coefficient of the material. The exponent r depends on the material and has values of 1/2 for direct semiconductors and 2 for indirect semiconductors. [52]

The evaluation of the band gap of the material is done by extrapolating the linear region with the x-axis.

Chapter III

Fabrication of the catalyst and physical characterization

3.1 Fabrication of the substrate

Introduction

The aim of this chapter is to shows the fabrication procedure followed to obtain the TiON/Pt catalyst. Fundamental is the role of pulsed laser deposition as the technique chosen for the deposition of titanium nitride thin films since it provide the starting point for the fabrication of the full catalyst. The physical characterization made by SEM images, UV-vis spectroscopy and XRD is also fundamental to study the materials property necessary for the catalysis of methanol oxidation.
The fabrication procedure will follow different steps:

- Deposition of TiN by pulsed laser deposition
- Vacuum annealing of TiN
- Oxidation of TiN to TiON by air annealing
- Electrodeposition of Pt catalyst

The choice of electrodepositing over a pre oxidized substrate is also discussed and compared to another fabrication path in which the oxidation step is carried out after the electrodeposition.
Pulsed laser deposition play a fundamental role in the preparation of the thin film and a precise choice of the deposition parameters must be done to obtain a correct morphology of the substrate in order to enhance the methanol oxidation reaction.

3.1.1 Pulsed laser deposition parameters

TiN thin films are deposited through Pulsed Laser Deposition in order to achieve high surface area and porosity to promote the reaction when immersed in the electrolyte. Mechanical stability of TiN films is also requested to avoid delamination and damage during the processing.

As already described, PLD is a versatile technique able to deposit thin films with different morphologies by just modifying operative parameters.

This thesis work continues the work done by Giuffredi [53] in the realization of nanostructured TiN thin films with high surface area and the optimization of the deposition process has been carried out by a fine tuning of the deposition parameters.

First of all, the background gasses chosen for the deposition inside the PLD chamber, is a N_2+H_2 (<5%) gas mix differently from previous depositions [53] where pure nitrogen were used (N_2 9,9995%) in order to keep the deposition process under a reducing atmosphere avoiding unwanted oxidation during the process. The gas background pressure is set at 60Pa and a pumping system made by a primary pump and a turbomolecular pump allows the chamber to reach value of HV up to 10^{-4} Pa before introducing the gas. Reaching this low value of pressure is a fundamental step in order to achieve a clean process during deposition. The ablation is carried out by a KrF excimer laser (wavelength 248 nm) and the titanium nitride target (99.5%, Testbourne) used is accurately polished before deposition in order to obtain a smooth flat surface and undergoes a first ablation to remove any sort of contamination on its surface. A key aspect in the deposition process is the calculation of all parameter to find the value of the fluence. In particular, using a powermeter, the transmittance of the optics used to focus the laser beam on the target is calculated in order to know exactly the energy of the incident beam entering the deposition chamber. After the measure of the spot size, the parameters are changed to obtain a value of fluence of 2.5 J/cm^2 is evaluated. At this point, setting the frequency of the plasma pulses (20Hz) and the number of pulses (20000), we are able to obtain films with a thickness of 1 μm.

The target to substrate distance is set constant to the value of 50 cm and is not variated in this work. The deposition is carried out with the laser pulse ablating the target under rototraslation to maximize the target ablation uniformity. Also the sample holder is kept under rotation during the deposition.

Before deposition, the substrates are prepared in the following way:

- Glassy carbon (GC) are first polished with different abrasive paper and finally with an alumina abrasive paste (0.3 μm size particle suspension) in order to achieve a mirror like surface.
- Glassy carbon, FTO, glass and Silicon substrate are then cleaned in an ultrasonic bath with different solvents (acetone, isopropyl alcohol and water)

3.1.2 As deposited TiN films

As deposited TiN films over silicon are then analyzed through Scanning electron microscopy (SEM) JEOL Touchscope JSM-6010LA.

Top view of the films has been reported in the figures below at different magnifications.

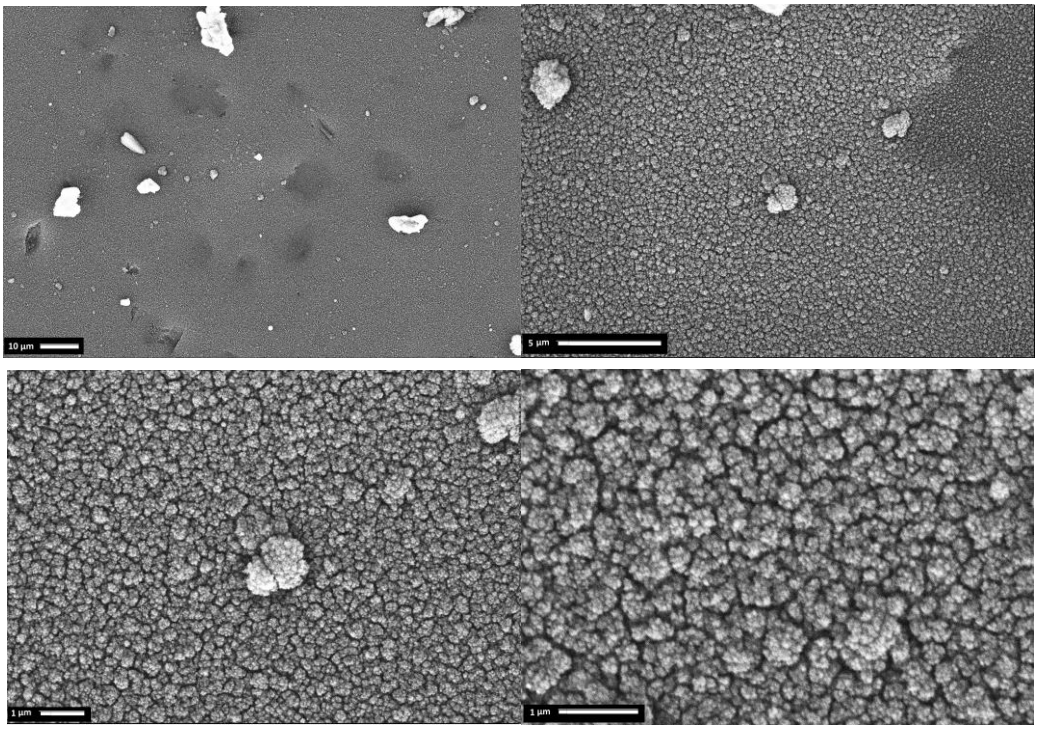

Figure 26: SEM top view of as deposited TiN at different magnification

It can be clearly seen the nanostructuration of the films characterized by the isolated round shaped tips of the nanotrees also shown by cross section SEM images reported in *Figure 27*.

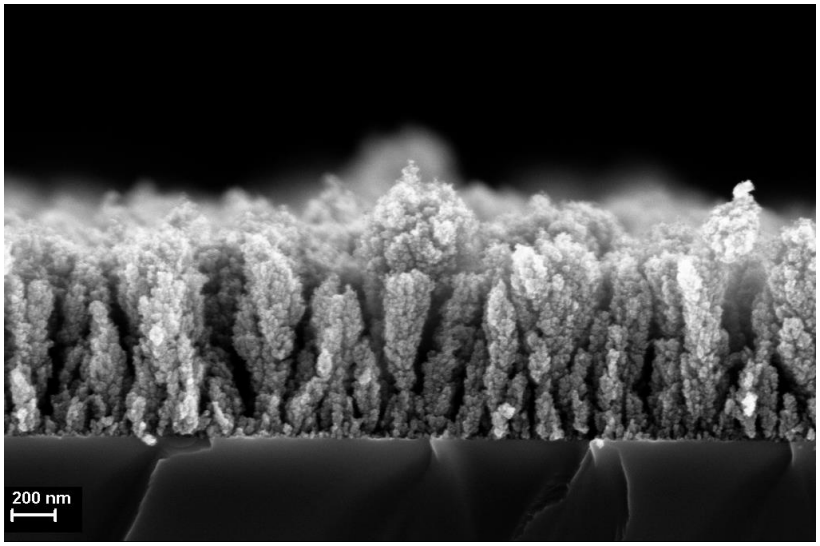

Figure 27: SEM cross-section for as deposited TiN

Cross section SEM performed on the TiN films deposited over silicon is also useful to verify the thin film thickness.

As also described by [53], the titanium nitride deposited at 60Pa as background pressure fulfill the requirements for an efficient catalyst support. In particular, SEM images easily show the high porosity and nanostructuration of the films while mechanical resistance upon manipulation is acceptable with no delamination of the films exposed to the atmosphere.

TiN nanotrees with a width ranging from 100 to 300 nm can be observed and a good uniformity can be achieved without any agglomeration effect. The characteristic hierarchical structure has a tree-like shape with a main direction and characterized by the presence of small branches that spread from the central body. The directionality of nanotrees is ideal for an active catalyst support since it combines a high surface area with the ability to easily extract the carriers in the vertical direction. The high aspect ratio (length/width) allows us to approximate the structure to quasi-1D structure particularly useful in enhancing the performance of a fuel cell electrode.

These preliminary observation obtained by SEM for as deposited TiN films are satisfactory for a porous, high-surface area support and cocatalyst. Nevertheless, the presence on the surface of large (>10 μm) droplets clearly seen at low magnifications is an unwanted phenomena due to problems during pulsed laser deposition caused by a non-uniformity of the ablating spot and consequently unavoidable.

3.1.3 Vacuum annealing

Vacuum annealing is the first process that as deposited TiN films undergoes after the deposition by PLD. The vacuum annealing is performed using a tubular furnace show in the figure below and characterized by the presence of a quartz tube able to reach temperature up to 1000°C surrounded by heating coils embedded in a thermal insulating matrix. The system is linked to a vacuum system made by a primary pump and a turbomolecular pump so high vacuum can be achieved inside the tube.

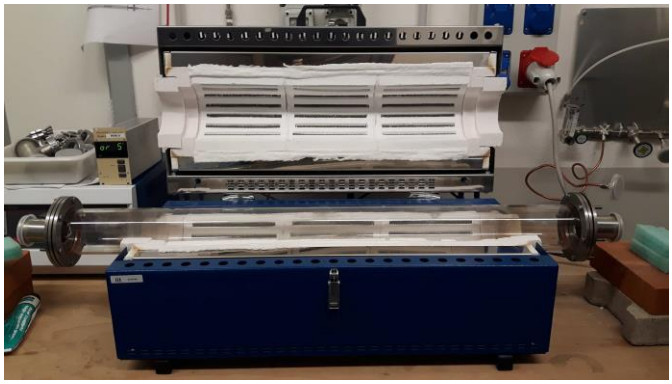

Figure 28: The tubular furnace used for vacuum annealing

The main problem associated with the described set up is the severe carbon contamination of the quartz tube followed by an unwanted carbon contamination of the annealed samples. In order to avoid this problem, a homemade set up is used and consist of an inner chamber of stainless steel AISI 316 connected to the vacuum system able to provide a clean and not contaminated atmosphere during the annealing process.

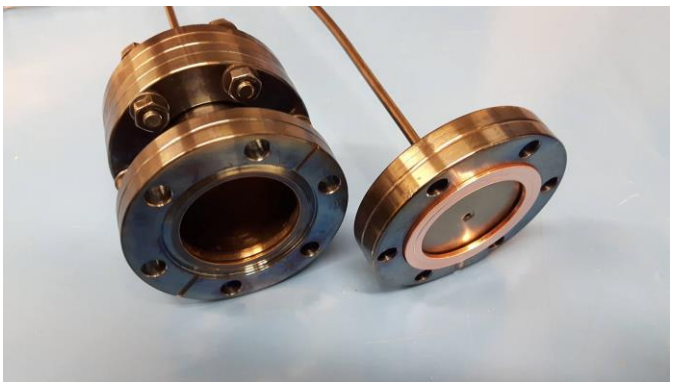

Figure 29: AISI 316 inner chamber used to protect samples from contamination during vacuum annealing

Vacuum annealing parameters

Before annealing, the chamber has to be evacuated to a vacuum level of $3.0x10^{-3}$ Pa using the pumping system aforementioned.

The annealing is carried out setting the temperature to 500°C and the dwelling time to 4 hours. Careful attention must be paid to the ramping velocity setting a value of 4°C/min for the heating ramp and a value of 1°C/min for the cooling ramp in order to favor the crystallinity and avoid thermal shock of the substrates. As described in section 2.1.2, different types of substrate has been used for PLD deposition and consequently the choice of the maximum temperature must take into consideration the response of the different materials to the annealing process. In particular, glass and FTO substrate have the more restrictive parameters since their operative temperature is maximum 500°C and an overheating can cause the substrate to melt. Glassy carbon instead does not suffer from these problems but at the same time, to avoid carbon self-contamination of the samples associated to a damage of the GC substrate, it must be annealed carefully.

SEM images of the vacuum annealed TiN samples are shown below

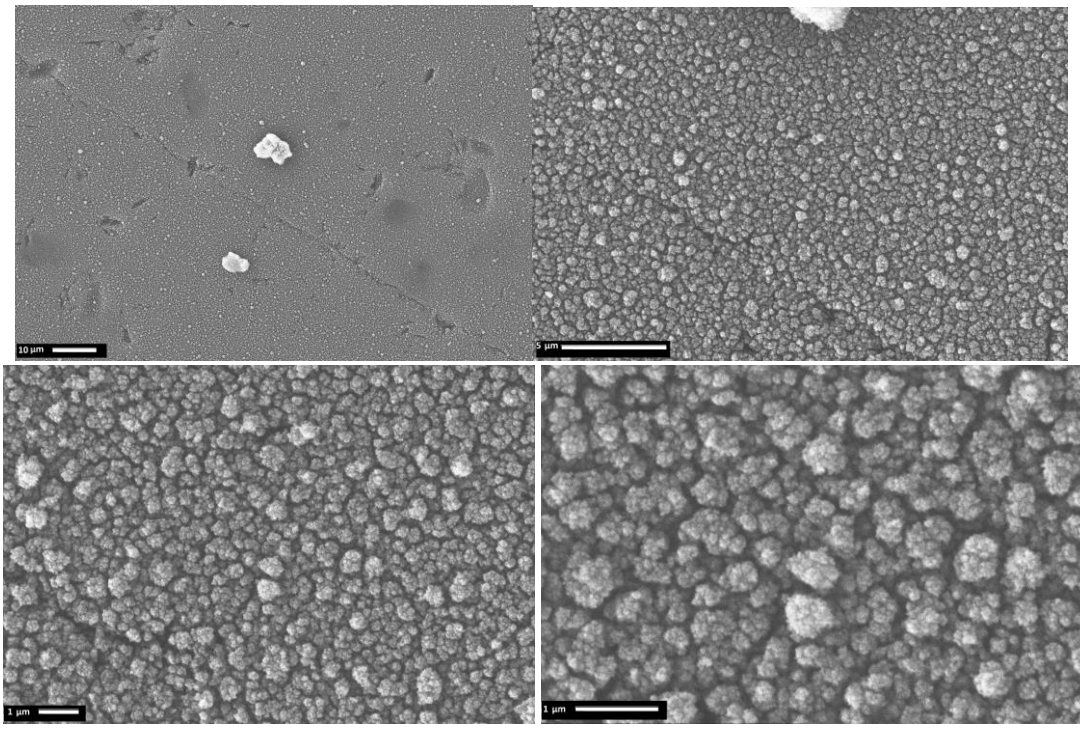

Figure 30: SEM top view of vacuum annealed TiN at different magnification

No carbon contamination can be seen after the vacuum annealing of the TiN films confirming the fact that the AISI 316 inner chamber is able to protect from contamination and grant a clean atmosphere during the process. TiN large droplets are still present after the annealing and could not be eliminated from the surface.

After the vacuum annealing, the TiN samples are ready to be oxidized at different temperatures in order to obtain titanium oxynitride thin films.

3.1.4 Oxidation of TiN

Air annealing has been chosen as the method to oxidize the titanium nitride thin films. As described in literature [33], exposing TiN to air at high temperature is an effective method to oxidize the material in order to create a titanium oxynitride phase able to photocatalyze the methanol oxidation reaction. The extent of oxidation can be finely controlled by choosing appropriate annealing parameters and the oxidation is caused by a substitutive process between oxygen atoms and nitrogen atoms in the TiN lattice forming a progressive titanium oxynitride layer on its surface (TiON) up to a complete oxidation to titanium oxide.

In this thesis work, attention has been paid to the dwelling temperature and the dwelling time since a correct choice of this parameters can lead to different oxidation extent of the material and consequently different properties.

Measurements at constant annealing time

A preliminary annealing test has been carried out by setting the annealing time to 1 hour and varying the annealing temperature. Heating and cooling velocities has been set to 4°C/min while the investigated temperatures ranged from 100°C up to 500°C with a variation of 100°C from each sample. The preliminary annealing were carried out on samples deposited over glass substrates in order to further analyze them using UV-Vis spectroscopy.

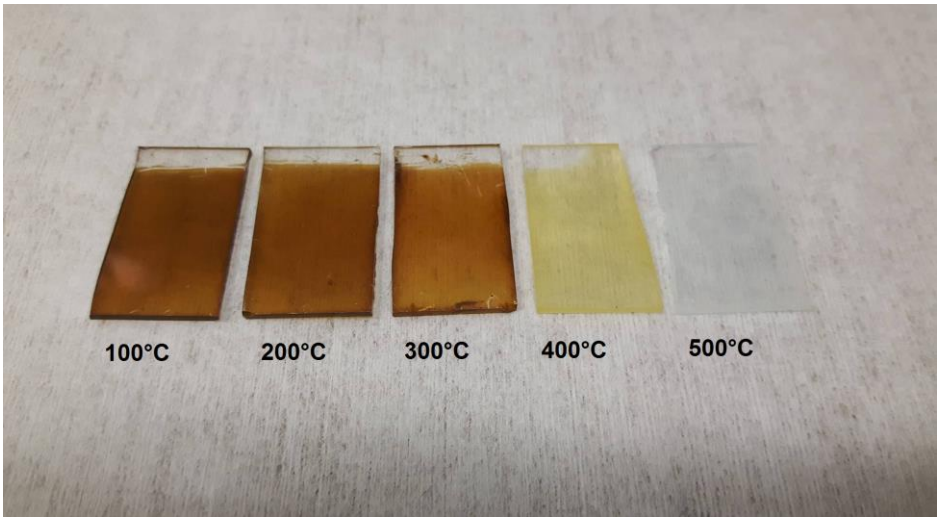

Figure 31: TiN oxidized at different temperatures for 1 hour

It can be clearly seen that the extent of oxidation modify the optical properties of the different TiON samples by changing the colors of the deposited films starting from a brown color for the vacuum annealed sample , moving to a pale yellow for the 400°C air annealed and reaching a white color for the 500°C one.

UV-vis spectroscopy plays a fundamental role for the study of the optical properties of the TiON films and the result is shown below:

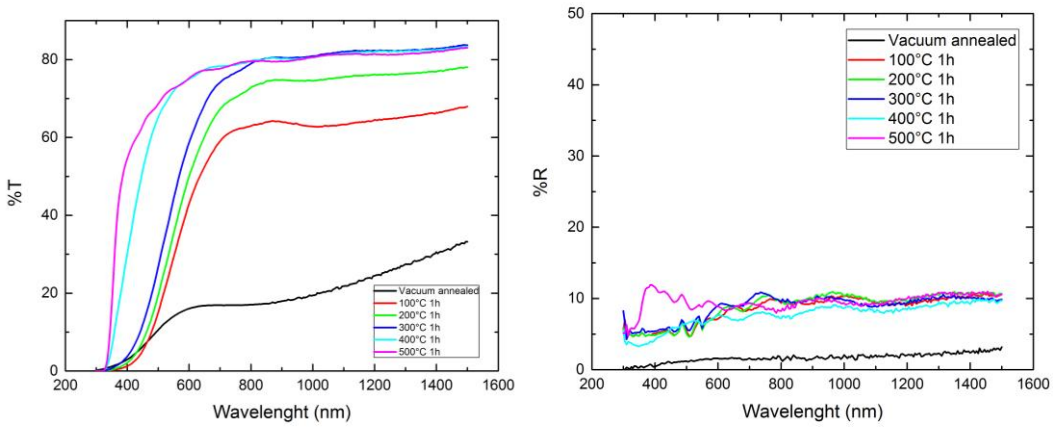

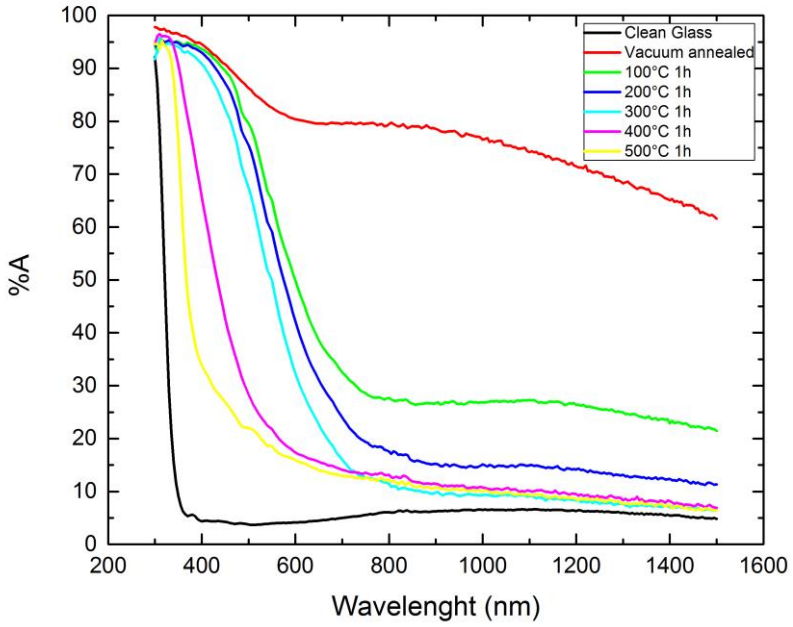

Figure 32: Transmittance, reflectance and absorptance spectra of TiON oxidized at different temperatures for 1 hour. Clean glass absorption is also shown as reference

Transmittance and reflectance measurement are performed by using a Perkin Elmer Lambda 1050 UV/Vis spectrophotometer. The spectral range analyzed (in wavelength) is between 1500 to 300 nm with a scan resolution of 5 nm. After the measurement of transmittance and reflectance with the use of an integrating sphere, the absorptance is obtained using the formula:

$$A(\%) = 100 - T(\%) - R(\%) \tag{3.1.1}$$

Where T is the transmittance(%) and R is the reflectance(%) of the sample. As shown in the graph, also the absorption spectrum of clean glass is shown in order to provide a reference of the substrate over which the thin film is deposited.

The main absorption edge shifts to lower wavelength with the increasing oxidation temperature and in particular, for the TiN oxidized at 500°C the behavior is similar to a pure TiO_2.

After the evaluation of the absorption of the TiON films, Tauc plots have been performed knowing the optical path in order to calculate the absorption coefficient. As already describe in section 2.5.2, this plots are

performed using the photon energy on the x-axis and $(\alpha h\nu)^{1/r}$ on the y-axis and, being TiO_2 an indirect semiconductor, the value of r is equal to 2 (indirect allowed transitions)

Tauc plots of the analyzed samples are shown in *Figure 33*

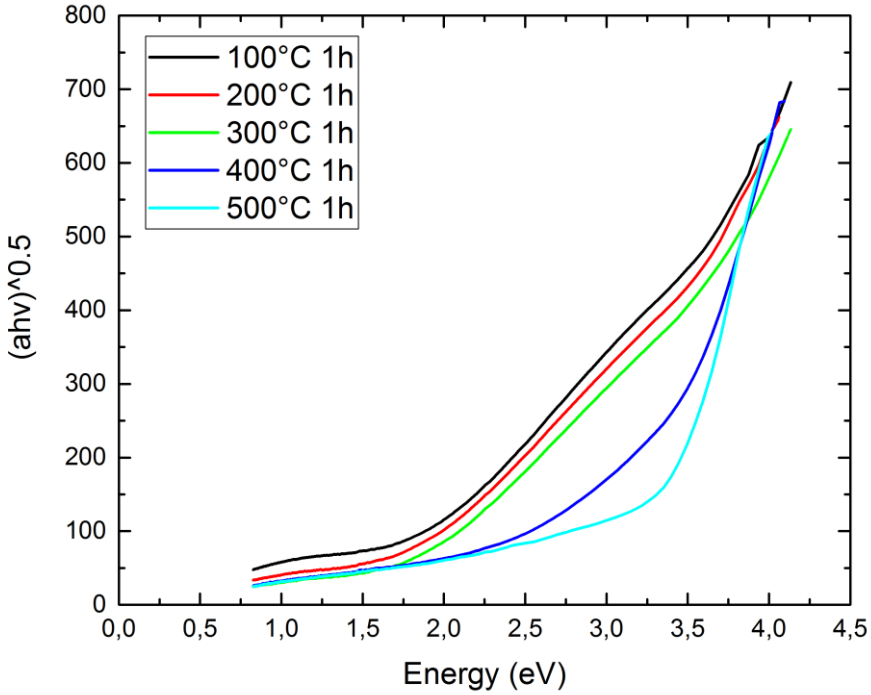

Figure 33: Tauc plots of TiON samples

The estimation of the band gap of the material is directly done by extrapolating the linear region to the abscissa. As for the absorption plots, also in this case a definite trend is shown with the band gap of the TiON samples increasing as the oxidizing temperature increase. For the sample oxidized at 500°C a value of the bandgap of 3.2 eV is measured confirming the fact that the material is completely oxidized to titanium oxide.

Measurements at constant temperature

In order to study the effect of the annealing time on the oxidation degree of the TiON thin films, measurement at constant temperature has been

carried out. In particular, temperature has been set to the value of 300°C and the annealing time has been variated from 1 hour to 8 hours.

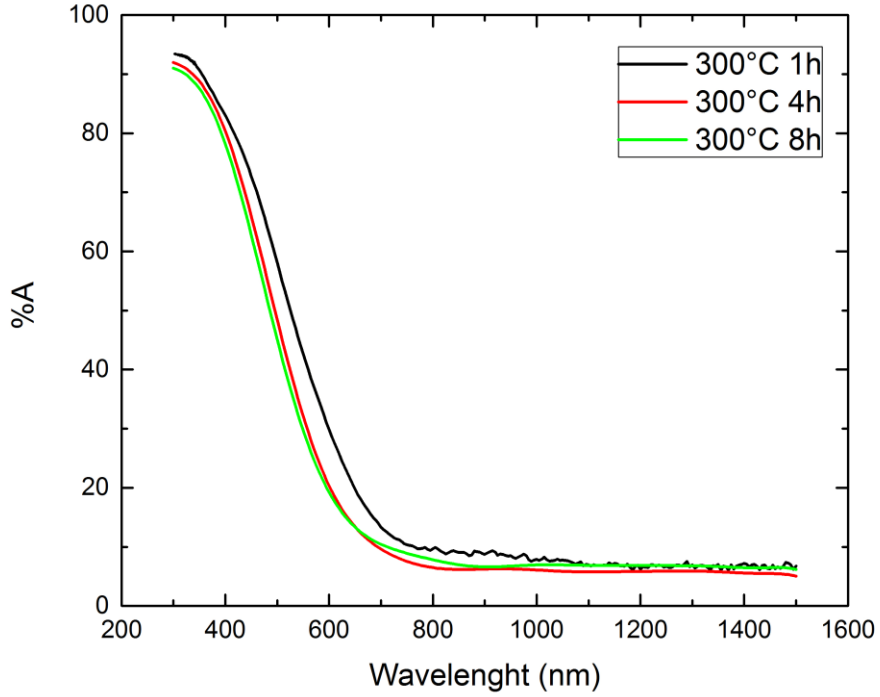

Figure 34: Absorption spectra of TiON oxidized at constant temperature (300°C) for different times

The absorbance spectra of the different films clearly show a correlation between annealing time with the absorption edge: with the increasing of the annealing time there is a shift to lower wavelength of the absorption edge witnessing the increased oxide extent of the material.

The role of the annealing time is predictably similar to that of the temperature both influencing the oxidation degree of the material but we can see a saturation effect with the oxidation at constant temperature probably associated to achieving equilibrium. Since the variation of the absorption edge is more pronounced in the case of annealing at different temperatures, the annealing time has been set to 1 hour without other changes.

From the preliminary results and following also the literature [33], the oxidation temperature range has been restricted to the values 300°C – 400°C. In particular, also the intermediate temperature 350°C has been investigated. This choice of temperature range has been made since we want to obtain an N-doped TiO_2 with a small band gap but at the same time able to generate energetic holes able to catalyze the methanol

reactions. TiO_2 for this reason is the ideal material since it can produce highly energetic holes due to its deep valence band but the introduction of N states above the valence band minimum with the N-doping even if it decrease the band gap, it will also reduce their energy.

In order to favor the crystallinity of the oxidized samples, the cooling velocity has been reduced to 1°C/min and the results are shown in *Figure 35*

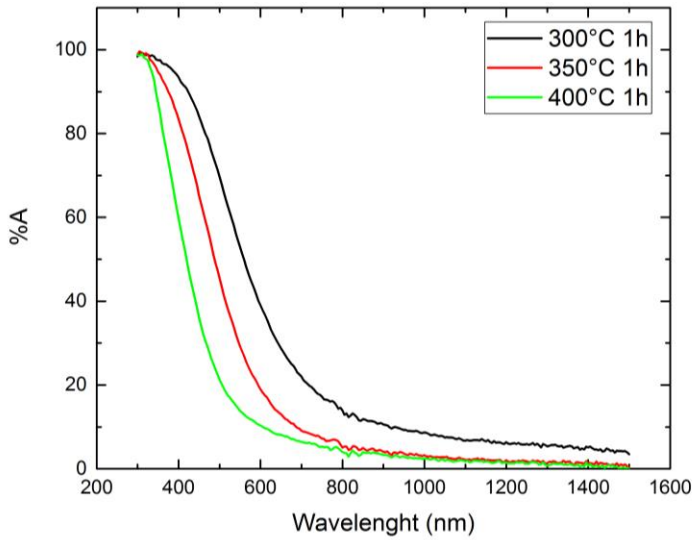

Figure 35: Absroption spectra of TiON for the three chosen temperatures

Predictably the behavior of the TiN annealed at 350°C is intermediate between the 300 and 400°C samples. Tauc plots are also reported.

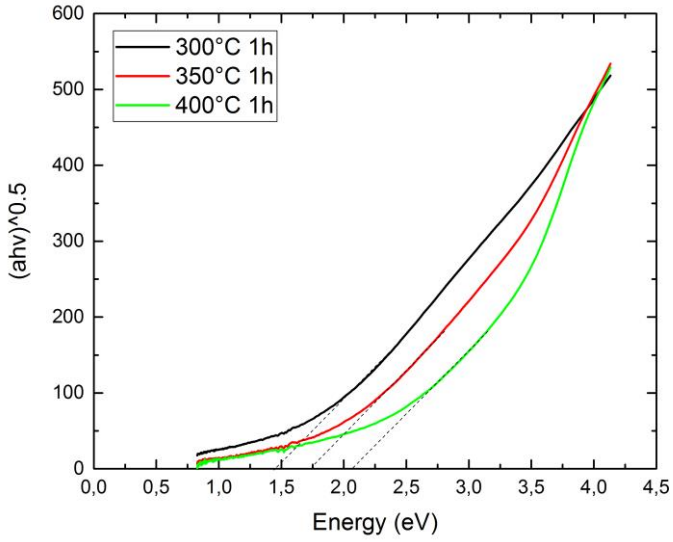

Figure 36: Tauc plots of TiON for the three chosen temperatures. Extrapolation of the band gap is shown

Extrapolation of the linear region in order to obtain the estimation of the band gap has been performed and the value obtained are 1.49 eV for the 300°C oxidized sample, 1.74 eV for the 350°C sample and 2.06 eV for the 400°C.

Being the band gaps estimated in the range 1.5 – 2 eV, make the chosen materials promising for photocatalytic application under visible light illumination and confirm the effective bang gap engineering of the titanium oxynitride thin films. As described by the Shockley–Queisser limit [54], the maximum efficiency that a photocatalytic device can obtain is dependent on the band gap and is maximum for a material with a band gap of 1.34 eV value really close to the analyzed band gap obtained for TiON in this thesis work.

Morphological analysis of oxidized samples at different temperatures has been performed by SEM measurements in order to study the modification of the structure after the air annealing step.

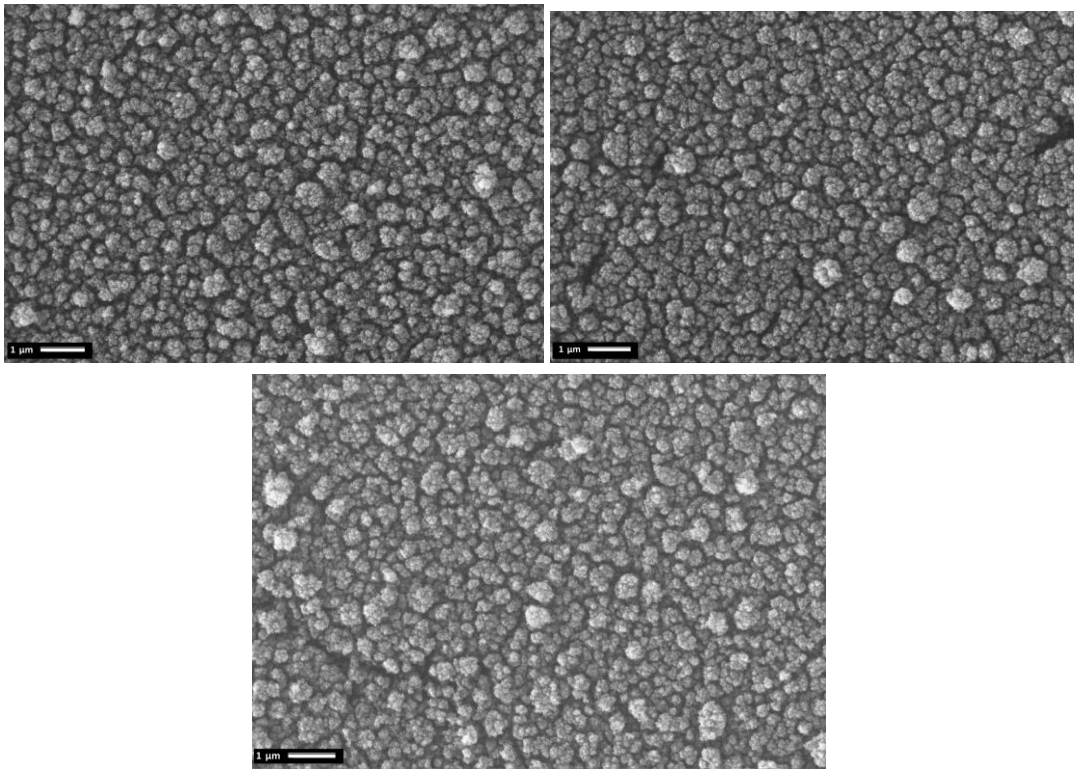

Figure 37: SEM top view of TiON300°C (top left), TiON350°C (top right) and TiON400°C at the same magnification

Neither modification of the nanostructure nor a variation of the size of the nanotrees is present among different oxidized samples and no agglomeration effects show up since the tips of the nanotrees are well

defined. We can therefore assume that the surface area of the TiON samples is equal despite their different oxidation degree.

3.1.5 XRD measurements of TiON

After the oxidation of the TiN thin films, the samples deposited over glass substrate are analyzed by X-ray diffraction in order to study the degree of crystallinity and the modifications of the crystal structure after the oxidation step.

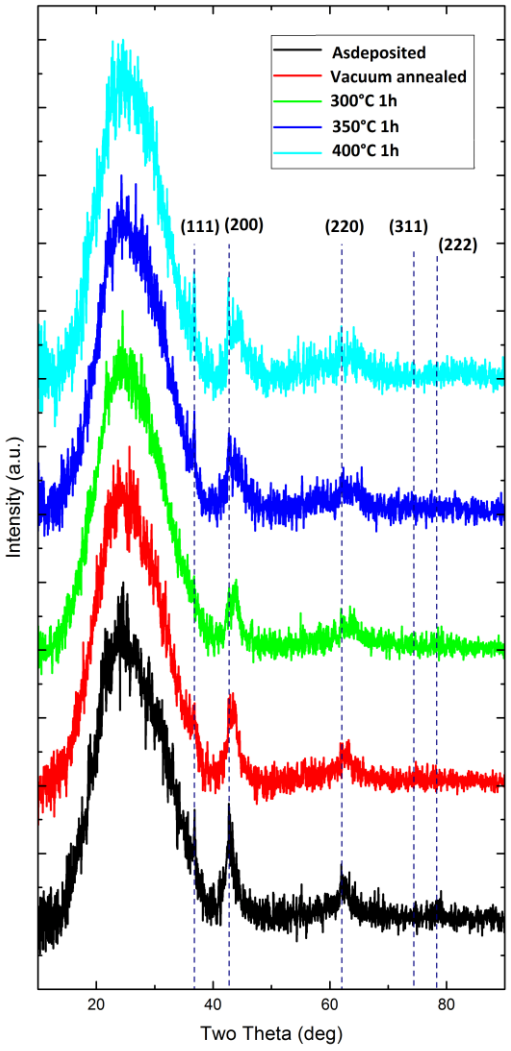

Figure 38: XRD spectra of different TiON samples. Stoichiometric TiN reference peaks are also shown

In the XRD spectra, the TiN reference peaks are plotted while the broad band peaked at 25° is characteristic of the glass substrate. The presence of bands instead of sharp peaks witnesses the fact that the investigated materials are not crystalline even after the annealing. The mean crystal size of the film has been evaluated using the Scherrer equation

$$\tau = \frac{K\lambda}{\beta \cos\theta} \qquad (3.1.1)$$

Where τ is the mean crystal size, K is the shape factor (dimensionless), λ is the wavelength of the x-ray, β is the FWHM and θ is the Bragg angle (degrees). Analyzing the peak corresponding to TiN(200), the material result to be nanocrystalline with a grain size in the order of 10 nm.

In the table below, the peak position of stoichiometric TiN is reported with the associated TiN planes.

TiN peaks	Stoichiometric TiN [37]
	2 theta (θ)
111	36.66°
200	42.59°
220	61.81°
311	74.07°
222	77.96°

Table 2: Stoichiometric TiN peaks position

Respect to the stoichiometric TiN, the TiON samples analyzed in this work show a shift in the peak positions to higher theta angles. In particular, the most evident shift is recorder for the peak corresponding to TiN(200). Passing from the as deposited TiN sample to the vacuum annealed sample, the shift from 42.65° to 42.8°can be attributed to the building up of internal stresses inside the material.

The shift of the TiN(200) peak is more pronounced for the TiON samples and increase progressively with the oxidizing temperature with values of 43° for the 300°C , 43,3° for the 350°C and 43.5° for the 400°C sample.

As described by [37], the shift to higher angles of a TiN peak can be attributed to the oxynitride phase present on the material. In particular, the Vegard's rule states that the lattice constant of TiON should lie

between the two values of TiN and TiO lattice constant since TiON can be seen as a solid solution of this two constituent both with a NaCl lattice structure.

As described by [55], the analysis of TiON films is complicated because the TiN and TiO peaks are very close so only for highly crystalline films they can be seen separately while in the shown graphs, the spectra appears to be noisy with broad bands with no distinction.

For this reasons, XRD result to be a non-effective methods for substrate analysis.

3.2 Electrodeposition of the catalyst

3.2.1 Pulsed electrodeposition parameters

After the fabrication of the titanium oxynitride films, a fundamental step in the catalyst preparation is the deposition of the platinum catalyst. Electrodeposition is the chosen method as consequence of the study done by [53] on effective methods for catalyst dispersion over TiN substrates. In particular, using puled electrodeposition and accurately tuning the parameters, we can achieve a good coverage of Pt nanoparticles over the TiON substrates. The choice of the pulsed electrodeposition is in galvanostatic mode in order to impose a given current pulse and consequently a known mass of Pt deposited. In a potentiostatic electrodeposition instead, the resulting current is linked to the voltage applied by the electrode resistance and since the electrode material change depending on the extent of oxidation of the different TiON substrates, the current will be different.

Since Faraday's law affirms that there is a direct proportionality between the mass deposited and the total charge that is transferred to an electrode, a fundamental parameter to be considered is the total charge density delivered to the electrode (in C/cm^2). A study on the effect of different charge density for Pt electrodeposition over TiN has been already carried out by [53] and it's not in the objective of this work. For this reason, the total charge density has been chosen to 10 C/cm^2 and this value has not been changed. The other deposition parameters were optimized by the previous work and are here reported:

- Current on-time (t_{on}) of 50 ms
- Current off-time (t_{off}) of 500 ms
- Current density of 50 mA/cm^2 for each pulse
- Total Charge density of 10 C/cm^2 corresponding to a value of 4000 pulses with the parameters described above

The pulsed current parameters strongly affect the crystallization of the deposited metal particles that occurs by incorporation of adatoms in crystal lattice. Two different mechanisms can occur as described by [46]:

- **Formation of new crystals**: the formation of new metallic crystals will be favored by an high adatom population and by a low surface diffusion of these species and this conditions can be achieved by an high value of current density per pulse in a short period (t_{ON})
- **Building up of old crystals**: growth of old crystal instead is favored by an high surface diffusion and an higher pulse time

With an excessive increase of the on-time pulse, the particles are able to reorganize and the formation of metal clusters cannot be avoided with consequent reduction of the catalytic area. The optimization of the Pt electrodeposition recipe is done in order to achieve Pt nanoparticles with a dimension lower than 10 nm.

The electrodeposition process is carried out in an electrochemical cell with the following experimental set up:

- Working electrode: TiON over glassy carbon substrate
- Counter electrode: Pt mesh
- Reference electrode: Saturated calomel electrode (SCE, E_o = +0,244 vs RHE)
- Electrolyte: the electrolyte is a liquid solution of the Pt precursor $H_2PtCl_6 \cdot xH_2O$ with a concentration of 1mM and H_2SO_4 0.5 M.

  The solution is prepared by mixing an appropriate amount of solid Pt precursor (Pt-salt) to the sulphuric acid-water solution.
- Bubbling system: The cell is fluxed with nitrogen through a glass frit to stir the solution during the electrodeposition process and to provide an inert atmosphere while the exhaust gas are expelled under the fume hood

In order to precisely control the exposed surface area of the TiON over glassy carbon samples, a masking process must be performed and in the specific case, a PTFE tape or a Vinyl tape is used. Both the tapes have an extremely high hydrophobicity and a good resistance in acidic environment to avoid degradation and contamination of the samples.

A preliminary way to test the Pt amount after the pulsed electrodeposition process was to measure the weight of the sample before and after the deposition process by a microbalance with a resolution in the order of micrograms. Before measuring, the samples were dried but

infiltration of solution under the masking tape cannot be avoided and consequently invalidate the measurement. This method was quickly discarded in favor of more precise measurements. Up to now the evaluation of the catalytic loading is still uncertain but a future collaboration with another research group would provide a correct measurement thanks to ICP mass spectrometry.

3.2.2 XRD OF TiN/Pt

After the electrodeposition, XRD measurements are carried out in order to investigate the changes introduced by this fabrication step on the material. An XRD graph of TiN after electrodeposition of Pt nanoparticles is shown in *Figure 39*.

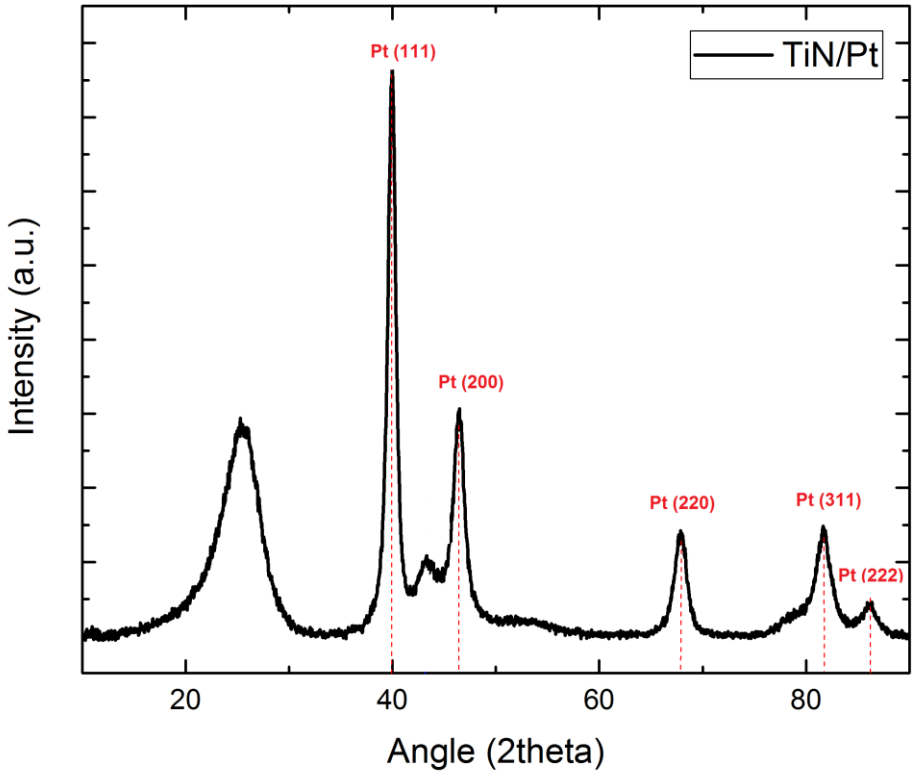

Figure 39: XRD spectra of Pt electrodeposited TiN. Pt peaks are reported

Characteristic of the analyzed spectra is the presence of sharp peaks associated to the different platinum planes as shown in the graph while the peak centered at 26,5° is attributable to a graphite peak since the

analyzed catalyst was deposited over a glassy carbon substrate instead of a glass substrate.

The fact that the platinum peaks are sharp is an indication of the crystallinity of the deposited nanoparticles by electrodeposition and using the Scherrer equation we can estimate a mean dimension of 9.8 nm.

3.3 Oxidation and electrodeposition process

To study the effect of the different oxidation extent of the material on the electrodeposition process, two main experiments have been carried out: the electrodeposition has been done on pre oxidized sample(TiON) and on pure TiN samples. In particular, the fabrication path was the following:

- **Oxidation of the TiN samples and subsequent ED**: in this experiment, the TiN substrate is oxidized at the three chosen temperature 300, 350 and 400°C and afterward the Pt catalyst is deposited over it by pulsed electrodeposition. In this situation, the ED is carried out with the hypothesis that the substrate partially oxidized is less conductive respect to a pure TiN film. Since the deposition happen after the oxidation of the substrate, Pt can be deposited only over TiON layer and not over TiN.

- **ED over TiN and subsequent oxidation of TiN/Pt**: in this experiment, the ED is performed over a pure TiN sample with the hypothesis that the not oxidized substrates should show an higher conductivity. The preliminary hypothesis in this situation is that Pt will deposit over TiN nanotrees and the subsequent oxidation will oxide the surface to TiON while the not exposed film covered by Pt nanoparticles will be less or completely not oxidized. In this case, Pt nanoparticles would be surrounded by TiON while contacting with the non oxidized TiN.

  Different considerations must be taken into account for this kind of fabrication path: since the electrodeposition step happens before the thermal oxidation, the masking tape must be removed and the substrate must be accurately cleaned before proceeding with the oxidation in order to avoid unwanted contamination during the annealing. Another important consideration is that the TiN/Pt catalyst is put inside the furnace after the electrodeposition so Pt itself can be oxidized during the process.

  A schematic representation of the full fabrication path is shown in *Figure 40*

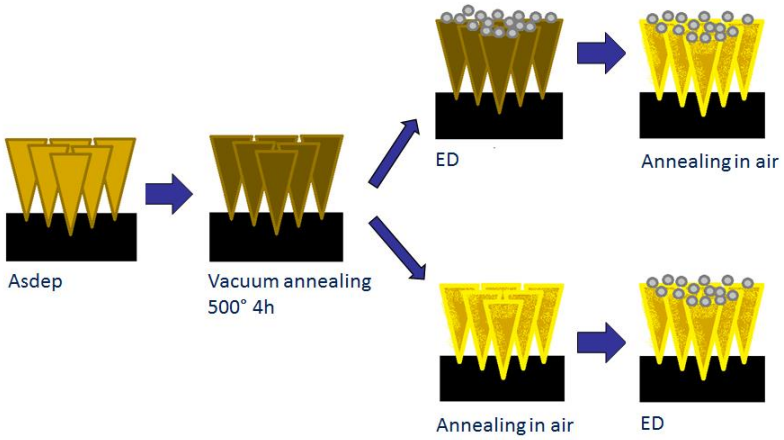

Figure 40: Fabrication path scheme of the final TiON/Pt devices. The two fabrication routes are shown

As consequence of the electrodeposition, structural modification of the TiON substrate has been investigated by SEM images

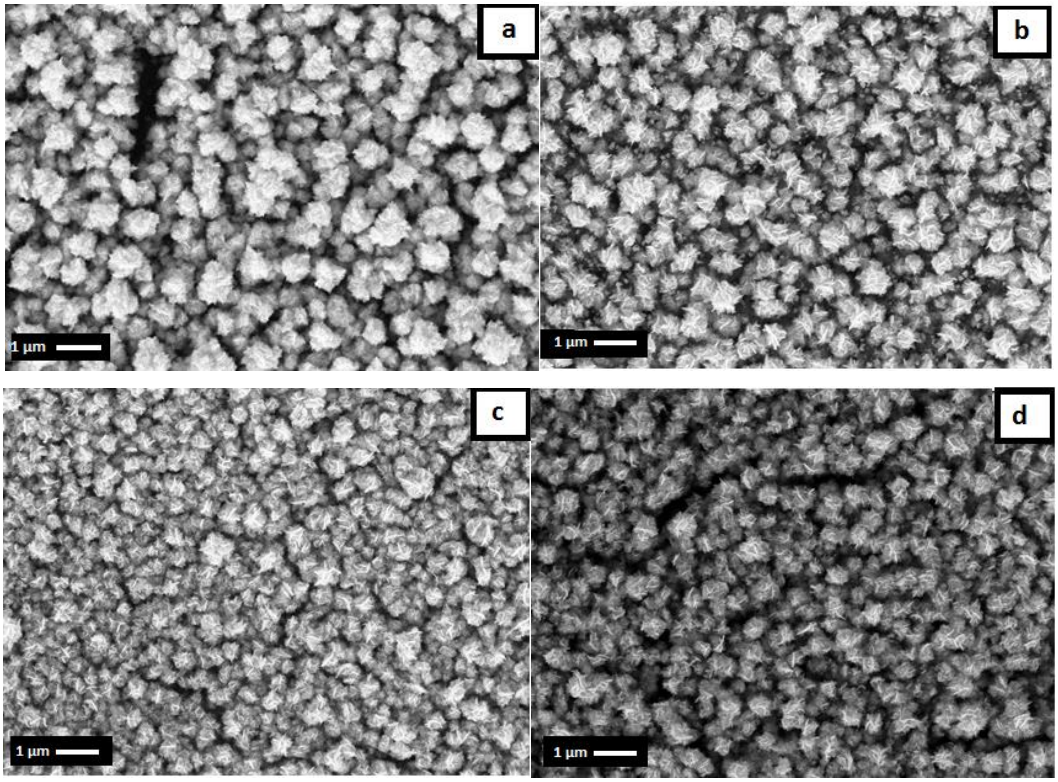

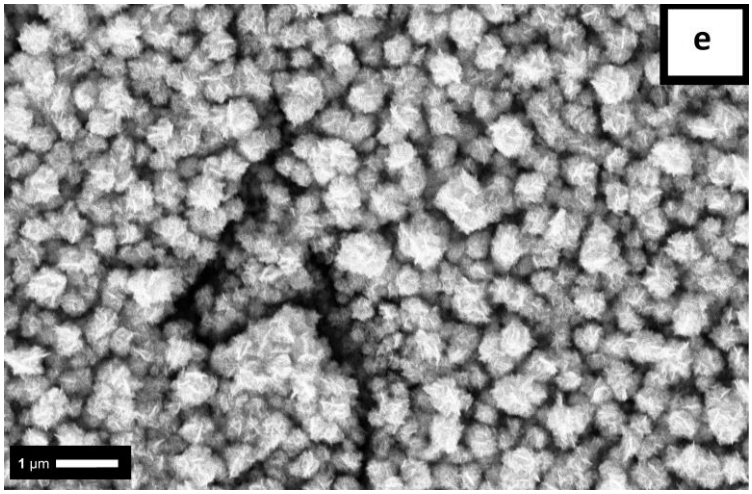

Figure 41: SEM top view of the lamellae structure resulting after the ED process. (a) E/O 400, (b) O/E 400, (c) E/O 300, (d) O/E 300, (e) O/E 350

Characteristic of all samples is the presence of a lamellar structure on top of the nanotrees with a directional growth. This modification takes place only during the electrodeposition of the catalyst and does not depend on the degree of oxidation of the sample or on the choice of the fabrication path. The explanation of the phenomenon is still unclear but probably associated to a modification caused by the electric field during the ED caused by a tip effect on top of the nanostructures. Platinum nanoparticles on this lamellar structure and can be shown only with higher magnification as shown by [53].

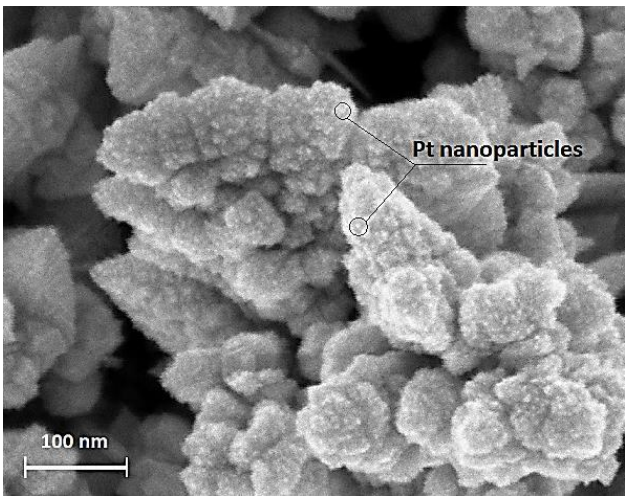

Figure 42: SEM top images at higher magnification of the lamellae structure. Pt nanoparticles are shown. From [53]

The modification of the structure and deposition of the nanoparticles only on top of the nanotrees, introduce a strong limitation of the electrodeposition as a catalyst deposition method. In particular, platinum nanoparticles can't effectively be dispersed over the entire TiON surface area not fully exploiting the nanostructuration of the film.

This limitation cannot be avoided with the chosen catalyst deposition method while other techniques such as wet techniques [50] used in literature could solve this problems since in that case no issues linked to the electric field are present.

Chapter IV

Electrochemical characterization of the catalyst

Introduction

In this chapter, particular attention will be given to the electrochemical and photoelectrochemical response of the fabricated TiON/Pt catalyst under both potentiostatic and potentiodynamic tests. The aim of this thesis work is to provide a description of all the phenomena that occur when the device is in contact with different electrolytes. In particular, the TiON/Pt will be tested both in acidic solutions with the presence or the absence of methanol to study both the stability of the catalyst in harsh environments and also its activity toward methanol oxidation reaction.

- The titanium oxynitride substrate obtained by different oxidation of titanium nitride is first analyzed in acid solutions to study its behavior under many potential cycles to verify its stability under potential cycling fatigue.

- TiON/Pt is then analyzed in acid environment by cyclic voltammetry to verify the catalytic activity toward hydrogen evolution synonym of the presence of Pt on top of the TiON nanostructures and consequently evaluate the electrochemical surface area.

- Cyclic voltammetry in acid electrolyte is performed both for the pre-oxidized and electrodeposited samples (O/E) and also for the electrodeposited and post-oxidized samples (E/O) to study the behavior resulting from different fabrication paths.

- Cyclic voltammetry in an acidic solution of methanol is a crucial step to verify the catalytic ability of TiON/Pt toward the oxidation of methanol simulating the conditions of a DMFC device.

- Further analysis of the better oxidation ability of a TiON/Pt catalyst are done by chronoamperometric experiments in methanol solution

- Finally the photocatalytic effect is also demonstrated by performing the aforementioned measurements under chop illumination provided by a solar simulator to study the behavior under an hypothetical solar radiation illumination.

The first step in the electrochemical analysis must be done on the bare TiON substrate in order to show its behavior in harsh environments since stability is a key parameter for a good catalyst.

4.1 Stability of Ti-based support

After the fabrication and physical characterization of the nanostructured TiON as a high surface area catalyst with a high directionality useful for anode support in DMFCs, the electrochemical study of the scaffold must be performed. The particular morphology of the scaffold is not the only key parameter that a support material must fulfil but also the long term stability in harsh environment must be achieved.
For this reason, electrochemical testing of the TiON thin films is performed following the described procedure:
Cyclic voltammetry in 0.5 M H_2SO_4 solution are carried out in order to verify the stability of the material. CV cycles, from 0 V to 1,3 V (vs RHE) with a scan rate of 150 mV/s, are performed plotting the behavior every 200 cycles up to 1000 cycles corresponding to more than two hour testing. The choice of the potential range is done in order to study the behavior in a wide range of potentials. The stability of the material should be witnessed by the presence of no peaks in the range of potential scanned since a current peak is synonym of a reaction undergoing at a given potential.
The electrochemical setup used for these experiments is briefly described and is made of:

- 3 electrode configuration cell: TiON (WE), Pt mesh (CE), Ag/AgCl (RE)
- Electrolyte: 0.5 M H_2SO_4 solution (pH=0.3)
- Bubbling system: glass frit insufflating nitrogen inside the cell in order to provide an inert atmosphere eliminating the oxygen.

The electrochemical stability test is performed on the TiON samples oxidized at the two extreme temperatures 300, 400°C for 1 hour.

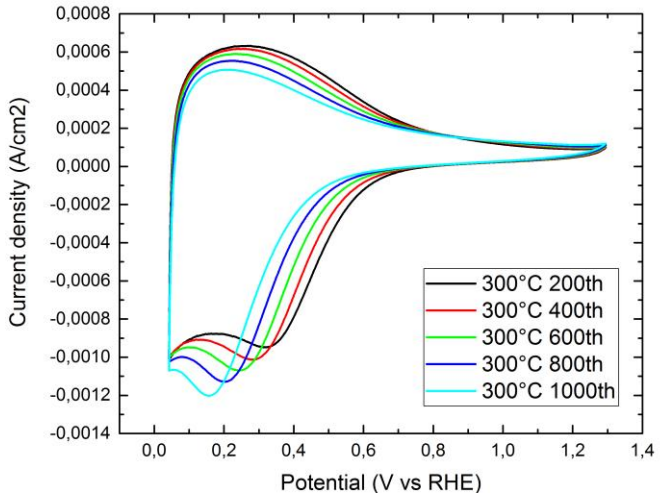

Figure 43: Cyclic voltammetry in 0.5M H_2SO_4 . Stability test of TiON300

Starting with the 300°C annealed sample (TiON300) we can clearly see the presence of a wide peak at 0.2 V vs RHE decreasing in intensity with the increase of number of cycles. Associated to the oxidation peak in the forward scan, the reduction peak in the backward scan is present and it shift from 0.35 V to 0.15V with the increasing number of scan. As also described by [53], the presence of this peak also on TiN is not attributed to the evolution of hydrogen following the reaction $H_2 \rightarrow 1/2O_2 + 2H^+$ and is still unclear.

The TiON oxidized at 300°C will present on its surface a mixture of different sub stoichiometric oxides resulting from the not complete oxidation of the material and with a different behavior in the harsh environment. The presence of the peak at 0.20V vs RHE can be attributed to a slow oxidation of the already not oxidized material with the formation of stable oxides (TiO_xN_y) that reduce further oxidation of the underneath remaining TiN. This hypothesis can also explain the fact that the oxidation peak decrease in intensity with the increasing number of cycles.

In the range of potentials 0.6 – 1.3 V, no peaks can be seen witnessing the stability of the material in this potential range since no reactions occur.

After the CV fatigue test, the TiON300 is analyzed by SEM images

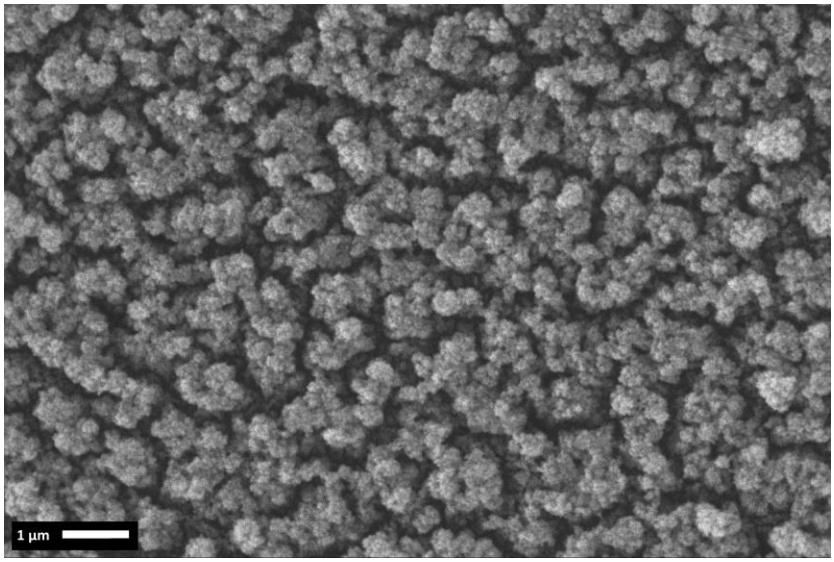

Figure 44: SEM top view of TiON300 after the stability test

The damage caused by the extensive potential cycling is evident on the nanostructure with an agglomeration effect of the nanotrees now separated by canyons inside the films. Despite the variation of the morphology with associated a reduction of the exposed area, the TiON300 thin film nanostructuration is still present and demonstrate the ability of this material to resist in a harsh environment for long time under potential cycling. The hypothesis of stable oxidation of the material seems to be confirmed also by these results.
The same electrochemical test is performed for TiON400 and the cyclic voltammetry results are shown below.

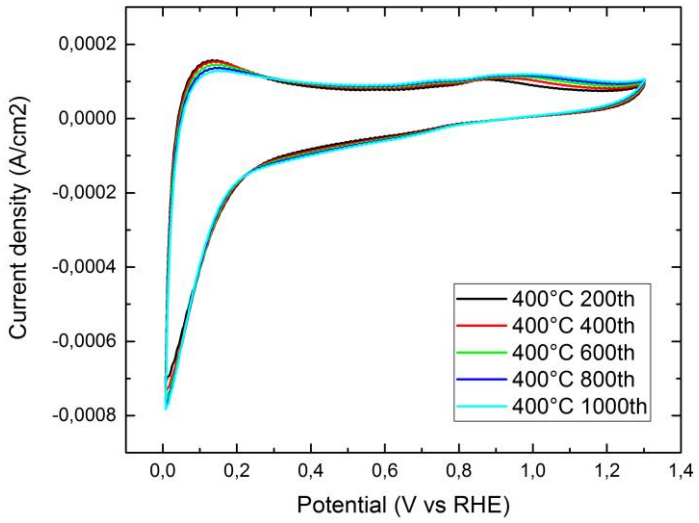

Figure 45: Cyclic voltammetry in 0.5M H_2SO_4 . Stability test of TiON400

Differently from TiON300, TiON400 presents a small peak at high potentials probably associated to the formation of hydroxides. As suggested by [37], in the range 1.0 -1.5V, TiN can undergoes oxidation with formation of unstable hydroxides following the reaction:

$$TiN + 3H_2O \rightarrow Ti(OH)_3 + N_2 + 3H^+ + 3e^-. \quad (4.1.1)$$

Nevertheless the peak intensity is very low probably because the formation of stable oxide after the air oxidation step at 400°C passivates the surface and prevents further reactions. After the intensive fatigue test of TiON400, also in this case, the nanostructure is still present.

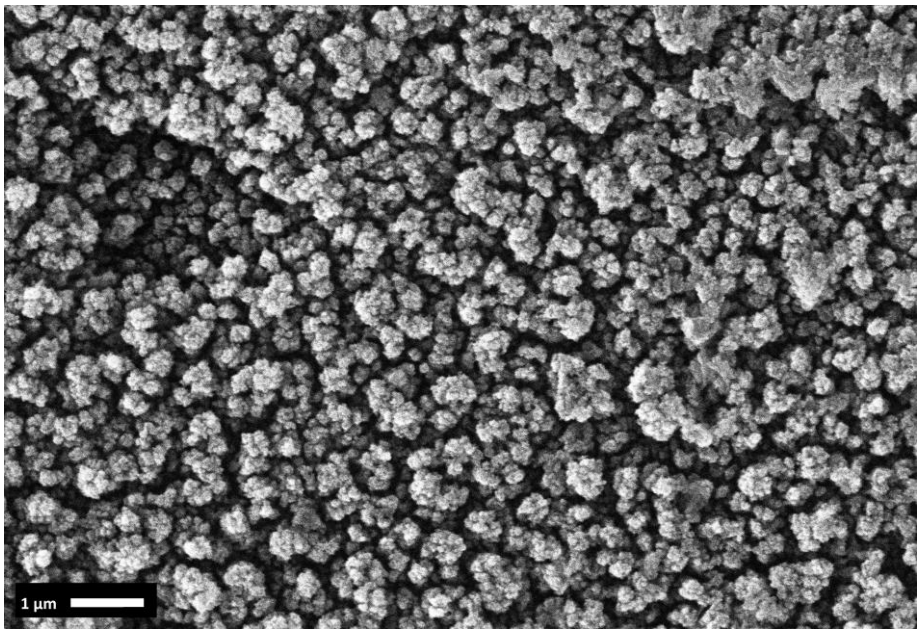

Figure 46: SEM top view of TiON400 after the stability test

The morphology variation of TiON400 is similar to that of TiON300 and an agglomeration effect of the nanostructure is evident. Instead of a uniform film, also in this case, "islands" of nanotrees are separated by canyons and deep channels.

It's important to remark that the stability test has been carried out only for single samples so it's hazardous to make some hypothesis with these results. In order to really understand the behavior of the material, a statistical study covering a large number of samples must be performed and will be addressed to future developments.

4.2 Testing of TiON/Pt in acid environment

4.2.1 Cyclic voltammetry analysis

After the evaluation of the behavior of the different TiON substrate in acid environment, cyclic voltammetry is performed to the TiON/Pt i.e. after the electrodeposition of the Pt catalyst over the substrate. As already mentioned, two different fabrication path has been employed in this work that is the electrodeposition over TiN and oxidation of the catalyst (E/O) or the oxidation of TiN and electrodeposition over TiON (O/E). In this chapter will be discuss the behavior of these two differently produced materials in acid environment (0.5 M H_2SO_4) under cycled potential scan between 0 – 1.3 V vs RHE. In particular, the followed protocol is:

- 10 cycles of CV with a scan rate of 150 mV/s, to activate the catalyst after the deposition process
- 50 cycles with a scan rate of 150 mV/s followed by other 50 cycles in order to test the behavior of the material after a consistent number of cycles

The total number of 110 cycles is a good choice for testing the material in stable conditions after the activation and without degradation happening at prolonged testing times.
In order to understand the behavior of the material, the results of CV for the sample (E/O)TiON300 are used as an example to describe all the phenomena that occurs during potential cycling of a Pt based catalyst in the potential range 0 – 1.3V vs RHE.

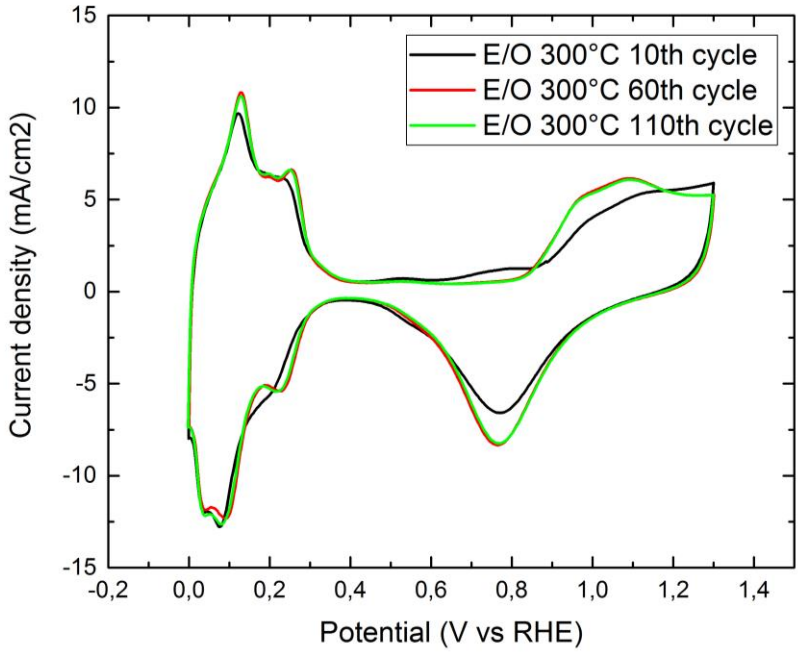

Figure 47: Cyclic voltammetry in 0.5M H_2SO_4 of (E/O)TiON300

The description will proceeds analyzing the graph at the different potentials following the direction of a scan so starting from 0V, reaching 1.3V with the forward scan and then analyzing the backward scan from 1.3V to 0V.
Forward scan:

- 0 – 0.4 V: in this potential range the hydrogen desorption from Pt nanoparticles occurs and is witnessed by the high anodic current measured in this region [59]. The presence of 3 peaks are associated to the desorption of hydrogen from the 3 different Pt planes (100), (111), (110) but in this types of measurement, precise information cannot be extracted.

- 0.4 – 0.85V: this region is also called double layer region since the small anodic current is not due to faradaic process but just to the charge of the double layer so no reactions associated to the Pt catalyst take place in this region. [59] The small peak observed for the curve corresponding to the 10th scan is associated to the oxidation of small impurities that are easily eliminated in the first scans.

- 0.85V – 1.3V: in this final region different phenomena occur in particular, the oxidation of Pt sites to platinum oxides is detected [59] and since we reach values of pH above 1.23V the oxygen evolution reaction should start but is not witnessed.

Backward scan:

- 1.3V – 0.5V : in the backward scan reduction reactions happens and are correlated to peaks with negative (cathodic) currents. In this potential region the reversible reduction of the Pt oxides happens and the increasing cathodic peak with the increasing number of cycles demonstrate the activation of the catalyst. [59]
- 0.4V – 0V : in this final region the adsorption of hydrogen over Pt surface happens witnessing the reversibility of the process and also in this case the presence different peaks correspond to the reaction occurring on different Pt faces. [59]

Once the description of the main features of a CV for TiON/Pt is complete we can now show the CV corresponding to all the different fabricated catalysts. In order to easily identify the fabrication path of a given sample, the different TiON/Pt will now be identified by a code in which the TiON formula will be preceded by (E/O) for the electrodeposited and successively oxidized devices or (O/E) for the catalysts first oxidized and then electrodeposited and followed by the oxidation temperature while the oxidation time is fixed at 1 hour. Electrodeposition parameters are also omitted since the ED recipe is kept constant for the entire fabrication path as already described in section 3.2.1.

For this reason, a sample called (O/E)TiON300° will correspond to a catalyst prepared by pre oxidation of a TiN substrate at 300°C for 1 hour followed by the electrodeposition of Pt (10C/cm^2, 50mA/cm^2, t_{on} 50ms).

The description will start showing the behavior of (E/O)TiON annealed at the three chosen temperatures (300, 350, 400°C)

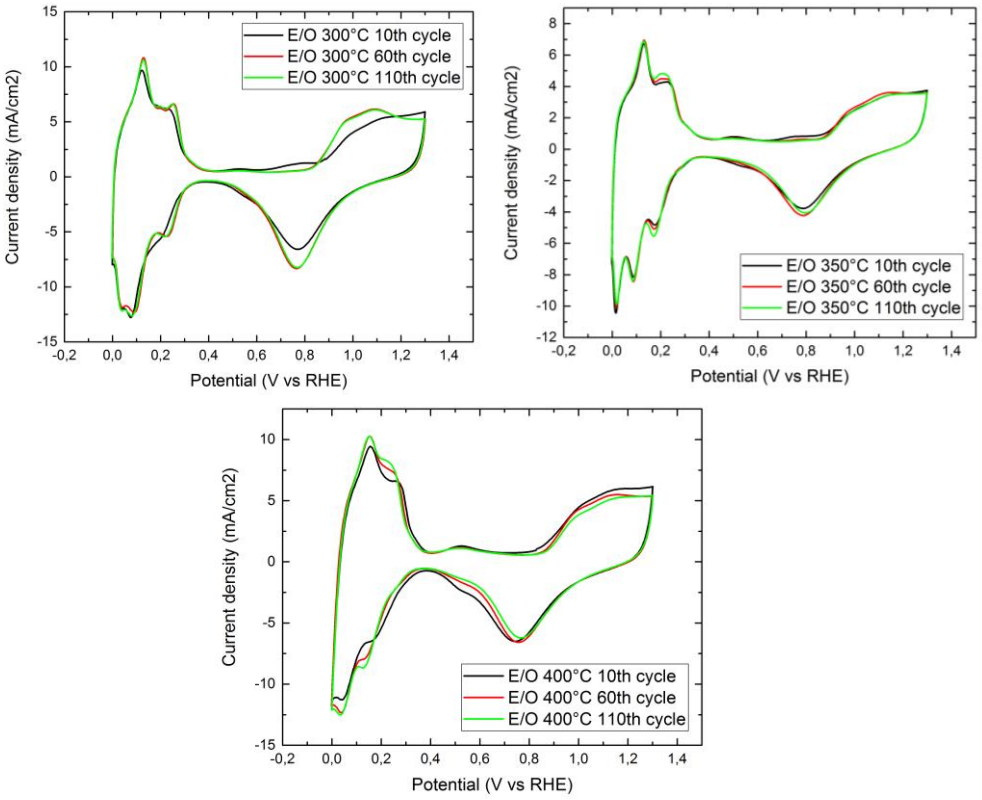

Figure 48: Cyclic voltammetry in 0.5M H2SO4 of (E/O)TiON300 (top left), (E/O)TiON350 (top right), (E/O)TiON400 (bottom)

The three samples show the same features when cycled in acid media with the characteristic peaks of Pt oxidation and reduction and with the presence of the hydrogen desorption and adsorption region. The presence of this features demonstrate that the electrodeposition process is able to effectively deposit the Pt catalyst over the TiN nanostructure and that the Pt is present also after the oxidation at the three temperatures. In particular, (E/O)TiON300 and (E/O)TiON400 both show similar values of current densities in correspondence of the peaks in the hydrogen desorption region from which a similar Pt loading can be estimated. (E/O)TiON350 instead shows lower values of current but this strange behavior cannot be associated to the particular annealing temperature but just to a bad electrodeposition process.

One of the main problems associated to the fabrication path is indeed the difficulty to have a reproducible process since all the different fabrication steps can easily induce variation of the final catalyst. A single device

analysis so can be misleading if take alone and not analyzed in more general context.

To confirm this concept, another important consideration can be made on the analyzed catalysts and is the presence of a small peak observed for the (E/O)TiON400 at 0.5V vs RHE. This peak can be attributed to carbon corrosion as also described by [37] [53] and is caused by unwanted carbon contamination of the sample during the whole fabrication process. The presence of carbon contamination is even more significant on the (O/E)TiON CV's shown in *Figure 49*.

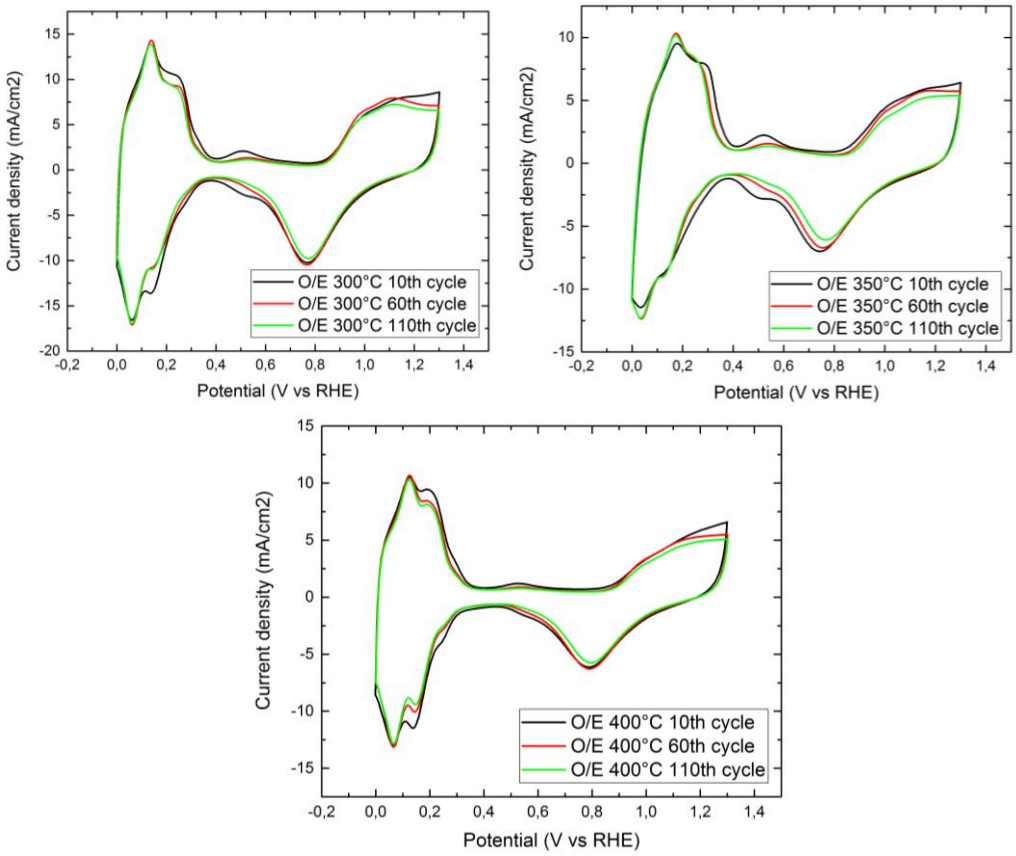

Figure 49: Cyclic voltammetry in 0.5M H2SO4 of (O/E)TiON300 (top left), (O/E)TiON350 (top right), (O/E)TiON400 (bottom)

The peak at ~0.5V is present in all the three samples regardless of the temperature of the oxidation and in general is more intense respect to the (E/O)TiON samples. The redox couple associated to the carbon graphite in sulphuric acid involves the quinone/hydroquinone surface groups as exposed in literature [37]. The presence of these groups has to

be attributed to contaminations probably introduced during the electrodeposition step due to a contaminated precursor solution. The fact that the intensity of the peak is higher for the (O/E)TiON can be addressed to the fact that the (E/O)TiON undergo oxidation after the electrodeposition and in this way the contamination introduced by the ED process can be partially or completely removed by oxidizing the sample at high temperatures while for the (O/E)TiON this process do not happen.

Despite the presence of the unwanted peak at 0.5V vs RHE, the features that characterize a correct deposition of Pt over the TiON substrates are evident and the current densities for the hydrogen evolution region are comparable to the values obtained for the (E/O)TiON samples.

Further analysis on the CV of TiON/Pt in acidic media is performed to obtain information about the electrochemical surface area of the described samples and will be exposed in the next chapter.

4.2.2 ECSA evaluation

A fundamental step in determining the quality of the electrodeposition process is the evaluation of the electrochemical active surface area (ECSA) key parameter need to estimate the catalyst loading over the deposited substrate. The evaluation of ECSA is done by analyzing the hydrogen evolution region in CV of TiON/Pt in acidic media.

As described in section 2.4.2, the ECSA is dependent on Q_H that is the total charge density associated to the hydrogen evolution process calculated by integrating the curve in the potential region 0 – 0.4V and dividing the result for the scan rate as shown for the (E/O)TiON300.

$$Q_H = \frac{\int_0^{0.4} i - i_{doublelayer} dV}{Scanrate} \tag{4.2.1}$$

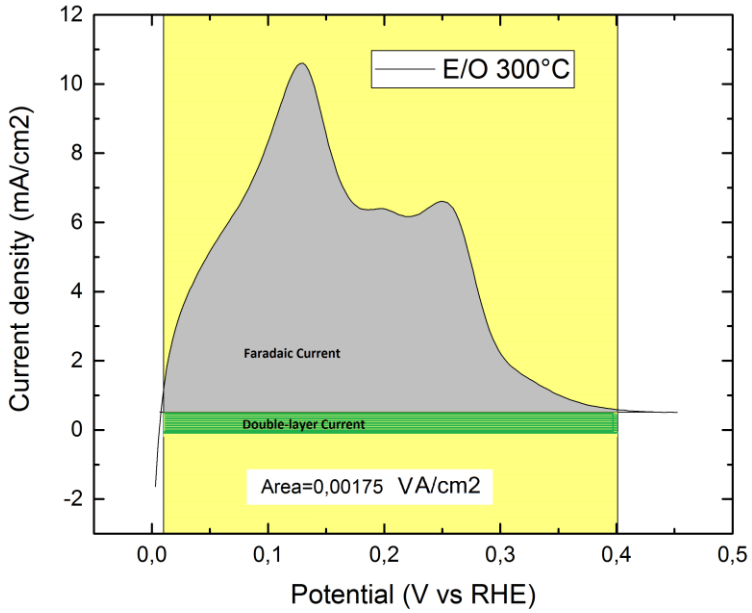

Figure 50: Example of integration of the hydrogen desorption region between 0 - 0.4V vs RHE excluding the double layer current

The exact estimation of the ECSA in m^2/g_{Pt} cannot be done since the catalytic loading i.e. the mass of the Pt deposited after the electrodeposition process cannot be measured precisely. The ECSA is reported in cm^2_{Pt}/cm^2 in order to show a qualitative trend.

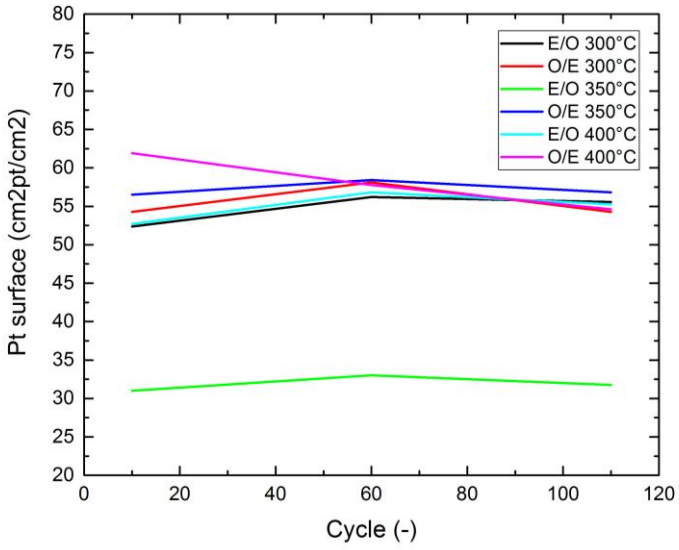

Figure 51: ECSA evaluated as cm^2 of Pt per cm^2 of substrate for the different TiON samples

As it can be seen, the value of Pt surface of all the samples spans in a range between 52 – 58 cm^2_{Pt}/cm^2 with a first increasing value with the number of cycles followed by a slow decrease when reaching the 110^{th} cycle. The sample (E/O)TiON350° confirms low Pt surface as already predicted probably due to a wrong electrodeposition process.

The increase in the Pt surface in the first 60 cycles can be attributed to an activation effect in which the Pt nanoparticles can effectively take part in the HER after the oxidation of surface impurities that happens in the first scans while the slight decrease in the next scans can be caused by a small degradation effect of the structure that will reduce the ECSA.

With the hypothesis of a constant Pt mass deposited for all the samples i.e. no variation in the Faradaic efficiency for the different electrodeposition processes we can therefore assume that all the analyzed samples will show close values of ECSA.

Considering the fact that the ED process is carried out in a galvanostatic mode, choosing the same value of current pulse for all the substrate should lead to the same amount of Pt deposited irrespective of the different oxidation degree of TiN that can present different values of conductivity. With the hypothesis of a faradaic efficiency of the electrodeposition of ~2% as estimated by [53] since we are working with similar operative conditions, we can calculate a possible mean value of ECSA of 56 m^2/g, a much higher value respect to the TiN/Pt devices obtained by [53] but incorrect because in that case, the electrodeposition efficiency estimation was too rough. We expect a much higher value of η and consequently a much lower value of ECSA. If we use η = 50% as an estimation from the efficiency evaluation in pulsed electrodeposition [53], the value of ECSA results of 2.2 m^2/g.

4.3 Testing of TiON/Pt in methanol

After the electrochemical testing of TiON/Pt in acid environment, a fundamental step in the catalyst analysis is performed by a series of measurements in methanol in order to study the ability of the fabricated catalyst to catalyze the methanol oxidation reaction.

Two different types of electrochemical testing are performed in methanol and are:

- **Potentiodynamic testing**: cyclic voltammetry in methanol to study the reactivity of the analyzed material in a scan over a wide range of potentials
- **Potentiostatic testing:** chronoamperometry experiments to study the ability of the fabricated material to catalyze the methanol reaction at a given potential and its ability to depoisoning from adsorbed CO

Both the measurements are performed with the following electrochemical setup:

- 3 electrode configuration cell: TiON/Pt (WE), Pt mesh (CE), Ag/AgCl (RE)
- Electrolyte: 0.5 M H_2SO_4 + 1M CH_3OH solution
- Bubbling system: glass frit insufflating nitrogen inside the cell in order to provide an inert atmosphere eliminating the oxygen.

Furthermore, the samples are also tested under dark or illuminated conditions by using a solar simulator able to replicate an AM 1.5 spectrum in order to study the photocatalytic effect of the oxidized TiN since, with the UV-vis experiments we are able to demonstrate that the TiON support for the three analyzed temperatures 300, 350 and 400°C have a band gap between 1.5 – 2.0 eV able to effective absorb the solar radiation.
The first measurements performed are the potentiodynamic tests and will be discussed in the next chapter

4.3.1 Cyclic voltammetry in methanol

Cyclic voltammetry in acidic media was able to demonstrate the presence of Pt nanoparticles over TiON substrate by analyzing the hydrogen evolution region and the behavior of the TiON/Pt in the range of potentials 0 – 1.3V vs RHE. In this chapter, a similar analysis on the catalyst is made performing the measurement in an acidic solution of methanol (MeOH) 1M to study how the fabricated material behaves toward the MOR. The first approach to methanol oxidation analysis will be performed in DARK conditions so with no illumination since we have to first study only the elctrocatalysis of the material before introducing the photocatalytic effect.
Cyclic voltammetry in methanol are performed in the following way:

- 10 cycles of CV with a scan rate of 150 mV/s in the potential range 0 – 1.3V vs RHE
- 40 cycles of CV in the same conditions to verify the variation of the curve after a consistent number of cycles

As also done for the CV in acid environment, we will use the results of CV for the sample (E/O)TiON300 as an example to describe all the phenomena occurring during the potential cycling.

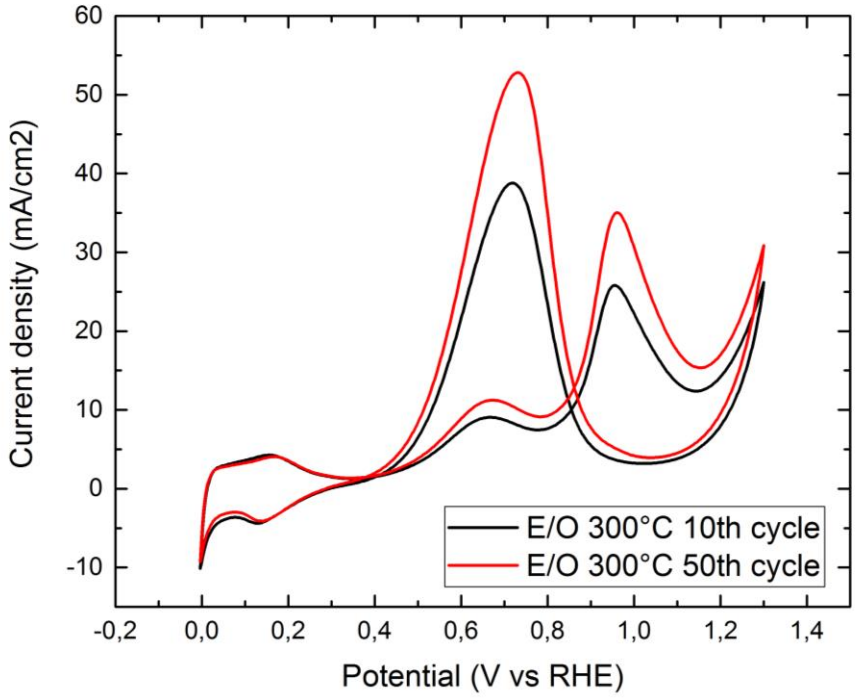

Figure 52: Cyclic voltammetry in 0.5M H_2SO_4 + 1M MeOH of (E/O)TiON300

Differences can be immediately recognized between the behavior of (E/O)TiON300° in acid environment as described in section 4.2.1 and the behavior in a solution containing MeOH and in particular the presence of the two huge peaks at 0.7V and at 1.0V are both associated to the oxidation of methanol. The fact that no reduction peaks (negative currents) are shown is due to the fact that the methanol oxidation reaction is completely non reversible and happen in both forward(1.0 V) and backward(0.7 V) scans.
The analysis of the behavior of (E/O)TiON300° at different potential regions will be done on the first 3 cycles in order to highlights important considerations.

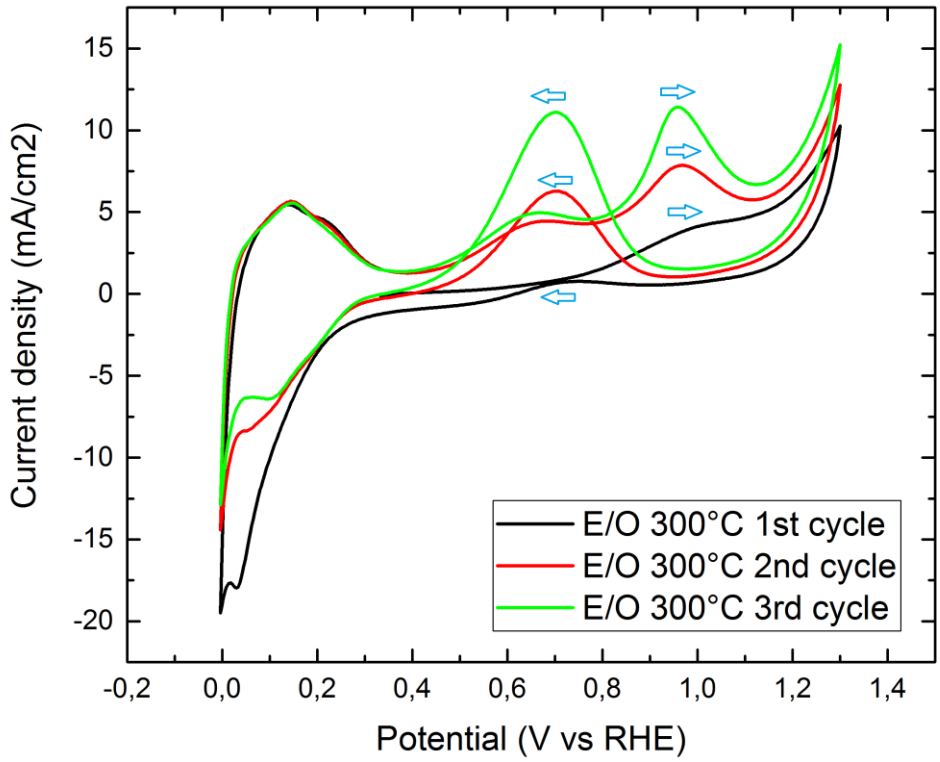

Figure 53: Highlight of the first 3 cycles of CV in methanol solution for (E/O)TiON300. Blue arrows indicate the direction of the scan

Forward scan:

- 0 – 0.4V: in this potential range, the behavior is similar to that of the measurement in acid environment and is characterized by the hydrogen desorption from Pt nanoparticles. The 3 peaks corresponding to the different Pt surface cannot be distinguished and are convoluted in a single wide peak.

- 0.4 – 0.8V: this potential region is extremely interesting and must be analyzed carefully. The behavior of the material is different between the first cycle and the other since in the first case no peaks are seen while from the second scan onward, a peak at 0.65V show up and increase in intensity. This peak is correlated to the CO oxidation step and is not present in the first scan since no CO is already adsorbed on Pt surface. Carbon monoxide is the strong poisoning intermediate in the reaction of methanol oxidation so it will accumulate on the Pt sites during the oxidation process. After the first potential scan indeed the residual CO adsorbed on the surface deriving from the precedent oxidation is bounded to the catalyst sites and starts to get oxidized to CO_2 depoisoning the Pt site and letting the methanol oxidation reaction to continue. The intensity of this peak gets higher after many cycles and as is sign of an increased methanol oxidation reaction due to the activation of the catalyst. [60]

- 0.8 – 1.3V: in this potential region different phenomena occurs. First of all the presence of a peak at 1.0V vs RHE corresponds the main oxidation peak of methanol and its intensity increase widely within the first cycles due to the activation of the catalyst. Secondly, as already described, after 0.85V vs RHE Pt catalyst starts to get oxidized to Pt oxides not able to catalyze the MOR. [60]

Backward scan:

- 1.3 – 0.4V: in the back scan, no reduction peaks show up with the curve always in the positive current region. The lack of the Pt oxides reduction peak seems to be masked by the more intense oxidation peak of methanol at 0.7V vs RHE [60]. The absence of an oxidation peak of CO in the back scan before the methanol oxidation peak as in the forward scan can be addressed to the fact that the oxidation at these high potentials is complete and the catalyst is able to undergo a complete depoisoning. The intensity of the methanol oxidation in the backward scan has also in this case an increasing trend with the number of cycles since the catalyst must be properly activated.

- 0.4 – 0V finally in this range of potentials, hydrogen adsorption over the Pt catalyst occurs. An important consideration can be made on the intensity of the cathodic current in this region. Since the adsorption happens after the methanol oxidation at higher potentials, the Pt surface will be partially poisoned by CO produced

in the previous steps and consequently the adsorption of hydrogen will happen only on the depoisoned Pt. The catalyst will be progressively get poisoned by the MOR up to a steady state situation in which a given number of Pt sites will be free due to the depoisoning ability of the TiON/Pt catalyst.

After the investigation of the main features of a CV in MeOH, we can now show the result obtained for all the different fabricated samples. Also in this case, the description will start showing the behavior of (E/O)TiON annealed at the three different temperatures and followed by (O/E)TiON to see if differences show up.

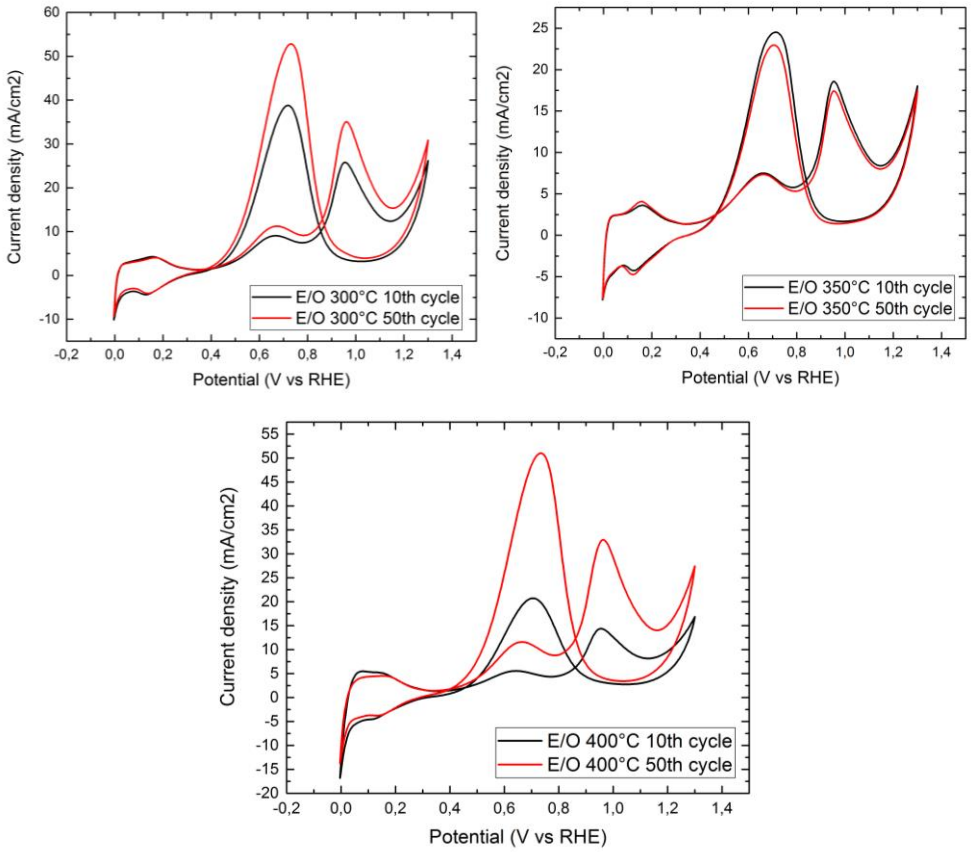

Figure 54: Cyclic voltammetry in 0.5M H_2SO_4 + 1M MeOH of (E/O)TiON300 (top left), (E/O)TiON350 (top right), (E/O)TiON400 (bottom)

Despite the three graphs show similar behavior, small consideration can be made:

- (E/O)TiON300 and (E/O)TiON400 have both the same peak current densities for the 50th scan while (E/O)TiON350 has much lower values. This can be attributed to the fact that the sample annealed at 350°C has a lower Pt loading as also highlighted by the ECSA calculation reported in section 4.2.2.
- (E/O)TiON350 differently from the other two samples shows the maximum current density values for the 10th scan while both the others show much better behavior at the 50th scan. This can be the result of a fast degradation of the material during the scans with consequently reduction of the ECSA.

A complete different situation is obtained for the (O/E)TiON samples and are here reported

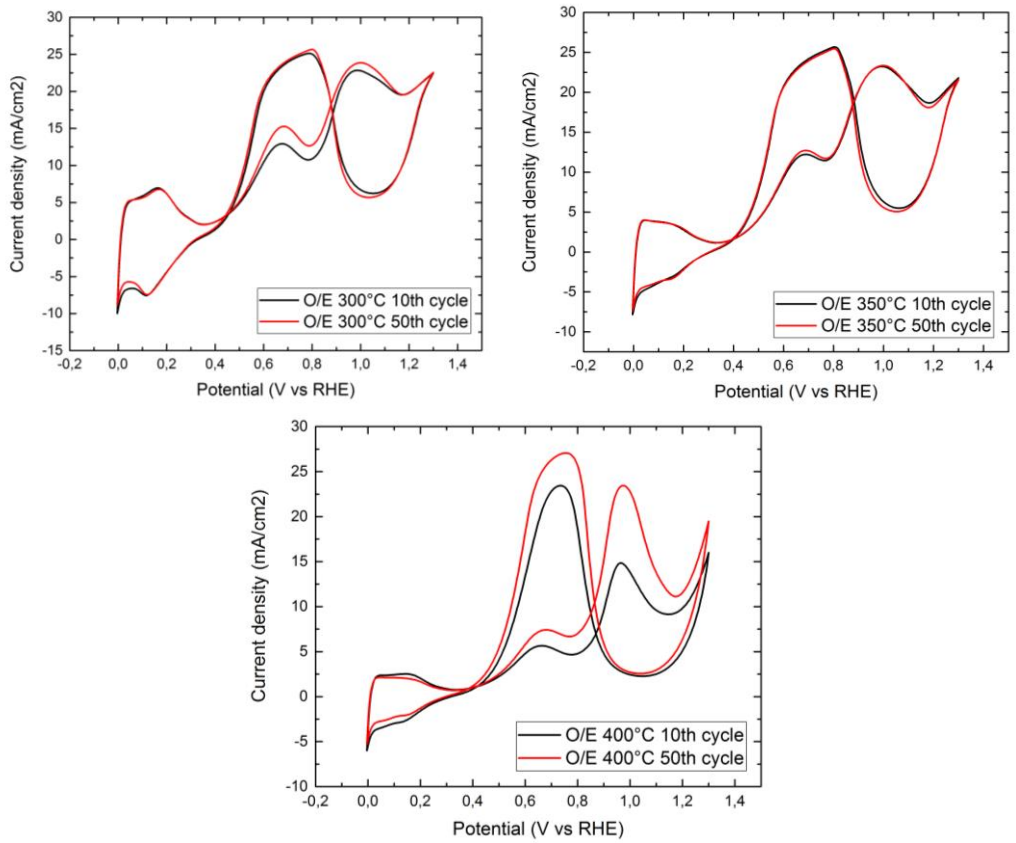

Figure 55: Cyclic voltammetry in 0.5M H_2SO_4 + 1M MeOH of (O/E)TiON300 (top left), (O/E)TiON350 (top right), (O/E)TiON400 (bottom)

Characteristic of (O/E)TiON300 and (O/E)TiON350 is the presence of a wide distorted peak in the back scan associated to the methanol oxidation peaked at 0.8V vs RHE while (O/E)TiON400 shows a slight distortion only in the 50th scan. It's interesting to note that the strong distortion is present on the samples that have shown previously a carbon corrosion peak at 0.5 V characteristic of the oxidized and electrodeposited samples as already discussed. The real cause of the distortion is still under investigation and how this will affect the methanol oxidation reaction is still unclear. Nevertheless since this phenomenon occurs only for the samples that undergo oxidation followed by electrodeposition, the cause must be associated to this fabrication path. Unfortunately SEM analysis is not useful to understand this strange behavior since the analyzed samples shown in section 3.2 present a good nanostructure and no sign of corrosion are evident.

4.3.2 Photocatalytic effect during CV

After the evaluation of the activity of the fabricated catalysts toward the MOR in DARK conditions, a particular set of measurements is performed under illumination. The solar simulator employed in these experiments is a tungsten lamp able to replicate the solar spectrum and calibrated in order to obtain a value of power density of 1000 W/m^2 corresponding to AM 1.5 spectrum.
The electrochemical set up used in this experiment is identical to the previous one but differences in the cyclic voltammetry parameters are introduced. The experiment is carried out after the 50 scans in dark and following the described procedure:

- 10 CV under LIGHT illumination in the potential range 0.2 – 1.2V vs RHE with a scan rate of 50 mV/s
- 10 CV in DARK conditions with the same CV parameters.

After the measurements, both the 10th scan of the CV in dark and in light is extracted and plotted together to show the differences.

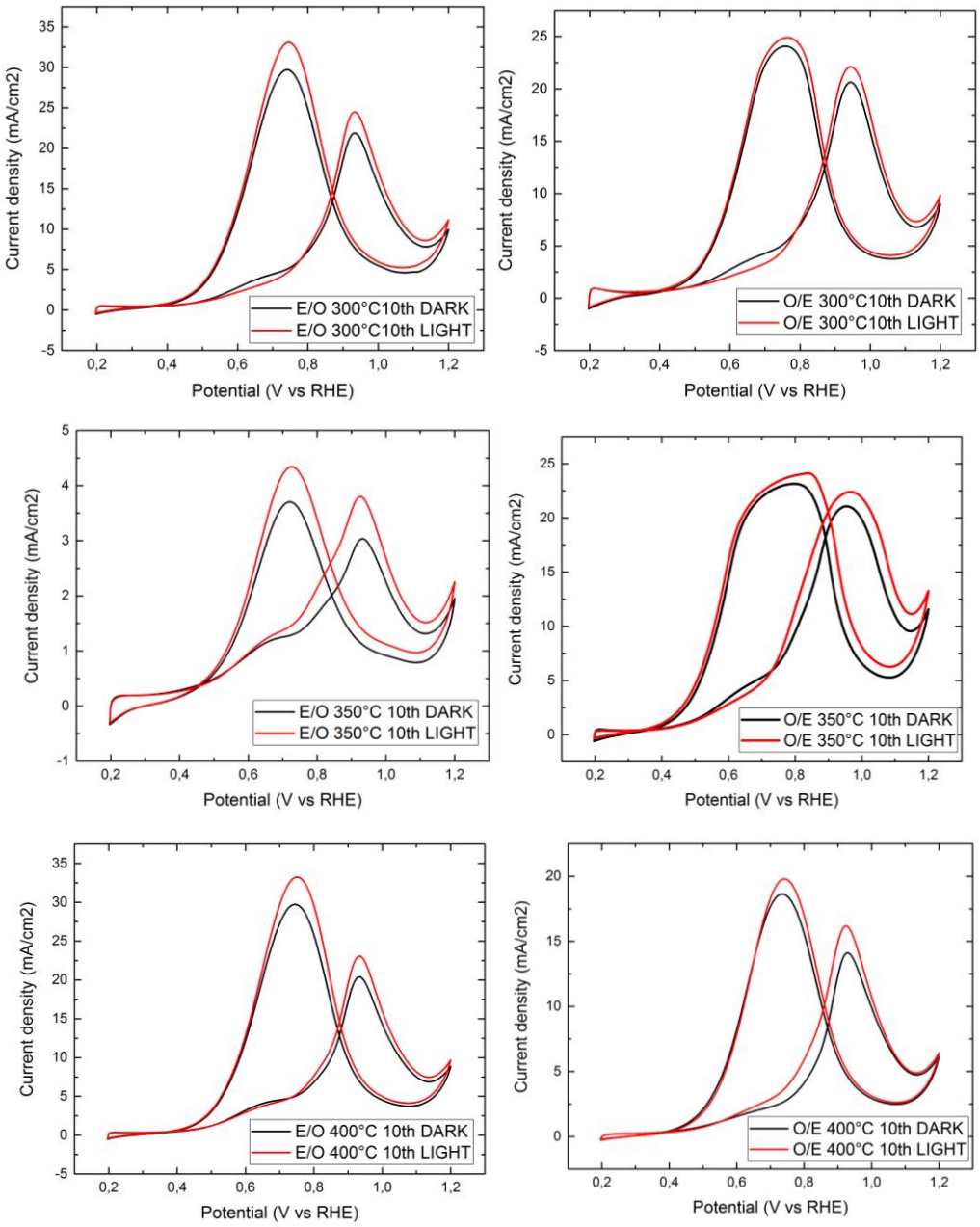

Figure 56: Photocatalytic effect shown in CV in methanol solution by plotting the 10th cycle in dark and under illumination for all the analyzed samples

It can be clearly seen an increase of the current density for all the illuminated samples respect to the dark conditions. This phenomenon is verified for both he forward and backward oxidation peaks of methanol and the effect is more pronounced for the E/O samples respect to the O/E.

The described phenomena has been investigated for TiON/Pt catalysts supported over glassy carbon so in order to study the photoactivity, the samples were illuminated by the top of nanotrees. A more efficient way to illuminate the samples instead is the use a back illumination to better extract photo generated carriers. For this reasons, the transparent substrate FTO has been tested. Unfortunately, FTO has an electric conductivity much lower than GC and it affected the overall performance of the device. In particular, showing the CV experiment in H_2SO_4 of (O/E)TiON300 deposited over FTO we can clearly see the presence of a high capacitive current density and an overall decrease of the features associated to a correct Pt deposition over TiON.

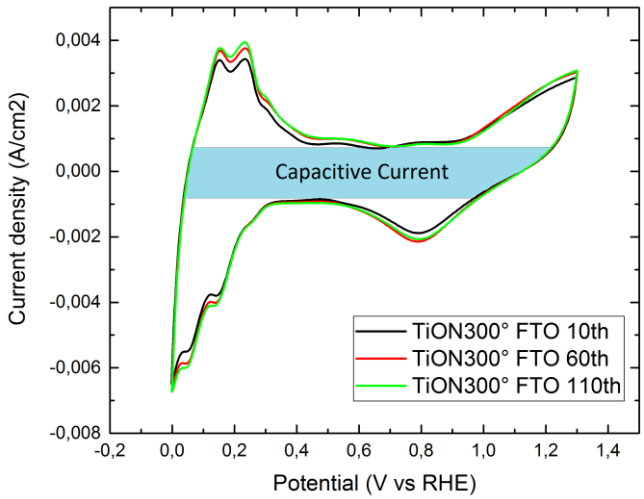

Figure 57: Cyclic voltammetry in 0.5M H_2SO_4 of (O/E)TiON300 deposited over FTO. The high capacitive current is highlighted

For these reasons, FTO has been quickly discarded for TiN deposition and GC has been chosen as the only substrate used for electrochemical analysis of the catalysts.

In order to further study the performance of the prepared samples both in dark conditions and under illumination, chronoamperometry experiments have been carried out and described in the next chapter.

4.3.3 Chronoamperometry in methanol

After the verification of the activity of the catalyst toward MOR both in dark and in light conditions, experiments are carried out to test the material after prolonged time in methanol and to verify its depoisoning ability from CO intermediates.
For this reasons, a chronoamperometry measurement is performed with the following protocol:

- 3 electrode configuration cell: TiON/Pt (WE), Pt mesh (CE), Ag/AgCl (RE)
- Electrolyte: 0.5M H_2SO_4 + 1M CH_3OH
- Set potential: 0.7V vs RHE
- Experiment time: 2 hours

The description starts with the chronoamperometry experiments performed in dark with duration of 2 hours. The results are shown in the graph below.

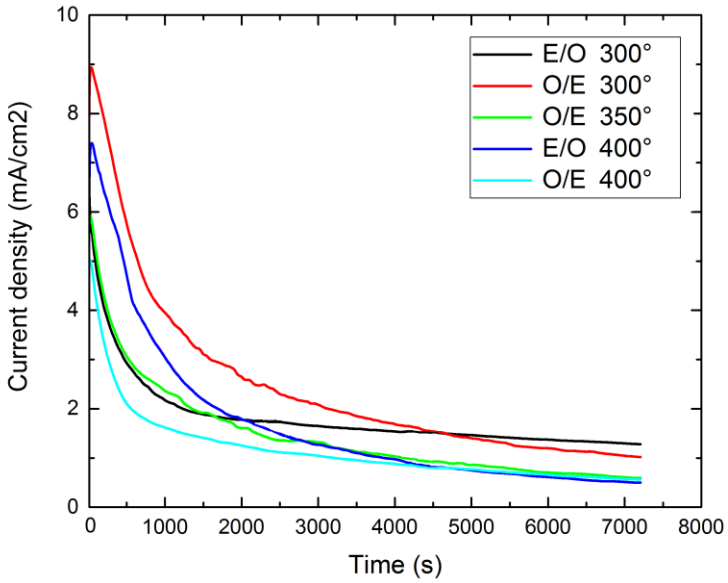

Figure 58: Chronoamperometry performed at 0.7V vs RHE in methanol solution for the different analyzed samples. The experiment is carried out in dark conditions for 2 hours

It can be easily notice the sharp decrease in current density for all the samples in the early testing. This first decrease is caused by diffusion phenomena of reactants inside the electrolyte toward the catalyst surface

since these experiments are carried out without stirring of the solution. Non faradaic current i.e. capacitive current decrease more rapidly respect to faradaic current so after a prolonged time it is negligible. Further decrease of the current density instead can be associated to the progressive poisoning of the catalyst during methanol oxidation reaction along with the degradation of the material. It's important to notice that even after 2 hours, a non zero current density is shown witnessing the ability of the material to catalyze the removal of the strong CO intermediate. Between the analyzed samples, (E/O)TiON300 and (O/E)TiON300 show the best performance with a higher current density respect to the other catalysts.
The best way to verify the effective depoisoning ability of TiON/Pt would be that of comparing the performance of the fabricated catalyst with a traditional C/Pt catalyst with the same catalytic loading and comparable ECSA. C/Pt since is not able to eliminate CO on Pt surface, is expected to get easily poisoned in a short time with a current density drastically dropping to 0. Unfortunately we were not able to perform the comparison in this thesis work so we address this comparison to the future developments.

As described previously, the strong mass transport limitation reduces the ability to describe all the possible phenomena occurring during time. In order to solve this problem, the use of a Rotating disk electrode (RDE) should be recommended since this device helps to avoid mass transport limitation inducing a laminar flow of electrolyte over the analyzed substrate by rotation.
Not having the possibility to use this instrument, we performed a different experiment in which the chronoamperometry experiment was stopped every 30 minutes to allow the stirring of the solution with a magnetic stirrer. Measuring the current density produced by the catalyst after the removal of concentration gradients of methanol close to the surface can be used as a rough estimation of the effective depoisoning ability of the analyzed samples. In particular, if the measured current density results to be higher than the plateau value obtained before the stirring, the limitation to the current density is provided by mass transport rather than poisoning; in other word, the catalyst is able to remove CO adsorbate on its surface.
Nevertheless, a decrease in performance is expected during time since the experiment is carried out at high potential so degradation effects can show up.

The results of the described chronoamperometry are reported for (E/O)TiON300 since it was the sample showing the best performance in precedent experiment.

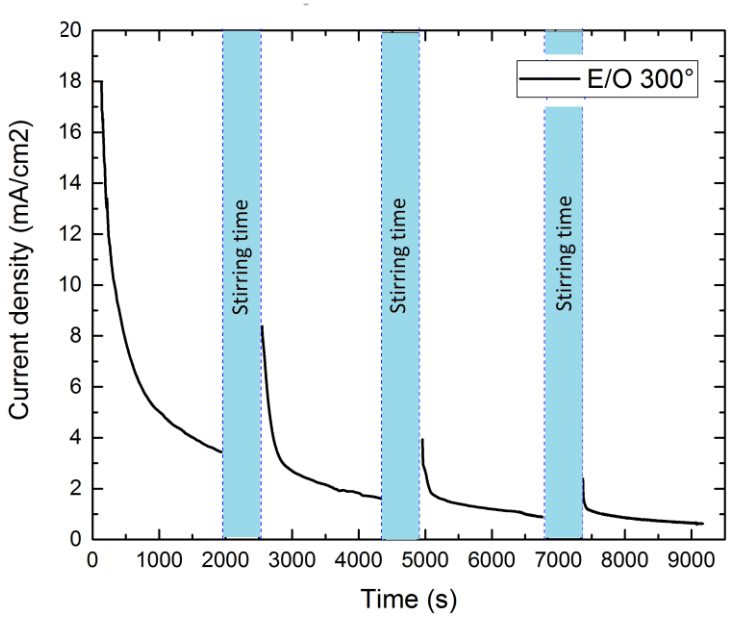

Figure 59: Chronoamperometry performed at 0.7V vs RHE in methanol solution for (E/O)TiON300. The experiment is divided into four parts of 30 minutes each divided by 10 minutes of solution stirring

We can clearly see the drop in current density due to the mass transport phenomena in the early stage of the experiment and, after the first stirring time, a net current density recover is shown witnessing the mass transport limitation rather than the poisoning of the catalyst. This behavior is confirmed by the other two segments in which the recover even if progressively lower is seen.

4.3.4 Photocatalytic effect during chronoamperometry

In order to verify the photocatalytic effect shown by cyclic voltammetry experiments, chronoamperometry tests are performed using the solar simulator. In particular, to highlight the photo-enhancement effect, chopping illumination measurements are carried out. In this experiment, illumination provided by the solar simulator is switched on and off in a limited period of time and the current density variation is recorded. An

example is shown for a (O/E)TiON300 in which on time periods of 50s are alternated to off times of 150s.

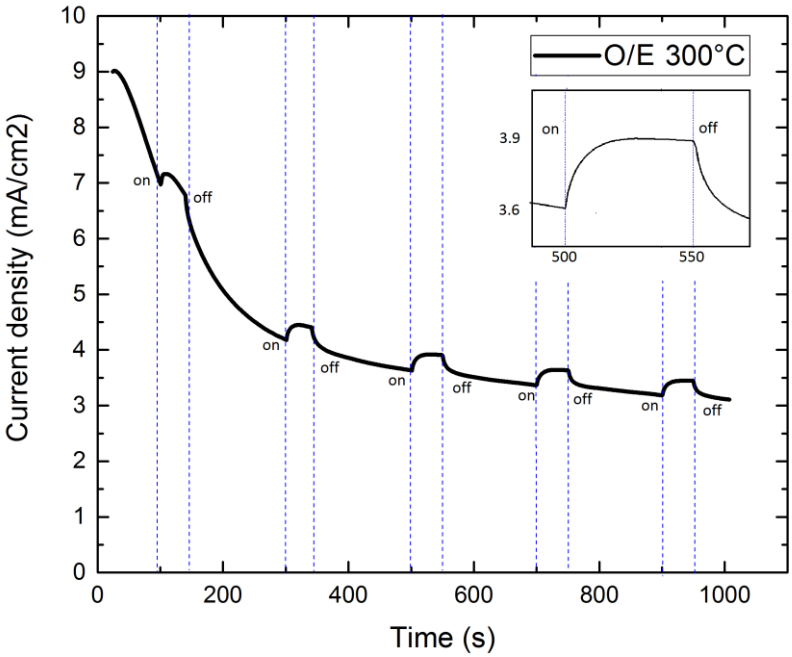

Figure 60: Chopped chronoamperometry performed at 0.7V vs RHE for (O/E)TiON300. On time: 50s, Off time: 150s. The insert shows the transient behavior up to the plateau current during illumination

It can be clearly seen the presence of a discontinuity in current density when the light is switched on and off. The increase of the current density when the light illuminates the samples is a clear sign of a photo induced effect on the reaction. This increase is not abrupt as also shown in the insight but rather follows a charging behavior up to a plateau current density. The difference between the value in dark condition and under illumination is used to estimate the photocurrent using the formula 2.4.4. and for the specific case the photocurrent percentage results to be + 9%.

In order to show the behavior of the catalyst after a prolonged time, chronoamperometry under chopped illumination is performed for (E/O)TiON300 with duration of 2 hours.

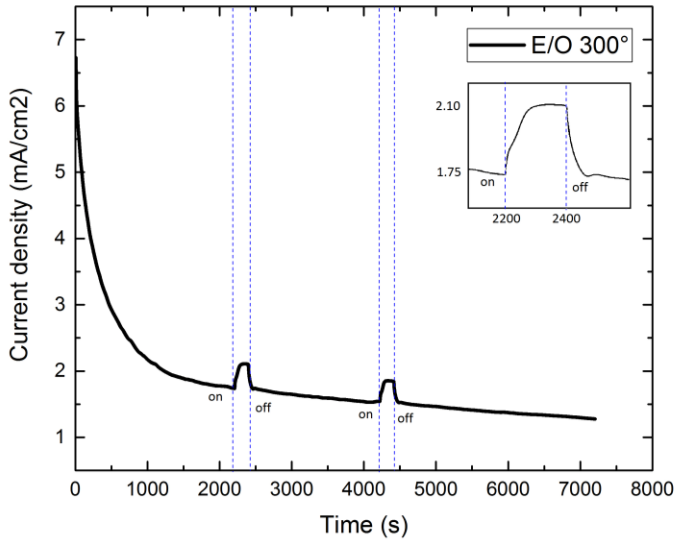

Figure 61: Chopped chronoamperometry performed at 0.7V vs RHE for (E/O)TiON300. On time: 200s. The insert shows the transient behavior up to the plateau current during illumination

The sample is illuminated after the initial drop in current density for 200s at 2200s and the chop measurement is repeated at 4200s. Also in this case, a net increase in current density due to illumination is recorded and the photocurrent increase results to be +20% evaluated at both the chopping times.
Different behavior is shown for (E/O)TiON400

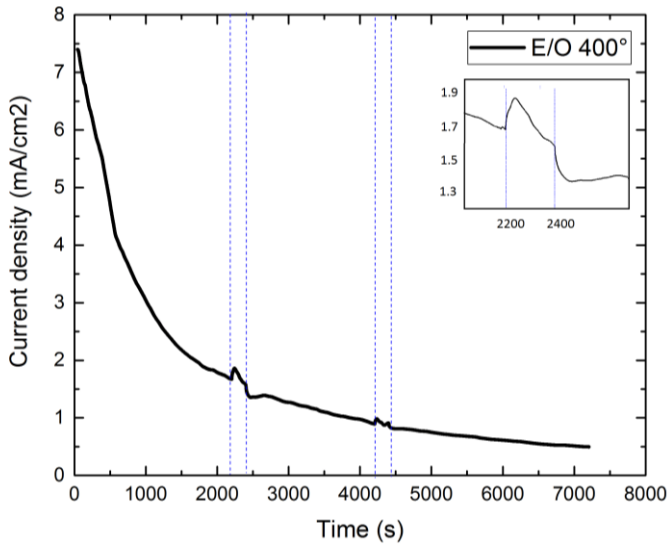

Figure 62: Chopped chronoamperometry performed at 0.7V vs RHE for (E/O)TiON400. On time: 200s. The insert shows the transient behavior up to the plateau current during illumination

In this case, the photocurrent density, after a first increase, rapidly decays and no formation of a plateau is seen even at higher times. This strange behavior is still not clear and can be attributed to the bad photocatalytic ability of TiON annealed at 400°C probably associated to recombination phenomena or the inability to effectively exploit the photogenerated carriers in the methanol oxidation reaction.

The enhanced current obtained in the photocatalytic experiments can be attributed to the ability of the oxynitride phase present to photo-generate carriers and in particular, photogenerated holes (h^+) reaching the surface can interact with adsorbed OH species to give OH radicals ($OH^\bullet$) extremely reactive compounds able to promote the methanol oxidation reaction especially during the depoisoning of CO intermediates.
(E/O)TiON300 seems to exploit this mechanism in an efficient way with an increase of photocurrent up to 20% while (E/O)TiON400 is not able to sustain a photocurrent probably due to recombination issues.

Conclusions

In this thesis work, we present an advanced catalyst support for DMFC anodes able to enhance the methanol oxidation reaction and exploit a photocatalytic effect.
We fabricated and characterized nanostructured thin films of titanium oxynitride with large surface area deposited by pulsed laser deposition and the following steps has been followed in the realization of the full TiON/Pt catalyst:

- PLD is the chosen deposition technique for the creation of a porous nanostructured titanium nitride thin film with 1μm thickness and characterized by the formation of quasi-1D hierarchical nanotrees able to provide outstanding values of surface area as shown by SEM images.

- Annealing and oxidation steps play a key role in the variation of composition of TiN leading to the formation of an oxynitride phase. Vacuum annealing at 500° for 4 hours is done to favor the crystallinity of the deposited substrate and consequently, the oxidation step in the range 300 – 400°C for 1 hour is performed to oxidize the material. TiON can be seen as an N-doped TiO_2 and is characterized by the presence of a band gap which value is directly correlated to the oxidation degree of the metallic-like TiN as seen by UV-vis experiments. XRD is also a useful technique able to study the crystallinity and composition of the analyzed samples.

- Electrodeposition is chosen as the deposition technique of the catalyst nanoparticles over the engineered TiON substrate since the fine tuning of the pulsed ED recipe can lead to the deposition of small Pt nanoparticles. We adapted a previous recipe used by [53] choosing the following parameters: total charge density of 10C/cm² with

current density pulses of 50mA/cm² and on/off time of 50/500ms. Unfortunately, the uniform deposition of the catalyst can't be achieved with this technique since the catalyst was deposited only on the top of the TiON nanostructures with a modification of the structure and the creation of lamellae.

- Two different fabrication path are chosen to create the final TiON/Pt in order to see if differences show up with the electrodeposition over TiN and consequent oxidation or depositing over an already oxidized substrate. Both the two path show activity toward the methanol oxidation reaction as shown by electrochemical measurements.

- Electrochemical measurements play a fundamental role to study the behavior of the fabricated catalysts in different electrolytes: first, the stability of TiON is analyzed by performing 1000 cycles of cyclic voltammetry in 0.5M H_2SO_4 in a potential range 0 - 1.3V showing that the TiON annealed at 300° is the most stable material. The evaluation of ECSA of the TiON/Pt is done by performing cyclic voltammetry in the same conditions showing a value of surface area in the range of 2÷50 m²/g guessing the possible faradaic efficiency in the electrodeposition step. The activity toward MOR is verified by performing potentiostatic and potentiodynamic test in 0.5M H_2SO_4 + 1M CH_3OH showing the ability of the material to recover from CO poisoning.

- Finally the photocatalytic effect toward MOR is verified by performing the aforementioned measurements under visible light illumination with the use of a solar simulator. TiON/Pt annealed at 300°C shows the best performance with an increase of the current density of up to 20% witnessing the ability of the fabricated material to absorb end exploit this radiation.

This thesis work demonstrates how PLD can be used to fabricate advanced TiON/Pt catalyst for DMFC anodes able to be active toward methanol oxidation reaction.
Despite the good results obtained, some problematics have to be solved. Among these, the fabrication path is still influenced by the presence of carbon contaminants which could reduce the catalytic ability of the

fabricated material and witnessing the problem of non-reproducibility of the results. Furthermore, we demonstrate how electrodeposition, even if a good catalyst deposition method, is still inefficient since is not able to uniformly distribute Pt nanoparticles over the whole substrate surface.
Concerning the catalytic ability of the fabricated material, to confirm the effective CO depoisoning of the catalyst, CO stripping voltammetry is the needed technique since can immediately show the behavior of the catalyst when covered by this strong intermediate. Photocatalytic effect demonstrated in this work must be optimized and fully understood since we obtained different results within the analyzed samples.
Finally, to fully characterize the material, future developments will lead to perform advanced and expensive measurements like TEM and XPS, the last one able also to verify the electronic effect of TiON on Pt.

List of Figures

Chapter I

Chapter II

Chapter III

Chapter IV

List of Tables

References

[1] K. A. Mauritz and R. B. Moore, “State of understanding of Nafion,” *Chem. Rev.*, vol. 104, no. 10, pp. 4535–4585, 2004.

[2] D. Dohle, H.; Mergel, J.; Stolten, “Heat and power management of a direct-methanol-fuel-cell (DMFC) system,” *J. Power Sources*, vol. 111, pp. 268–282, 2002.

[3] R. Parsons, “Manual of Symbols and Terminology for Physicochemical Quantities and Units - Appendix-3 - Electrochemical Nomenclature,” *Denki Kagaku*, vol. 48, no. 1, pp. 46–55, 1980.

[4] M. T. M. Koper, S. C. S. Lai, and E. Herrero, “Mechanisms of the Oxidation of Carbon Monoxide and Small Organic Molecules at Metal Electrodes,” *Fuel Cell Catal.*, pp. 159–207, 2008.

[5] T. Iwasita, “Electrocatalysis of methanol oxidation,” *Electrochim. Acta*, vol. 47, no. 22–23, pp. 3663–3674, 2002.

[6] T. Iwasita, “Chapter 41 Methanol and CO electrooxidation,” vol. 2, 2003.

[7] F. Seland, *Electrochemical oxidation of methanol and formic acid in fuel cell processes*, vol. 2005:204. 2005.

[8] S. Gilman, “The Mechanism for Electrochemical Oxidation of Carbon Monoxide and Methanol ,’” *J. Phys. Chem.*, vol. 68, no. 1, pp. 70–80, 1964.

[9] L. Giorgi and A. Pozio, “H 2 and H 2 / CO oxidation mechanism on Pt / C , Ru / C and Pt-Ru/C electrocatalysts,” *J. Appl. Electrochem.*, vol. 31, pp. 325–334, 2001.

[10] J. Rodriguez and D. Goodman, "The nature of the metal-metal bond in bimetallic surfaces" Science New series Vol 257. 1992.

[11] A. McNaught, A. D.; Wilkinson, *Compendium of Chemical*

Terminology, 2nd ed. (the "Gold Book"). 2006.

[12] G. L. Spessard, G. O.; Miessler, *Organometallic Chemistry (2nd ed.)*. New York Oxford University Press, 2010.

[13] H. Igarashi *et al.*, "CO Tolerance of Pt alloy electrocatalysts for polymer electrolyte fuel cells and the detoxification mechanism," *Phys. Chem. Chem. Phys.*, vol. 3, no. 3, pp. 306–314, 2001.

[14] F. Buatier de Mongeot, M. Scherer, B. Gleich, E. Kopatzki, and R. . Behm, "CO adsorption and oxidation on bimetallic Pt/Ru(0001) surfaces – a combined STM and TPD/TPR study," *Surf. Sci.*, vol. 411, no. 3, pp. 249–262, 1998.

[15] M. Roca-Ayats, G. García, J. L. Galante, M. A. Peña, and M. V. Martínez-Huerta, "TiC, TiCN, and TiN supported Pt electrocatalysts for CO and methanol oxidation in acidic and alkaline media," *J. Phys. Chem. C*, vol. 117, no. 40, pp. 20769–20777, 2013.

[16] H. Liu, C. Song, L. Zhang, J. Zhang, H. Wang, and D. P. Wilkinson, "A review of anode catalysis in the direct methanol fuel cell," *J. Power Sources*, vol. 155, no. 2, pp. 95–110, 2006.

[17] J. Chen, J. B. Siegel, T. Matsuura, and A. G. Stefanopoulou, "Carbon Corrosion in PEM Fuel Cell Dead-Ended Anode Operations," *J. Electrochem. Soc.*, vol. 158, no. 9, p. B1164, 2011.

[18] T. I. Valdez, S. Firdosy, B. E. Koel, and S. R. Narayanan, "Investigation of Ruthenium Dissolution in Advanced," *ECS Trans.*, vol. 1, no. 6, pp. 293–303, 2006.

[19] S. Jayaraman, T. F. Jaramillo, S.-H. Baeck, and E. W. McFarland, "Synthesis and characterization of Pt-WO3 as methanol oxidation catalysts for fuel cells.," *J. Phys. Chem. B*, vol. 109, no. 805, pp. 22958–22966, 2005.

[20] P. Shen, K. Chen, and A. C. C. Tseung, "Co-deposited Pt-WO , Electrodes," vol. 90, no. 20, pp. 3089–3096, 1994.

[21] C. Xu, R. Zeng, P. K. Shen, and Z. Wei, "Synergistic effect of CeO2 modified Pt/C catalysts on the alcohols oxidation," *Electrochim. Acta*, vol. 51, no. 6, pp. 1031–1035, 2005.

[22] J. O. M. Bockris, A. K. N. Reddy, and M. Gamboa, *Modern electrochemistry 2A: Fundamentals of electrodics*, vol. 2A. 2015.

[23] J. O. M. Bockris, A. K. N. Reddy, and M. Gamboa, *Modern electrochemistry 2B:Electrodics in Chemistry, Engineering, Biology and Environmental Science*, vol. 2B. 2015.

[24] K. Rajeshwar, "Fundamentals of Semiconductors Electrochemistry and Photoelectrochemistry," *Encycl. Electrochem.*, pp. 1–51, 2007.

[25] K. Fujishima, Akira; Honda, "Electrochemical Photolysis of Water at a Semiconductor Electrode," *Nature*, vol. 238, 1972.

[26] A. Y. Ahmed, T. A. Kandiel, I. Ivanova, and D. Bahnemann,

"Photocatalytic and photoelectrochemical oxidation mechanisms ofmethanol on TiO2in aqueous solution," *Appl. Surf. Sci.*, vol. 319, no. 1, pp. 44–49, 2014.

[27] N. Su *et al.*, "Plasma-induced synthesis of Pt nanoparticles supported on TiO2 nanotubes for enhanced methanol electro-oxidation," *Appl. Surf. Sci.*, vol. 399, pp. 403–410, 2017.

[28] Y. H. Qin, Y. Li, R. L. Lv, T. L. Wang, W. G. Wang, and C. W. Wang, "Enhanced methanol oxidation activity and stability of Pt particles anchored on carbon-doped TiO2 nanocoating support," *J. Power Sources*, vol. 278, pp. 639–644, 2015.

[29] A. S. Polo, M. C. Santos, R. F. B. De Souza, and W. A. Alves, "Pt-Ru-TiO2 photoelectrocatalysts for methanol oxidation," *J. Power Sources*, vol. 196, no. 2, pp. 872–876, 2011.

[30] K. Drew, G. Girishkumar, K. Vinodgopal, and P. V. Kamat, "Boosting fuel cell performance with a semiconductor photocatalyst: TiO 2/Pt-Ru hybrid catalyst for methanol oxidation," *J. Phys. Chem. B*, vol. 109, no. 24, pp. 11851–11857, 2005.

[31] T. Yoshida, S. Niimi, M. Yamamoto, T. Nomoto, and S. Yagi, "Effective nitrogen doping into TiO2 (N-TiO2) for visible light response photocatalysis," *J. Colloid Interface Sci.*, vol. 447, pp. 278–281, 2014.

[32] R. Asahi, T. Morikawa, T. Ohwaki, and Y. Taga, "Visible-Light Photocatalysis in Nitrogen-Doped Titanium Oxides," *Science (80-.).*, vol. 293, no. 5528, pp. 269–271, 2001.

[33] X. Cui, M. Ma, W. Zhang, Y. Yang, and Z. Zhang, "Nitrogen-doped TiO2 from TiN and its visible light photoelectrochemical properties," *Electrochem. commun.*, vol. 10, no. 3, pp. 367–371, 2008.

[34] H. Allmaier, L. Chioncel, and E. Arrigoni, "Titanium nitride: A correlated metal at the threshold of a Mott transition," *Phys. Rev. B - Condens. Matter Mater. Phys.*, vol. 79, no. 23, pp. 1–7, 2009.

[35] D. S. . K. B. Y. W. D. S. Stone, "Hardness and elastic modulus of TiN based on continuous indentation technique and new correlation," *J. Vac. Sci. Technol. A*, pp. 2543–2547, 1991.

[36] K. Lal *et al.*, "Electrical resistivity of titanium nitride thin films prepared by ion beam-assisted deposition," *Phys. B Condens. Matter*, vol. 307, no. 1–4, pp. 150–157, 2001.

[37] B. Avasarala and P. Haldar, "Electrochemical oxidation behavior of titanium nitride based electrocatalysts under PEM fuel cell conditions," *Electrochim. Acta*, vol. 55, no. 28, pp. 9024–9034, 2010.

[38] O. T. M. Musthafa, S. Sampath, and O. Muhammeda, "High performance platinized titanium nitride catalyst for methanol oxidation," *Chem. Commun.*, vol. 1, no. 1, pp. 67–69, 2008.

[39] M. M. Ottakam Thotiyl, T. Ravikumar, and S. Sampath, "Platinum particles supported on titanium nitride: an efficient electrode material for the oxidation of methanol in alkaline media," *J. Mater. Chem.*, vol.

20, no. 47, p. 10643, 2010.

[40] Passoni L., D. Program and I. N. Physics, “Titanium dioxide hierarchical nanostructures for photonic applications,” no. December, 2015.

[41] J. Schou, “Physical aspects of the pulsed laser deposition technique: The stoichiometric transfer of material from target to film,” *Appl. Surf. Sci.*, vol. 255, no. 10, pp. 5191–5198, 2009.

[42] H. Krebs *et al.*, “Pulsed Laser Deposition (PLD) - a Versatile Thin Film Technique UHV-chamber,” *Adv. Solid State Phys. SE - 36*, no. July, pp. 505–518, 2003.

[43] D. H. Lowndes, D. B. Geohegan, a a Puretzky, and D. P. Norton, “Synthesis Thin-Film Materials by Pulsed Deposition Laser,” *Science (80-.).*, vol. 273, no. 5277, pp. 898–903, 2012.

[44] A. Baserga *et al.*, “Nanostructured tungsten oxide with controlled properties: Synthesis and Raman characterization,” *Thin Solid Films*, vol. 515, no. 16 SPEC. ISS., pp. 6465–6469, 2007.

[45] A. Ehl, Rosemary Gene; Ihde, “Faraday’s Electrochemical Laws and the Determination of Equivalent Weights,” *J. Chem. Educ.*, pp. 226–232, 1954.

[46] M. S. Chandrasekar and M. Pushpavanam, “Pulse and pulse reverse plating-Conceptual, advantages and applications,” *Electrochim. Acta*, vol. 53, no. 8, pp. 3313–3322, 2008.

[47] Bard, *Electrochemical Methods Fundamentals and Applications*, vol. 8, no. c. 2015.

[48] R. S. Nicholson and I. Shain, “Theory of Stationary Electrode Polarography: Single Scan and Cyclic Methods Applied to Reversible, Irreversible, and Kinetic Systems,” *Anal. Chem.*, vol. 36, no. 4, pp. 706–723, 1964.

[49] I. Te Lu, Y. C. Hsieh, P. C. Chen, and P. W. Wu, “EQCM study on pulse current Pt electrodeposition,” *Int. J. Electrochem. Sci.*, vol. 10, no. 12, pp. 10199–10209, 2015.

[50] C. R. K. Rao and D. C. Trivedi, “Chemical and electrochemical depositions of platinum group metals and their applications,” *Coord. Chem. Rev.*, vol. 249, no. 5–6, pp. 613–631, 2005.

[51] S. R. Skoog, Douglas A.; Holler, F. James; Crouch, *Principles of Instrumental Analysis (6th ed.)*. 2007.

[52] B. D. Viezbicke, S. Patel, B. E. Davis, and D. P. Birnie, “Evaluation of the Tauc method for optical absorption edge determination: ZnO thin films as a model system,” *Phys. Status Solidi*, vol. 11, no. 8, p. n/a-n/a, 2015.

[53] G. Giuffredi, “Hierarchical titanium-nitride scaffolds for Direct Methanol Fuel Cell anodes,” pp. 1–125, 2016.

[54] W. Shockley and H. J. Queisser, “Detailed balance limit of efficiency of

p-n junction solar cells," *J. Appl. Phys.*, vol. 32, no. 3, pp. 510–519, 1961.

[55] J. M. Chappé, N. Martin, J. Lintymer, F. Sthal, G. Terwagne, and J. Takadoum, "Titanium oxynitride thin films sputter deposited by the reactive gas pulsing process," *Appl. Surf. Sci.*, vol. 253, no. 12, pp. 5312–5316, 2007.

[56] Z. J. and Z.-J. Jiang, "Carbon Nanotubes Supported Metal Nanoparticles for the Applications in Proton Exchange Membrane Fuel Cells (PEMFCs)," 2011.

[57] A. McNaught, A. D.; Wilkinson, Compendium of Chemical Terminology, 2nd ed. (the "Gold Book"). 2006.

[58] M. K. Hirschfeld, C. Pfohl, and J. W. Schultze, "Corrosion properties of titanium based hard coatings on steel," 1998.

[59] Z. Dongping, J. Velmurugan, and M. V. Mirkin, "Adsorption/desorption of hydrogen on Pt nanoelectrodes: Evidence of surface diffusion and spillover," J. Am. Chem. Soc., vol. 131, no. 41, pp. 14756–14760, 2009.

[60] D. Y. Chung, K. J. Lee, and Y. E. Sung, "Methanol electro-oxidation on the Pt surface: Revisiting the cyclic voltammetry interpretation," J. Phys. Chem. C, vol. 120, no. 17, pp. 9028–9035, 2016.